

**IMMERSION COOLING OF SUSPENDED AND COATED  
NANO-PHOSPHOR PARTICLES FOR EXTENDING THE  
LIMITS OF OPTICAL EXTRACTION OF LIGHT  
EMITTING DIODES**

A Dissertation

By

Enes Tamdoğan

Submitted to the

Graduate School of Sciences and Engineering  
in Partial Fulfillment of the Requirements for

the Degree of

Doctor of Philosophy

in the

Department of Mechanical Engineering

**Özyeğin University**

August 2017

Copyright © 2017 by Enes Tamdoğan

**IMMERSION COOLING OF SUSPENDED AND COATED  
NANO-PHOSPHOR PARTICLES FOR EXTENDING THE  
LIMITS OF OPTICAL EXTRACTION OF LIGHT  
EMITTING DIODES**

**Approved by:**

---

**Prof. Dr. Mehmet Arık, (Advisor)**  
Department of Mechanical Engineering  
Özyeğin University

---

**Prof. Dr. Samuel Graham**  
School of Mechanical Engineering  
Georgia Institute of Technology

---

**Assoc. Prof. Dr. Göksenin Yaralıođlu**  
Department of Electrical Engineering  
Özyeğin University

---

**Assist. Prof. Dr. Altuđ Bařol**  
Department of Mechanical Engineering  
Özyeğin University

---

**Assist. Prof. Dr. Mete Budaklı**  
Department of Mechanical Engineering  
Turkish-German University

**Date Approved:** 23 August 2017

## ABSTRACT

Energy efficiency, long life, exceptional color and performance of solid-state light (SSL) sources have resulted in a rapidly increasing trend in a number of practical applications especially for general lighting after a long history of incandescent lamps. However, LEDs, as a solid state lighting technology, have some limitations as typical electronics so thermal management is vital for LEDs. Moreover, predicting the life and the light quality is essential to assess and enhance the performance of LED performance. Specifically, to improve the heat dissipation one major parameter used to evaluate the LED performance is thermal resistance.

The major obstacle in estimating the thermal resistance for LEDs is the accuracy of determining the junction temperature especially for high power LEDs. Ideally, the junction temperature is determined reliably by monitoring the device temperature at a position close to the junction. That could be achieved with small temperature sensors that are placed very close to the junction. But there are still physical limitations to this method due to the sensor itself would be larger than the junction, which would result in an additional error to the measurement and will not be very useful in most applications. On the other hand, to convert blue to white light, GaN LEDs are usually encapsulated with a phosphor-epoxy mixture that cures into a soft material at high temperatures. During LED operation, significant self-heating occurs causing the glass-like epoxy to undergo large displacements due to its high thermal expansion coefficient at a critical temperature. This enhanced displacement inside the LED package may fracture the gold wire bonds and ultimately lead to device failure. Thus, the inclusion of phosphor into a high brightness LED package is another complex task. In a typical 450 nm or 470 nm blue LED, YAG phosphor is introduced and combined with the blue emission to create what appears to the eye is white light. While, the common practice for phosphor carrier

medium is typically a silicone with high refraction index, the geometry of the phosphor is a primary design variable and can be classified as dispersed (dispersed inside the liquid coolant as particles), remote (remote coated under the dome), and local (coated over chip). In each case the geometry greatly affects the ultimate optical output of the LED color qualities and conversion efficiency.

Since there is limited information about individual losses in an LED system and there is no available correlation to predict the total losses, this study is for filling the gap for both of these fundamental problems; estimating the thermal resistance and increasing the ultimate optical output of an LED with different coating technologies.

Thus, the junction temperatures are first measured in the current work with Raman Spectroscopy, Infrared (IR) imaging as well as Forward Voltage method (FVM) for a 455 nm bare blue LED chip (without any phosphor coating). Then, the same samples have been coated with a phosphor-epoxy (13%, 4300 CCT) mixture to convert blue light into white light. After that junction temperatures were measured experimentally with the previously mentioned three methods and compared to each other. While IR imaging shows better capability on capturing the possible hotspots over the surface, Raman and Forward Voltage methods were in reasonably good agreement on measuring the junction temperature for 455 nm blue (uncoated) LED chip. However, the measurements performed after coating have shown slightly different results with Infrared (IR) imaging and Raman method, while Forward Voltage method has still shown meaningful results for coated chips. To be able to have a reasonable comparison, all cases have been measured with FVM simultaneously with one other mentioned method as in couple.

As the second phase of the work, after identifying the junction temperatures accurately, LED effective liquid cooling is examined since it is tackling a major challenge “hot

phosphor losses” that provides unique information for both fundamental nano-fluid (phosphor based) heat transfer and improved light conversion efficiency. Thus, topside liquid cooling with optically-transparent liquids is utilized to reduce average chip temperatures and to improve the uniformity of chip and phosphor temperature, leading to higher light extraction efficiencies. Furthermore, computational models and experimental studies of heat transfer and optical behavior to validate modeling results were performed for three proposed coating configurations (coated over chip, dispersed inside the liquid coolant as particles and remote coated under the dome) with dielectric liquid cooling. While, the phosphor is in direct contact with the LED chip in the current coating applications, it has shown higher junction temperatures beside of lower conversion efficiency and possible color shifts. The dispersed phosphor idea inside the liquid coolant as particles has resulted with lower conversion efficiency beside of any important thermal enhancements on the LED junction. However, the phosphor in the remote coating system is not affected by the LED temperature and thus maintained a consistent conversion rate and overall color point. Moreover, the remote phosphor with immersion cooling system has extended the lumen extraction limits of white LEDs in excess of 53%, as long as the remote-phosphor system is well designed.

## ÖZETÇE

Uzun yıllar akkor lambaların kullanılmasının ardından, yarı-hal ışık kaynaklarının (LED'lerin) sahip oldukları yüksek verim, uzun ömür ve çeşitli renk imkânı sunabilmesi gibi özellikleri sebebiyle özellikle genel aydınlatma olmak üzere birçok uygulamada yer almaktadır. Bununla beraber LED'lerin de tüm elektroniklerde olduğu gibi bazı limitleri mevcuttur. LED'ler de jonksiyon sıcaklığı önemli bir faktör olarak önümüze çıkmaktadır. Ayrıca, LED'lerin ömür ve ışık kalitesinin elde edilmesi ve performansının belirlenebilmesi oldukça önemlidir. Performans ve ışık kalitesinde en önemli etken olan jonksiyon sıcaklığının belirlenmesinde ise kullanılacak en önemli parametre ısı direncidir dolayısıyla jonksiyon sıcaklığıdır. LED'lerde bu ısı direncin doğru bir şekilde hesaplanabilmesi ise oldukça zor ve hala tam bir kararlaştırılmış teknik olmamakla beraber, 3 farklı method ile hesaplanabildiği literatürde ki bazı çalışmalarda gösterilmiştir. Normalde, jonksiyon sıcaklığı çok ince sensörlerin jonksiyon bölgesine yerleştirilerek daimi veri alımı ile yapılabilmektedir. Ancak, LED'lerin jonksiyon bölgesi ölçüm sensörlerinden daha ufak olması bu tekniğe imkan sağlamamakla beraber olası bir ölçüm esnasında da ölçülen değerlerdeki hata payı beklenenden fazla olabilecektir.

Diğer bir yandan da, GaN yarı iletkenlerinden yapılmış bir LED'den çıkan mavi ışığın beyaza dönüştürülmesi için genelde fosfor malzemesi çip üzerine silikon yardımıyla kaplanır. Bu ışık dönüşümü de kendi içerisinde belli bir verime sahip olduğundan, çalışma esnasında buradaki fosforda oluşan ekstra ısınma bazen buradaki bu silikon yapının erime öncesi yumuşama seviyelerine ulaşabilmektedir. Bu da çip ile elektronik kart arasında elektriksel iletkenliği sağlayan ince tel kabloların kopmasına yol açabilmektedir ve LED çalışmaya devam edememektedir. Bu sebepten jonksiyon

sıcaklığının ölçülebilmesinin yanı sıra çip üzerine yapılacak kaplama da kendi içerisinde ayrı bir önem taşımaktadır.

Tipik bir 450-470 nm'lik mavi LED çipinden çıkan ışığı beyaza dönüştürmek için genellikle YAG fosforu kullanılmaktadır. Genel kaplama yöntemi ise direk çip üzerine silikon ile sıvı halde döküp orda katılaşmasını sağlamak şeklinde olmaktadır. Bu tekniğe alternatif olarak çip üzerine çipten uzakta bir cam yarım kürenin iç yüzeyine fosfor kaplanması ve elektrik iletkenliği olmayan sıvı dolumu; ve diğer bir teknik olarak fosfor partiküllerinin bu yarım küre içerisine elektrik iletkenliği olmayan sıvı içerisinde serbest bir biçimde doldurulması düşünülmüştür. Her bir teknik kendi içerisinde ışık çıkışını ve ışık dönüşüm verimini oldukça etkilemektedir.

Genel bağlamda, LED'lerde ki kayıpların ilgili yerlerinde ne kadar olduğunun hesaplanması konusunda yeterli çalışma ve korelasyonlar mevcut değildir. Bu çalışma da bu boşluğu doldurabilmek adına sunuyoruz. Bu çalışma da özellikle LED'lerin jonksiyon sıcaklığının ölçülmesi ve sıvı soğutma ile birleştirilmiş farklı fosfor kaplama tekniklerinin kıyaslanması yapılmıştır.

Jonksiyon sıcaklığının ölçülmesinde ki en önemli parametre olan ısı direncin doğru bir biçimde hesaplanabilmesi için literatür de bahsedilen üç farklı method; Raman spektrometresi, Termal kamera ve Voltaj değişim teknikleri kullanılmıştır. İlk olarak 465nm'lik bir mavi çipin jonksiyon sıcaklıkları üç method ile çok yakın değerlerle hesaplanabilmiştir. Ardından aynı çip önceden belirlenmiş 4300 CCT değerine göre %13 fosfor ve silikon karışımı ile kaplanarak tekrar ölçülmüştür. Kaplama sonrası yapılan jonksiyon ölçümleri bazı farklılıklar göstermiştir. Termal kamera, silikonun düşük termal iletkenlik katsayısı sebebiyle sebep olduğu merkezde yüksek sıcaklık değerleri okurken; Raman spektrometresi ise kaplama sonrası çipten çıkan yoğun beyaz ışık sebebiyle okunması hedeflenen tepe noktası bu yoğun ışık süzmesi içerisinde

kalmakta ve ilgili malzemenin çıkardığı dalga boyundaki tepelik gözlemlenmemiştir. Voltaj değişim tekniği ise her iki durum için ise aynı şekilde sıkıntısız ölçüm yapabilmektedir. Jonksiyon sıcaklığının doğru bir biçimde belirlenebilmesi ardından artık sıvı soğutmalı farklı kaplama tekniklerinin kıyaslaması üzerine çalışma devam etmiştir. Daha öncede bahsedildiği üzere fosfordaki ışık dönüşümü esnasında oluşan istenmeyen ısının giderilmesi amacıyla fosfor katmanının çipten uzağa alınması düşünülmüştür. Ardından çip ve fosfor arasına da elektrik iletkenliği olmayan sıvı ile doldurularak optik ve termal etkileri incelenmiştir.

Yapılan incelemelerde öncelikli olarak sayısal metotlar kullanılmış ve deneysel ölçümlerle birbirinin kıyaslanması yapılmıştır. Elde edilen sonuçlara göre, direkt çip üstü kaplama (sıvılı ve sıvısız) ve cam yarım küre içine sıvı ile serbest bir biçimde bırakılan fosfor partikülleri durumları yüksek jonksiyon sıcaklıklarına beklenen faydayı sağlayamamakla beraber ışık veriminde de kayda değer sonuçlar elde edilememiştir. Cam yarım küre içine yapılan fosfor kaplaması ve elektriksel iletken olmayan sıvı dolumu sonrası yapılan deneylerde ise jonksiyon sıcaklığında kayda değer derecede soğuma elde edilirken, ışık dönüşüm veriminde ilk duruma kıyasla (sıvı soğutmasız, direkt çip üstü fosfor kaplamalı durum için) kıyaslandığında %53 oranında ışık çıkışında artış gözlenmiştir.



## ACKNOWLEDGEMENTS

Financial support for this research project was provided by the EU FP7 Career Integration Grant (304013) and it was carried out at Özyeğin University.

First, I would like to extend my sincere appreciation for my advisor, Prof. Dr. Mehmet Arık, for giving me the opportunity to carry out this study under his supervision and who with his professionalism, advised me during the whole process of my PhD and offered constructive criticism and help. Also special thanks to the Engineering Faculty for giving me the opportunity to work as researcher during my PhD and being a part of Özyeğin University.

I would also like to extend my gratitude to my committee members: Assoc. Prof. Dr. Göksenin Yaralıoğlu, Assist. Prof. Dr. Altuğ Başol and Assist. Prof. Dr. Mete Budaklı for their advice during my research and also to Prof. Dr. Samuel Graham for his guidance and hospitality during my short visit at the Georgia Institute of Technology.

Next, I would like to thank my family and my wife for always encouraging me to pursue my interests and for making that pursuit possible. I truly lack words to express how grateful I am for all the sacrifices you made.

Lastly, I am grateful to all of my colleagues at EVATEG and ART-group for their special contributions, and criticisms. Specially, I appreciate all the technical discussions we have had during group meetings. I have benefited a great deal from our individual meetings and your technical expertise and creativity.

Thank you all.

# TABLE OF CONTENTS

ABSTRACT.....	IV
ÖZETÇE .....	VII
ACKNOWLEDGEMENTS.....	X
LIST OF FIGURES .....	XIII
LIST OF TABLES.....	XVI
NOMENCLATURE .....	XIX
<b>1 INTRODUCTION .....</b>	<b>1</b>
1.1 Historical Evolution of Lighting Technology and Thermal Management.....	1
1.2 Thermal Sensitivity of Light Emitting Diodes.....	5
1.3 Thermal Management Schemes .....	7
<b>2 LITERATURE REVIEW .....</b>	<b>11</b>
2.1 Passive Cooling Techniques for High-Power LEDs.....	11
2.2 Scope of the Current Research.....	19
<b>3 DESCRIPTION OF THE PROBLEM .....</b>	<b>22</b>
3.1 Test Facility.....	25
3.2 Operating Parameters and Boundary Conditions.....	27
<b>4 COMPUTATIONAL STUDY ON THE THERMAL MANAGEMENT SCHEMES FOR HIGH POWER LEDs .....</b>	<b>28</b>
4.1 Grid Sensitivity Analysis .....	29
4.1.1 Mesh Dependency Tests for Conduction and Natural Convection Cases	29
4.1.2 Mesh Dependency Test for Forced Convection Cases .....	32
4.1.3 Energy Balance Tests.....	34
4.2 Conduction Heat Transfer with Silicone.....	37
4.3 Immersion Cooling of LEDs with Single Phase Natural Convection.....	39
4.4 Immersion Cooling of LEDs with Single Phase Forced Convection.....	43
4.5 Immersion Cooling of LEDs with Boiling Heat Transfer.....	54
4.6 Immersion Cooling of Suspended and Coated Nano-Phosphor LEDs .....	55
4.7 Ideal Dielectric Coolant for LED Immersion Cooling.....	65

<b>5</b>	<b>EXPERIMENTAL STUDY ON JUNCTION TEMPERATURE MEASUREMENT TECHNIQUES</b> .....	70
5.1	Forward Voltage (FVM) .....	72
5.2	Raman Spectroscopy .....	75
5.3	Infrared (IR) Thermal Imaging .....	79
5.4	Comparison of Measurement Techniques.....	81
<b>6</b>	<b>THERMAL AND OPTICAL PERFORMANCE EXPERIMENTS FOR IMMERSION COOLED LEDS</b> .....	88
6.1	Immersion Cooling of Suspended and Coated Nano-Phosphor LEDs and Light Extraction.....	88
<b>7</b>	<b>SUMMARY AND CONCLUSIONS</b> .....	98
<b>8</b>	<b>SUGGESTIONS FOR FUTURE WORK</b> .....	107
8.1	Summary of the Present Work .....	107
8.2	Future Work .....	109
<b>9</b>	<b>REFERENCES</b> .....	112
	APPENDIX A.....	119
	APPENDIX B .....	125
	APPENDIX C .....	130
	BIBLIOGRAPHY .....	133

## LIST OF FIGURES

<b>Figure 1.</b> History of lighting [4].....	1
<b>Figure 2.</b> History of LED evolution [8-10].....	2
<b>Figure 3.</b> The first white LED from luminescence conversion is developed by Shuji Nakamura [13] .....	3
<b>Figure 4.</b> Variation of optical power with spectral distribution for a range of temperature [27].....	6
<b>Figure 5.</b> Carbon nanotube interface material placed under a high power LED [50]....	15
<b>Figure 6.</b> LED luminaire fixture with a loop heat pipe from Huang et al. [55].....	16
<b>Figure 7.</b> Vapor chamber system module with copper or aluminum spreader from Huang et al. [56] .....	17
<b>Figure 8.</b> Miniaturized heat pipe design Li et al. [57] .....	17
<b>Figure 9.</b> Examples of a) phosphor darkening b) local hot spots and chip failures [20]	22
<b>Figure 10.</b> Cross section view of the in-house made LED with an innovative single phase cooling concept.....	25
<b>Figure 11.</b> Schematic of CFD domain for the light engine with dome.....	28
<b>Figure 12.</b> Chosen grid for numerical analysis (mesh 1).....	29
<b>Figure 13.</b> Grid refinements through three different mesh structures and comparison of present CFD analysis with experimental results published in Arik et. al. [20] .....	30
<b>Figure 14.</b> Schematic of the CFD domain .....	32
<b>Figure 15.</b> Chosen grid for analysis (Mesh 4).....	33
<b>Figure 16.</b> Grid refinements through 7 different meshes.....	33
<b>Figure 17.</b> Geometry and compared boundary conditions.....	35
<b>Figure 18.</b> Average temperatures for different phosphor coating thicknesses.....	36
<b>Figure 19.</b> Contour plots for average temperatures for different phosphor coatings.....	36
<b>Figure 20.</b> Total heat flow through the phosphor layer .....	37
<b>Figure 21.</b> Computational comparison of thermal capability for air and silicone .....	38

<b>Figure 22.</b> Temperature distributions for air (left) and silicone (right) filled domes ....	39
<b>Figure 23.</b> Computational comparison of thermal capability for air and HFE7200 .....	40
<b>Figure 24.</b> Computational comparison of thermal capability for air and FC72.....	41
<b>Figure 25.</b> Temperature contour plots for each liquids and also silicone in comparison to dome with air. ....	42
<b>Figure 26.</b> Thermal resistances comparison for natural convection, forced convection and conduction heat transfer .....	44
<b>Figure 27.</b> Variation of thermal rate as a function of Re number for different chip powers with 1SI-1SO.....	45
<b>Figure 28.</b> Variation of thermal rate as a function of Re number for varying number of outlets.....	46
<b>Figure 29.</b> Variation of thermal rate with chip powers for air under forced convection	47
<b>Figure 30.</b> Variation of thermal rate with Re numbers for water under forced convection.....	47
<b>Figure 31.</b> Variation of thermal rate with chip powers for water forced convection with new designs.....	48
<b>Figure 32.</b> Variation of thermal rate comparisons for Re numbers with 1CI-4SO and 1CO-4SI designs with air under forced convection.....	49
<b>Figure 33.</b> Variation of thermal rate with Re numbers for new designs (1CI-4SO / 1CO-4SI) with water under forced convection.....	49
<b>Figure 34.</b> Variation of thermal resistance with Re numbers for water and HFE 7200	50
<b>Figure 35.</b> Variation of thermal resistance with Re numbers for air-water-HFE 7200 .	50
<b>Figure 36.</b> Variation of pressure drops with Re numbers for Air-Water-HFE 7200 .....	51
<b>Figure 37.</b> Thermal effectiveness for Air-Water-HFE 7200 with increasing Re numbers .....	52
<b>Figure 38.</b> Comparison of thermal resistances for natural convection, forced convection and conduction.....	53
<b>Figure 39.</b> Optical degradation with boiling .....	54
<b>Figure 40.</b> Effect of boiling over radiant power .....	55
<b>Figure 41.</b> Application approaches for phosphor in high brightness LED packages.....	56

<b>Figure 42.</b> Schematic of CFD domain for the light engine with remote phosphor under dome.....	57
<b>Figure 43.</b> Chosen grid for analysis (Mesh 1).....	58
<b>Figure 44.</b> Computational comparison of thermal capability for air and silicone .....	64
<b>Figure 45.</b> Temperature rise over ambient for different liquids at various driving conditions.....	67
<b>Figure 46.</b> Temperature rise over ambient for air, water and NS15 at various driving conditions.....	68
<b>Figure 47.</b> Nu and Pr numbers for dielectric liquids with NS fluids .....	69
<b>Figure 48.</b> Nu and Gr numbers for dielectric liquids with NS15.....	69
<b>Figure 49.</b> Devices under test a) Bare chip and b) Phosphor coated chip .....	71
<b>Figure 50.</b> Experimental results depicting the linear behavior of $V_f$ with the junction temperature .....	72
<b>Figure 51.</b> Schematic of the experimental apparatus for Forward Voltage experiments .....	73
<b>Figure 52.</b> Block diagram for the experimental procedure .....	73
<b>Figure 53.</b> Variation of forward voltages a) Coarse scale b) Fine scale pulse duration and current .....	74
<b>Figure 54.</b> Schematic of the experimental apparatus for Raman Spectroscopy .....	76
<b>Figure 55.</b> Variation of Raman peak wave number with temperature for uncoated LED chip.....	77
<b>Figure 56.</b> Variation of wavenumber shift for $\text{TiO}_2$ particles over uncoated LED chips .....	77
<b>Figure 57.</b> Raman test measurements through the surface at different positions .....	79
<b>Figure 58.</b> IR Imaging through the surface at different positions.....	79
<b>Figure 59.</b> Schematic of experimental apparatus used for Infrared Imaging (IR) test station.....	80
<b>Figure 60.</b> Emissivity correction process via QFI Infra Scope system, a) Unpowered LED chip, b) Emissivity correction, c) 5X magnified correction result; uniform temperature .....	80

<b>Figure 61.</b> Infrared Imaging measurement results for uncoated chips a) 150mA b) 300mA c) 450 mA .....	82
<b>Figure 62.</b> Infrared Imaging measurement results for coated chips a) 150mA b)300mA c) 450mA .....	82
<b>Figure 63.</b> Comparison of coated and uncoated chip junction temperatures at 150mA	83
<b>Figure 64.</b> Comparison of coated and uncoated chip junction temperatures at 300mA	85
<b>Figure 65.</b> Comparison of coated and uncoated chip junction temperatures at 450mA	86
<b>Figure 66.</b> PCB manufacturing processes .....	89
<b>Figure 67.</b> Spectral fluxes for three test samples at various currents.....	89
<b>Figure 68.</b> Experimental setups for three different phosphor application technologies	90
<b>Figure 69.</b> Junction temperature and optical experimental systems .....	90
<b>Figure 70.</b> Optical light extractions according to the experimented technologies.....	94
<b>Figure 71.</b> Spectral power distributions for proposed technologies .....	95
<b>Figure 72.</b> Both light extraction and junction temperature comparison results for all proposed technology .....	104
<b>Figure 73.</b> Visualization of invented technology .....	106
<b>Figure 74.</b> The experiment sample for unpainted case .....	126
<b>Figure 75.</b> Schematic of the temperature measurement points .....	127
<b>Figure 76.</b> a)Experimental setup, b)Painted and unpainted LED packages close up view .....	128
<b>Figure 77.</b> Change of efficiency with increasing board temperature.....	129
<b>Figure 78.</b> Experimental setup of street lighting.....	130
<b>Figure 79.</b> Temperature distribution on cut plane.....	132
<b>Figure 80.</b> Various design with different fin thickness.....	133
<b>Figure 81.</b> Various design with different number of fins.....	133

## LIST OF TABLES

<b>Table 1.</b> Comparison of possible cooling technology, advantages and disadvantages ..	10
<b>Table 2.</b> Temperature values obtained from CFD for different phosphor thicknesses ..	35
<b>Table 3.</b> Operating parameters and boundary conditions.....	60
<b>Table 4.</b> Computational junction temperature results for corresponding technologies .	62
<b>Table 5.</b> Computational junction temperature results for corresponding technologies .	63
<b>Table 6.</b> Proposed dielectric coolants with their differentiated properties.....	67
<b>Table 7.</b> Experimental junction temperature and light extraction results for corresponding technologies .....	91
<b>Table 8.</b> Experimental junction temperature and light extraction results for corresponding technologies .....	92
<b>Table 9.</b> Both light extraction and junction temperature comparison for uncoated bare LED package.....	102
<b>Table 10.</b> Both light extraction and junction temperature comparison for silicone coated LED package.....	102
<b>Table 11.</b> Both light extraction and junction temperature comparison results for phosphor coated bare LED package .....	102
<b>Table 12.</b> Both light extraction and junction temperature comparison results for liquid cooled and remote phosphor coated LED package.....	103
<b>Table 13.</b> Both light extraction and junction temperature comparison results for liquid cooled with suspending phosphor particles .....	103
<b>Table 14.</b> Both light extraction and junction temperature comparison results for liquid cooled and phosphor coated LED package .....	103
<b>Table 15.</b> Integrating sphere – Luminous flux (Lm) measurement uncertainty .....	120
<b>Table 16.</b> Integrating sphere – CCT measurement uncertainty.....	121
<b>Table 17.</b> Integrating sphere – CRI measurement uncertainty.....	122
<b>Table 18.</b> Electrical, thermal and optical readings from experiments for blue chip ....	123
<b>Table 19.</b> Uncertainty analysis for the junction temperature of blue chip .....	123
<b>Table 20.</b> Integrating sphere overall measurement uncertainty summary .....	123



<b>Table 21.</b> Optical properties of the LED package.....	126
<b>Table 22.</b> Optical and thermal performance results of the unpainted experiments.....	127
<b>Table 23.</b> Optical and thermal performance results of the painted experiments.....	128
<b>Table 24.</b> Measured temperatures on different location.....	131
<b>Table 25.</b> Temperature for different materials .....	133
<b>Table 26.</b> Temperature distribution for current material on variable thickness.....	134
<b>Table 27.</b> Temperature distribution for current material on variable fin number ( $k=205\text{W/m-K}$ ) .....	134



## NOMENCLATURE

$Nu$	[-]	Nusselt number, $hD_h/k$
$Re$	[-]	Reynolds number
$D_h$	[m]	Hydraulic diameter
$h$	[W/m <sup>2</sup> -K]	Heat transfer coefficient
$L$	[m]	Characteristic length
$Q$	[W]	Heat transfer
$T$	[K]	Temperature
$Gr$	[-]	Grashof number
$Pr$	[-]	Prandtl number
$Ra$	[-]	Rayleigh number
$E$	[W]	Optical power
$g$	[m/s <sup>2</sup> ]	Gravitational acceleration
$R$	[K/W]	Thermal resistance

### Special characters

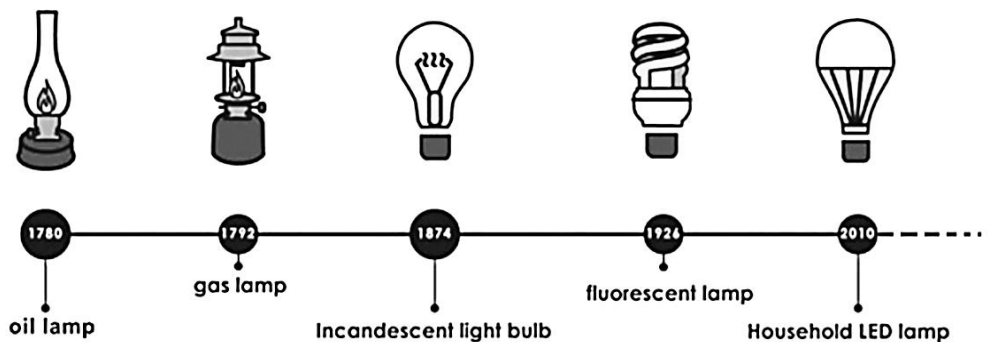
$\rho$	[kg/m <sup>3</sup> ]	Mass density
$\beta$	[1/K]	Volumetric expansion coefficient
$\vartheta$	[m <sup>2</sup> /s]	Kinematic viscosity
$\mu$	[mPa·s]	Dynamic viscosity
$c_p$	[J/kg-K]	Specific heat capacity at constant pressure
$k$	[W/m-K]	Thermal conductivity
$\alpha$	[m <sup>2</sup> /s]	Thermal diffusivity
$A$	[m <sup>2</sup> ]	Total convective area
$T_s$	[K]	Surface temperature
$T_J$	[K]	Junction temperature
$T_w$	[K]	Wall temperature
$T_\infty$	[K]	Ambient temperature

# CHAPTER I

## INTRODUCTION

### 1.1 Historical Evolution of Lighting Technology and Thermal Management

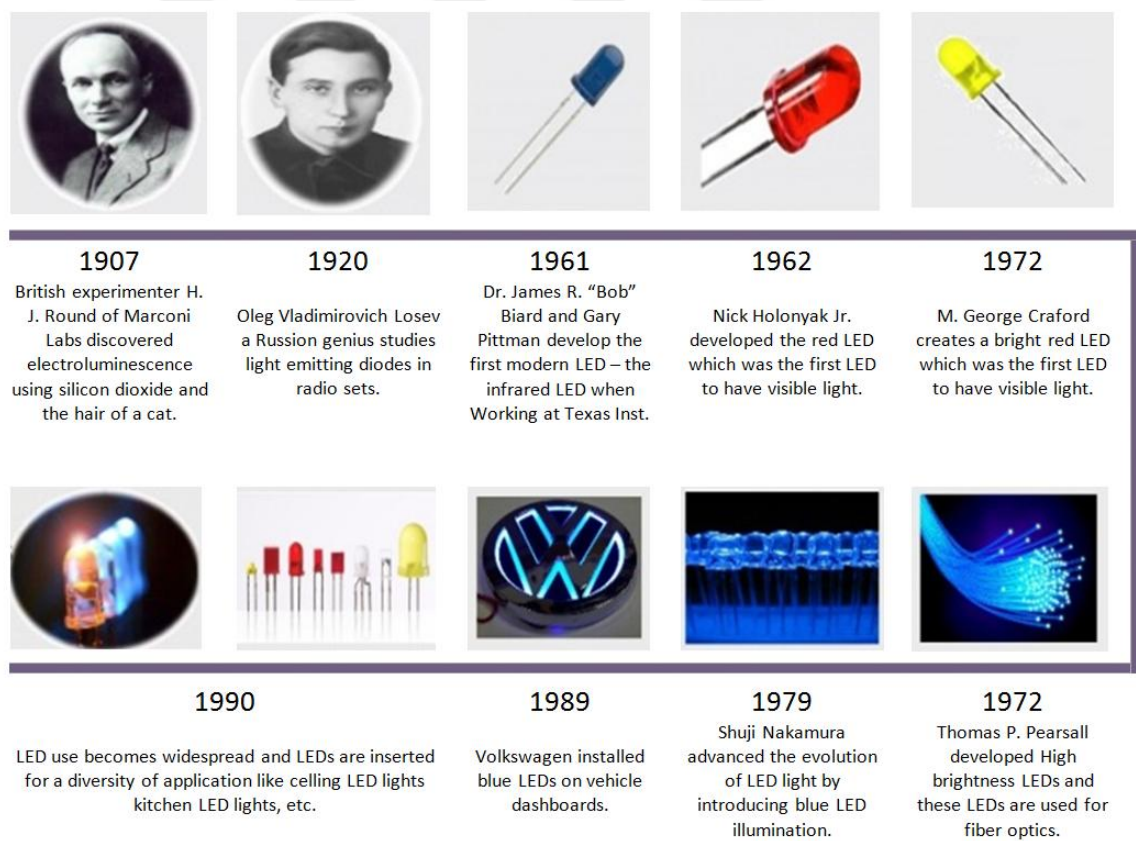
Different lighting systems have been invented during the history such as oil lamps, kerosene lamps, gas lighting, carbon arc, neon, and mercury lamps; while, incandescent lamps, fluorescent lamps and light emitting diodes (LED) are commonly used lighting systems nowadays [1]. Figure 1 presents the historical development of lighting systems. After extensively utilizing the incandescent lamps for more than a century, their disadvantages in terms of energy consumption and the short lifetime have forced the scientists to invent better lighting solutions for general lighting applications [2,3].



**Figure 1.** History of lighting [4]

The basic structure of a light emitting diode consists of multi-layered semi-conducting materials. While incandescent lamps emit continuous spectrum, in the active layer of an LED the light is produced at a particular color driven with a DC current. A wide range of color spectrum is achieved by changing the semiconductor material at the active layer. To reach a high degree of brightness in all colors, by means of luminescence conversion, two material systems are mainly used. When a DC current is applied, LEDs

emit light in many colors according to their composition of the semiconductor crystal compounds [5,6]. While, one of the methods for producing white light is exposing an additional yellowish fluorescent phosphor material layer over a blue LED; mixing the red, green and blue diodes (RGB) is another method of luminescence conversion from blue to white light. Since any number of color tones can be achieved by varying the proportions of the individual three RGB colors, mixing RGB LEDs is commonly chosen for decorative effects with various rich colors where the priority is not general white lighting. However, these technological developments were not that easy to invent, which took place in decades [7,8]. The development of LED lighting is summarized in Figure 2.



**Figure 2.** History of LED evolution [8-10]

For over 30 years, light emitting diodes have been used in various applications. While the first practical visible-spectrum of the light-emitting diode has been developed by

Nick Holonyak Jr. in 1960s, LED technical development starts from 1900s and continues to stride ahead [10-12]. In 1907, the first light up activity of inorganic materials is discovered by Henry Joseph Round under the chosen electric current. This light up activity has been published in the journal of "Electrical World" in the same year. While this "Round effect" of light emission was out of his focus, it was initially forgotten but again observed in 1921 by the Russian physicist Oleg Lossev and the fundamental phenomenon was described in a greater detail. In 1935, the same light emission effect is also discovered in zinc sulfide by the French physicist Georges Destriau and called as "Lossev light". However, a more detailed explanation of semiconductors physics is discovered with the development of a transistor in 1951. Then, it became easy to explain the light emission phenomenon. After all those achievements, Nick Holonyak has developed the first LED in the visible wavelength field (red), which also entered to the market as the first industrially-produced LED. With this ground breaking achievement, different semiconductor materials are used for having new colors such as green, orange and yellow in 1971.



**Figure 3.** The first white LED from luminescence conversion is developed by Shuji Nakamura [13]

Although, their performances and effectiveness were poor initially, they are continued to improve and the first brilliant blue LED in the green spectrum range (InGaN diode) were brought to market by Shuji Nakamura in 1993, seen in Figure 3. Just after two

years, he also introduced the first LED with white light and launched on the market [14]. Further improvements followed by the first LEDs with 100 lumens per watt to the market after 13 years. In recent years, LEDs luminous efficacy has reached to 250 lumens per watt under laboratory conditions.

Moreover, the technological developments in wide band gap devices have boosted the efficiency and performance of solid state lighting devices; hence they become a favorable choice for a number of general lighting applications. While, light-emitting diodes (LEDs) as solid state lighting devices have mostly been used as for indicators, signals and displays before, nowadays LEDs have increased their popularity with their superior advantages such as energy savings, long life, and exceptional color and performance. Especially high-power LEDs have already started playing a major role in general lighting applications. Moreover, they will be an important area for IoT (Internet of Things), control and smart house technologies in the coming years. Although, this technology offers very special features by the integration of those technologies and outdistances its potential competitors in advance, LEDs have some limitations on thermal management, as all electronics.

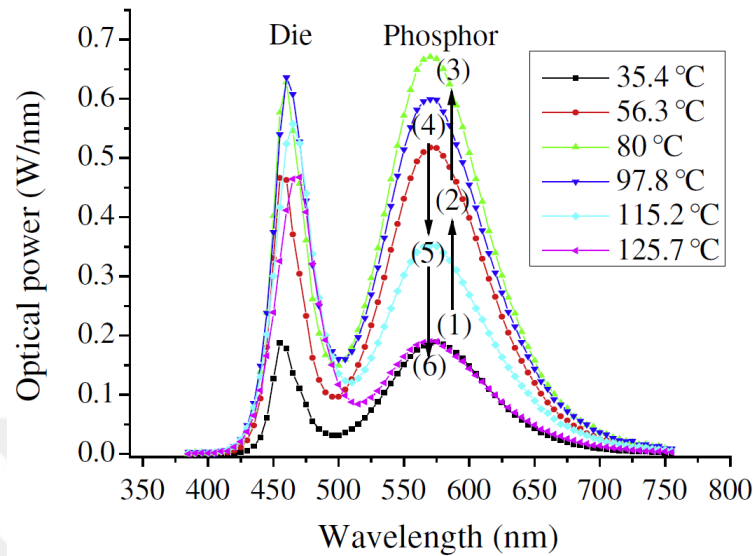
The miniaturization and the rise in processing power have increased the heat generation in LEDs. While this average heat flux is projected to further increase in upcoming years [15,16], a bigger challenge is posed by the spatial and temporal non-uniformity in power distribution [16,17]. Projected extreme heat fluxes in the next generation of high performance LEDs systems have created an unprecedented thermal management challenge for which a straightforward extension of the state-of-the-art cooling strategies cannot adequately address. Consequently, thermal management became a major limiting factor for implementing LEDs into lighting fixtures due to poor cooling capabilities that highly affects the performance and reliability of those lighting systems.

## 1.2 Thermal Sensitivity of Light Emitting Diodes

Even though the operating conditions of solid state lighting devices are significantly lower than metal halide lamps, LEDs as SSL devices have also much lower surface areas in comparison to the conventional light sources [18,19]. Every light source can achieve conversion of electric power into the light with a certain percentage according to its efficiency while the rest resides in the system as heat in different proportions. Thus, LEDs also generate undesired heat while operating like every other light source. Although, they are known as one of the most efficient system in lighting, about 75–85% of the total electrical power is still being converted and stored inside the package as undesired heat [20]. In comparison to white LEDs, lower conversion losses (60–70%) can be seen in green LEDs [21,22], but still a higher amount of power is being lost as undesired heat inside the enclosure that reduces the reliability and luminosity of packages [23]. Moreover, the trend of miniaturizing the overall system while desiring high-brightness LEDs causes to significant local heating problems that is called the hot-spot phenomenon and draws more attention to thermal management [23-25]. This is the reason why thermal design is one of the most challenging tasks to prevent the overheating of LEDs.

Inadequate design approaches might cause to performance drop of LED light sources in both short and long-term. Decreasing power conversion efficiency, wavelength shift, color changes in the spectrum can be counted as some of the short-term effects due to excess of heat [21, 26]. Moreover, the possible failures resulting from phosphor thermal quenching include a decrease in light output, color shift, and the broadening of full width at half maximum (FWHM). The driving forces are high drive current and excessive junction temperature, which are attributed to increases in temperature of the inside of the package [23]. The temperature dependency of phosphor thermal quenching

is also shown (see Figure 4), which is caused due to increased package temperature by high drive current and excessive junction temperature.



**Figure 4.** Variation of optical power with spectral distribution for a range of temperature [27]

Thus, the importance of thermal design becomes much clear, while a proportional increase in light extraction is not observed with increasing electrical current. This problem, called as thermal saturation, is the result of high junction temperature [28]. Moreover, complete thermal runaway, spontaneous failures and damages such as higher thermal stresses, broken wire bonds, delamination, detachment in the solder joints, and die-bond epoxy damages become inevitable, if higher temperatures occur [1,3,20]. Regarding long-term performance effects, local hot spots in phosphor layer due to poor color conversion, low quantum efficiency while accelerating the lumen depreciation, resulted in shortening the lifetime [3]. Thus, phosphor positioning within the package plays a critical role in thermal performance besides optics. Key considerations regarding the overall short and long term effects have to do with its thermal and optical flux limitations simultaneously. Indeed, the thermal design and cooling method play a key role for the success of conversion efficiency and reliability of LEDs [20].



### 1.3 Thermal Management Schemes

The heat generation at the device footprint and the associated rise in junction temperature can reduce device performance, reliability, and lifetime [29]. Moreover, the desired high power LEDs driving over 1000 mA over a smaller area ( $1 \text{ mm}^2$ ) is able to generate local temperature gradients. In addition, bonding failures at manufacturing or during operation (cracks and delamination) may also lead to local hot spots. Consequently, the semi-conductor industry is seeking an efficient thermal management solution. Traditional cooling solutions utilize stacks of thermally conductive solid-state heat spreaders such as copper, aluminum and extended surfaces (or fins) to increase the available surface area for heat transfer before ultimately dissipating the waste heat to the environment via convection [30].

The widely used cooling solution, air convection with extended surfaces, relies on both free convection and added effect of thermal radiation is effective at low heat flux densities. But the anticipated increase on the driving currents and chip frequency is resulting to higher heat fluxes. Therefore, current cooling technologies such as forced air convection cannot also provide an effective cooling performance. Thus, a very large heat sink and an unacceptably large chip-to ambient temperature difference is required to provide high heat flux cooling which also can't be applied due to the physical limitations of such systems. While, the impinging jet technology has also been used for large heat flux dissipation required systems such as lasers and x-ray anodes [30], resulting large impact force or momentum dissipation may not be allowable with delicate devices such as electronic devices. Another approach of air cooling for heat removal can be the use of an oscillating cantilever beam as a flow inducer, the piezoelectric fan. The piezoelectric fan is a low-power consumption fan that uses an applied electric voltage to produce material deflections and oscillations. Arik et al. [31]

examined the piezoelectric fan when coupled with a heat sink. This study indicated that metallic piezoelectric fans might have a considerable coefficient of performance. Acikalin et al. [32,33] studied an optimized design for the piezoelectric fan by changing the fan tip geometry. Moreover, Arik [34] studied the local and global heat transfer coefficients with high-frequency synthetic jet on a flat surface. At the resonance frequency of 4500 Hz, it is observed that the heat transfer coefficient values were 4 to 10 times higher than the natural convection values. Although, it may be an effective solution for electronics with its simple mechanism and its promising initial performance; its suitability for high power LEDs is up in the air and needs more research.

Moreover, recently advanced miniaturized thermoelectric coolers (TEC's), which have been evaluated for on-chip hot spot remediation [35], have received great attention for hot spot thermal management because these solid state devices can offer high reliability, can be locally and selectively applied for spot cooling, can provide high cooling heat flux. However, it can be only integrated to the bottom side of an LED package since the top side is required for light excitation. Thus, it should have enough cooling capability since the only possible cooling connection is from bottom side in the most of the current LEDs. Moreover, polarity reversing in overheated cases is another problem that might occur, while the system functioning under harsh conditions.

Compared to convective air cooling, some other well-known cooling techniques such as; pool boiling, flow boiling, spray cooling, and thin film evaporation, can also enhance the heat removal capacity and achieve heat fluxes that exceed  $100 \text{ W/cm}^2$ .

While, pool boiling is sensitive to orientation and limited by the critical heat flux (CHF); neighboring bubbles in CHF coalesce and form a vapor layer that separates the working fluid and the heated surface causing a significant rise in wall temperature. On

the other hand, the flow boiling in micro channels can be seen as an attractive cooling strategy that can improve temperature uniformity and achieve relatively higher heat transfer coefficient, in comparison to pool boiling [36-38]. Although, it is used for many engineering applications, it won't be also suitable for top side cooling of LED modules. As a result, phase change heat transfer is very powerful due to latent heat effect of the working fluids and provides several orders of magnitude higher performance than single phase heat transfer [39]. Moreover, it can also provide unique solutions for LED local hot spot problems. However, any decrease on the optical performance is not tolerable. Thus, to benefit from thermal superiority of multi-phase cooling, the special evaluation on light extraction is more crucial due to neighboring bubbles over the chips while operating. Although it might be chosen as a solution from the backside of LED, it will be dependent to the interface resistance between the chip and the heat sink. However, the direct liquid cooling, providing intimate contact with a bare chip, can eliminate that thermal resistance between the chip and the heat sink.

In direct liquid cooling, the LED chips with hot spots are immersed into a dielectric liquid within a closed loop system. While those liquids are electrically nonconductive, the optical properties (refractive index and transparency etc.) are also important since the fluid is located at the optical path [40]. As a result, single phase immersion (direct) liquid cooling systems present better optical light extraction with a reasonable thermal performance in comparison to other proposed thermal management schemes [40].

Although, each of those systems has individual advantages, they don't meet full of expectations due to some unacceptable results affecting overall LED performance, thus also has some disadvantages. Accordingly, the performance comparisons of each mentioned techniques were summarized in Table 1, where the basic advantages and disadvantages were listed.

**Table 1.** Comparison of possible cooling technology, advantages and disadvantages

Technology	Advantages	Disadvantages
<b>Natural Convection</b>	Solid-state heat spreaders such as copper, aluminum and extended surfaces (or heat sinks)	Increases surface area, distribute the local heat
	Thermoelectric Coolers	Suitable for low power electronics, low performance
<b>Forced Convection</b>	Rotating Fan	High mass flow rates, ease of use in many applications
	Piezo Fan	Not suitable for local hotspots, noise production, space required
	Synthetic Jet	Low-power consumption, smaller in size
<b>Multi-Phase Liquid Cooling</b>	Pool Boiling	Higher heat transfer coefficients due to latent heat effect of the working fluids and provides several orders of magnitude higher performance than single phase heat transfer
	Flow Boiling	
	Film Boiling	
<b>Single-Phase Liquid Cooling</b>	Immersion Cooling	Low performance
<b>Single-Phase Liquid Cooling</b>	Immersion Cooling	Direct contact with chip, better optical results, reasonable thermal performance
<b>Single-Phase Liquid Cooling</b>	Immersion Cooling	Special isolation required for possible leakage problems, gets heavier once the device gets bigger

## CHAPTER II

### LITERATURE REVIEW

The miniaturization trend of electronics has caused a significant increase of elevated heat flux levels. As this trend continues, the reliability of the solid state lighting systems may diminish, which eventually reveals the necessity for thermally higher performing technologies [29].

Two major approaches, active and passive cooling, are commonly in use as an effective thermal management solutions for LEDs. While the convection heat transfer is the main mechanism for heat removal in self (passive) cooling methods, local heat distribution from die to heat sink fins of the LED luminaire is also achieved with the use of heat pipes [30]. As the air movement happens naturally in passive systems, increased heat dissipation by forced air movement is the main mechanism of the active cooling techniques [41]. A number of such air movement devices such as micro pumps, forced convective heat exchangers or synthetic jets, are in use for different applications as explained in detail in previous chapter. Although, current passive cooling techniques are poor in terms of thermal performance for LEDs to achieve a satisfying light extraction, they are cost-effective on thermal management in comparison to the active cooling technologies [42]. Thus, a possible passive cooling technique with a reasonable cooling performance can be the best option for LEDs.

#### **2.1 Passive Cooling Techniques for High-Power LEDs**

In LEDs, undesired heat generation doesn't occur from a single point, while each part of those losses are generated in components of a luminaire system, have a specific percentage of effect on the thermal performance of LEDs. While the most of the

undesired thermal energy occurs at the LED die, the generated heat fluxes might be even greater than  $300 \text{ W/cm}^2$  in some applications, which reveals the vitality of advanced heat spreaders for LEDs [43,44]. While chip substrate and die attach materials are thermally performance limiting sections in the heat dissipation path, for dissipating this excess of heat from junction to ambient, thermally high conductive materials play an important role [44]. Especially, the low thermal conductivity of die attach material form a bottleneck in the dissipation path by decreasing the rate of heat flow.

Die attach materials can be summarized in two categories such as solder paste or metal (organic) adhesives. While metal adhesives perform better thermal conduction through the die attach due to the suspending metal particles in a polymer structure for providing the required mechanical strength and solder material; it is important to be aware of possible void problems in case of large amount of die attach materials needed since the required die attach material will include higher solder flux [45]. Moreover, the higher thermal resistances especially due to the voiding increase the junction temperature of LED thus raising the possibility of failure in the overall system [46]. Furthermore, organic metal adhesives are recommended for high power LEDs involves silicone encapsulation, instead of solder including die attach materials due to their sensitivity of silicone [45].

In another study, the conventional adhesive material is compared in terms of the thermal resistance of two types of high power LEDs with electrolysis and electroplating technique (EET) with a set of experiments by Chen et al. [47]. Individual high power LEDs (red, green and blue) were mounted on two separate metal heat sinks one with the mentioned conventional adhesive and other with EET without any adhesive resin. The experiments were conducted with a 350 mA input current and the junction temperatures were measured during the operation of the LED. While, junction temperatures with a

conventional method reported as 91°C, 117°C, and 82°C, respectively; by using EET, they are lowered by 10°C, 41°C, and 5°C respectively. Likewise, the thermal resistances of the red, green, and blue LEDs are reduced by 15.4 %, 43.1 %, and 14.0 %, while the luminous intensities are increased by up to 37.0 %, 19.5 %, and 26.0 %, respectively [47]. The importance of die attach material was thus clearly shown on thermal and optical performance of red, green and blue LEDs.

On the other hand, LED chip substrate material is another significant point affecting the thermal resistance and optical performance of LEDs. Two common chip substrate materials, SiC and sapphire, are in use with a thermal conductivity of 400 W/(m·K) and 30 W/(m·K) respectively. Moreover, the effects of those two types of substrate materials on the junction temperature were explored by Arik et al. [48].

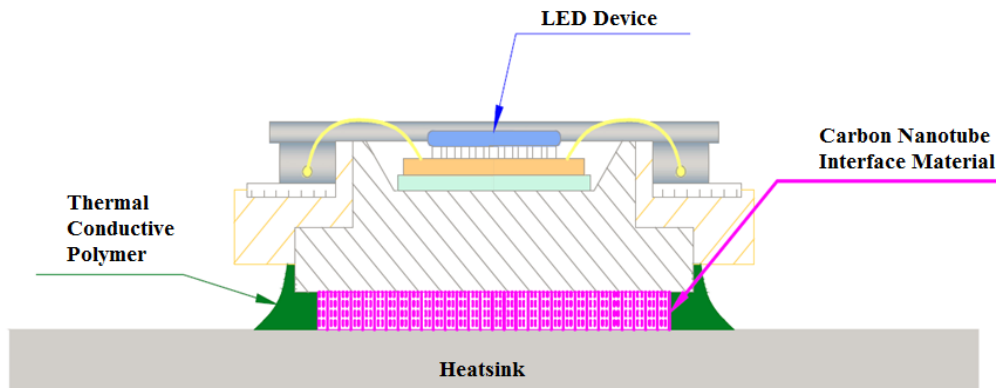
They made a comparison of both packages by evaluating the maximum junction temperatures measured for SiC and sapphire packages while operating as 120.1°C and 124.1°C, respectively. The junction-to-board resistance was reduced more than half as measurements have presented 4.4 K/W and 9.2 K/W for SiC and sapphire packages, respectively. Moreover, significant effect of the chip bump layout on the temperature distribution over an LED package has been stated by Arik and Weaver [23]. They have revealed the effect of substrate material on the temperature distribution. Due to the lower thermal conductivity, sapphire substrate was found to result higher temperature variations on the LED chip beside of the local maximum temperatures causing to local hot spots. As a result of their both studies, the higher thermal conductivity of SiC has proven its superiority over sapphire packages by presenting better thermal performances [27,48].

The thermal performance of high power LEDs were also explored computationally with a commercial software [49]. GaN based high power LED package with sapphire

substrate was placed on a heat sink. They aimed to show the effects of different parameters on the junction temperature including the substrate material within an accuracy of 4.8 %. Three different substrate materials, sapphire, SiC, and copper, have been simulated. Simulations have shown negligible difference between substrates. In case of 1 W power inlet to the LED package, the junction temperatures have been measured as 112°C, 105°C, and 102°C for sapphire, SiC, and copper substrates, respectively, once the inlet power has been increased to 5 W. Thus, a temperature difference of 10°C was shown in the simulations when the substrate material has been changed from sapphire to copper in case of 5 W input power to the LED package.

As another significant parameter, the thermal interface materials have also been evaluated in terms of thermal performance of an LED system. Increasing the thermal conductivities of interface materials, for which the current lower thermal conductivities stem from their polymer matrix within their structure, can accelerate the thermal performance of the system by decreasing the junction temperatures [50]. Thus, Zhang et al. have been proposed a new interface material for high power LEDs, that consists of vertically aligned carbon nanotubes while there wasn't any polymer matrix included. The location of the interface material and the side view of the LED package can be seen in Figure 5. The thermal resistance of proposed interface technology consists of carbon nanotubes were mentioned as 7 K/W in the experimental study. The measured data was also reported as only around 10 % of commercial silver epoxy thermal resistance with a thickness of 25  $\mu\text{m}$  [50]. Moreover, they have shown the capability of carbon nanotube interface material in terms of thermal and optical performance with the linearity behavior obtained between the light excitation and input current. Thus, they have stated that the nanotube arrays can be a promising technology for high power LEDs.





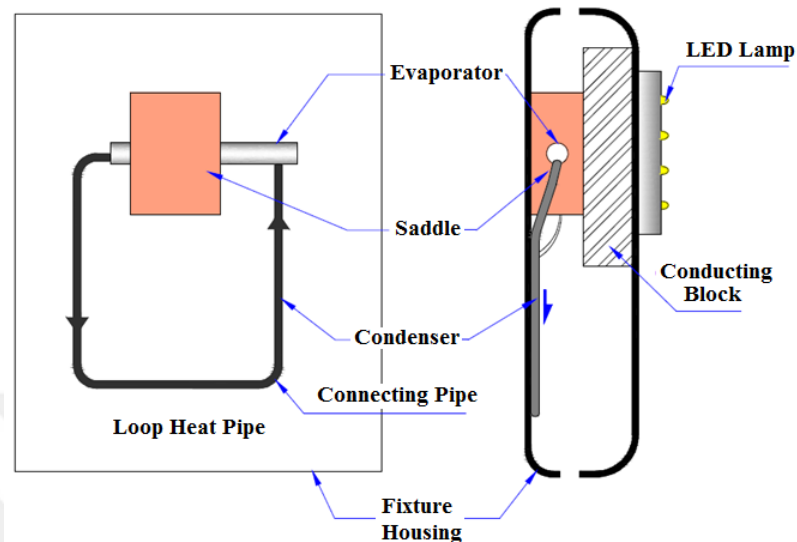
**Figure 5.** Carbon nanotube interface material placed under a high power LED [50]

On the other hand, the heat appeared from the die conducts to the substrate from where it is directed to and rejected from the heat sink usually with a natural convection passive air cooling. While, it relies on both free convection and added effect of thermal radiation, only natural convective cooled heat sink system will not be adequate to have optimal performance of lighting at higher heat fluxes generated by high brightness LEDs. Thus, the heat sink design and optimization in LED packaging is another important area to focus on, for which different type designs and optimization methods have already been presented in the literature [51-54].

Luo et al. have shown a new method optimizing the heat sink by determining the fin height, thickness and spacing for a 112 W street lamp [26]. Moreover, they conducted a set of experiments once the optimal height, thickness and spacing were determined. When the system reached to steady state condition, temperatures were measured as 45°C while the ambient temperature was 25°C, which has proven the new method and the optimized new structure as thermally well performing design.

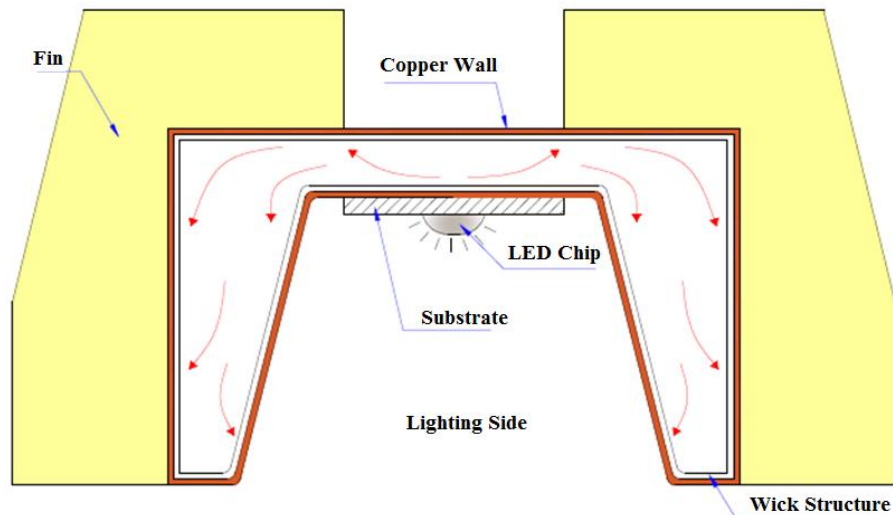
As another technique, loop heat pipe system is also commonly used in most of the electronics due to its higher dissipation capability of the locally generated heat. This technology enables the dissipation of large amount of locally generated heat due to capillary forces through flexible connecting pipes. Moreover, it is also specially chosen

where the system requirements don't allow any fans. A special design including a loop heat dissipation technology for a high power LED with an input power up to 150 W, seen in Figure 6, was utilized by Huang et al. [55].



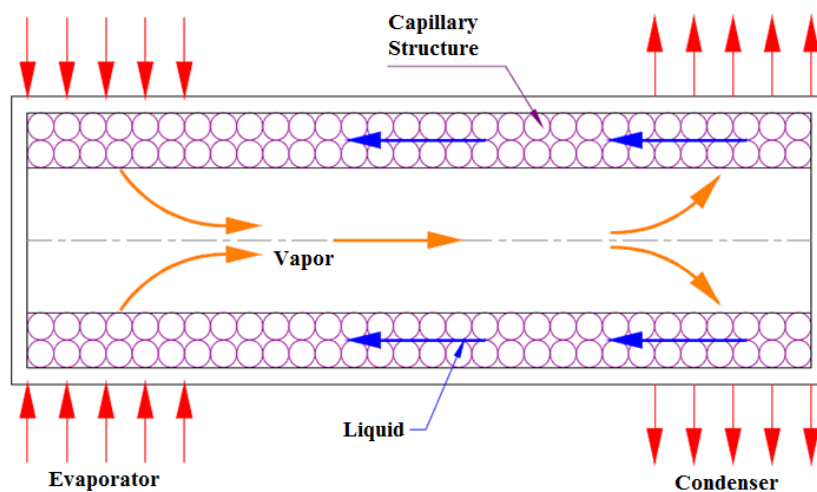
**Figure 6.** LED luminaire fixture with a loop heat pipe from Huang et al. [55]

A year later, they have proposed another design, seen in Figure 7, for cooling performance investigation of the proposed design module [55]. To establish the most appropriate design, diameter and material of vapor chamber and fin were varied. The circuit board was replaced with a vapor chamber. While the chamber was made up of copper, fins were manufactured from aluminum. As the working fluid, water was utilized. After the experiments, the effect of copper and aluminum spreaders were evaluated in terms of cooling performance of chamber. The experiments were performed at 15 W and the temperatures were recorded at different locations. The measured data from all three types of vapor chambers have shown the maximum temperatures as 62°C, 65.3°C and 67.1°C for the vapor chambered lamp, copper and aluminum spreader plate respectively. While the vapor chamber system is resulted in the lowest temperature distribution, a more uniform temperature distribution is also provided with a lamp-type vapor chamber.



**Figure 7.** Vapor chamber system module with copper or aluminum spreader from Huang et al. [56]

A miniaturized version of heat pipe technology based on copper/water, seen in Figure 8, was proposed by Li et al. [56]. A set of numerical models have been applied with a new design of a luminaire with nine 1.2 W LED chips to evaluate the performance of new miniaturized design in reducing the junction temperature for the same LED package. The computational studies were handled in ANSYS Icepak for analyzing the temperature distribution over electronics. Based on the computational results, they have proposed that the new miniaturized design would enable to keep junction temperature as low as 70°C, which is much lower than the allowable working temperature of 120°C.



**Figure 8.** Miniaturized heat pipe design Li et al. [57]

Furthermore, they have estimated the junction temperatures, after a set of optimization study was performed at the external parts of the heat sink including the height, thickness and the number of fins. Computational results for new optimized miniature system has shown a significant decrease on the maximum the junction temperature by estimating as  $56.7^{\circ}\text{C}$ , which has shown the enhancement capability of the current optimization levels. Another study attained a heat flux of  $790\text{ W/cm}^2$  from a surface in which microscopic channels were formed by Tuckerman and Pease [58]. They also developed heat transfer correlations for water forced through the channels with a flow rate of  $8.6\text{ ml/s}$ . Then, the thermal resistance was estimated for FC-77 (dielectric coolant) as 2.3 times greater than water [58].

Another similar study with a rectangular flow channel was conducted by Incropera et al. in which they obtained correlations for a single smooth heat source [59]. They have tested water and FC-77 as dielectric liquid coolant. Moreover, single-phase liquid cooling in a rectangular channel was tested by Samant and Simon [60]. But, they have used a small heater (length =  $0.25\text{ mm}$ , width =  $2.0\text{ mm}$ ) to achieve much thinner thermal boundary layers thus higher heat transfer coefficients. On the other hand, the resultant pressure drops might cause serious problems once the system consists of a large number of electronics, even though the obtained reasonable thermal resistance values.

Another solution has been tried to increase the heat transfer coefficient by Ramadhyani and Incropera. They performed a set of experiments with a special surface enhancement [61]. They have varied their surface with two types of fins: one with basic cylindrical pins and other with a series of square fins along its length. These two designs gave them extra surface area of the heated surface by factors of 8 and 12.8, respectively. Moreover, the experimental results for FC-77 showed much lower thermal resistances with a

moderate level of pressure drop ( $< 0.68$  kPa). Meanwhile, some researchers started thinking about immersed cooling systems which put both PCB and components inside working fluids. On the contrary to the fact that the feasibility of immersed cooling systems has already been demonstrated by constructing some practical models, very few analyses have been conducted yet.

Therefore, in the current study, a lighting system comprising a dielectric cooling fluid which directly contacts with LED chip; attached to a heat sink base. There, the heated dielectric coolant moves with its decreasing density as a result of the increased temperature due to the high temperature formed in the LED chip. Then, the same coolant, whose temperature thereof decreasing upon contacting with the heat sink base; moves towards the LED chip, and reduces the temperature of the LED chip by contacting the LED chip. While, these fluids are still not much rich in terms of thermal performance due to their lower thermal transporting properties; different coating ideas for owing higher optical and thermal performance have also been carried out in the current work. As a result, different phosphor coating applications were integrated with immersion liquid cooling and compared in terms of thermal and optical performance enhancements.

## **2.2 Scope of the Current Research**

The objective of this thesis is to investigate the local hot spots in LED systems and to understand the implications of different cooling mechanisms. Moreover, the effect of phosphor conversion efficiency by varying coating applications is also in the scope of the thesis. There, a novel idea has been developed for extending the limits of optical extraction of light emitting diodes beside of thermal performance enhancements. As the consensus of the current work, positive impact of direct immersion cooling over thermal

and optical performance for both bare and phosphor coated LEDs has been proved computationally and experimentally. The results have shown that immersion cooling can be used to cool LED lamps in an efficient manner, to increase the durability and the amount of light to be obtained from LED lamps, and to reduce the weight thereof. The greatest advantage of the embodiment according to the proposed idea is that it eliminates local temperature difference (local hotspots) in LED chips, while increasing the light extraction (i.e. lumen extraction) efficiency, with a proper dielectric liquid selection. Moreover, the work is extended to demonstrate the potential of phosphor coating strategies as a thermal management solution for localized heating (extreme heat flux) which formed in the phosphor layer, or in phosphor particles.

While the history of lighting, LEDs in the lighting history, and thermal problems on LEDs are explained in detail in Chapter 1, basics of the current thermal management technologies, their performances and the scope of the work are being presented in Chapter 2.

In Chapter 3, the general aim of the study is further expanded. Experimental approaches and the test facility are explained in detail. All the related dimensions and operating boundary conditions are discussed. Microfabrication steps, calibration procedures, and experimental error analysis are also discussed in detail.

In Chapter 4, a set of computational models, that acts as same as the novel idea, for different cooling technologies is developed. Moreover, the models are validated by comparing the experimental findings. These models solve the mass, momentum and energy equation simultaneously in a control volume. The model has been simulated separately for changing coating techniques, cooling methods and input power conditions. Then, the obtained thermal performances are compared and discussed.

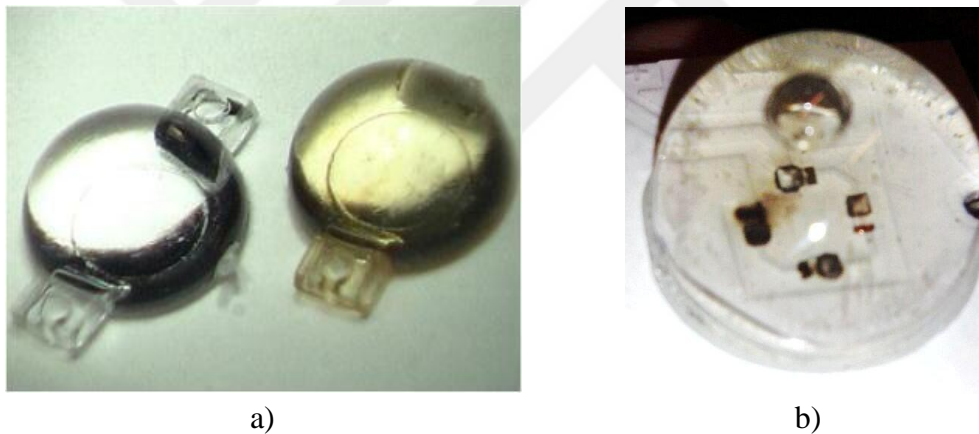
In Chapter 5, experimental studies for different cooling and coating techniques are reported and compared with a set of junction temperature measurements methods. Moreover, the experiments were repeated under different power conditions and their validations for the computational studies are also reported in this chapter. Furthermore, consideration of optics is also vital in lighting. Thus, a set of experiments for light extraction are studied in this chapter too. Since the poor heat dissipation of the package and undesired extra heat generation inside the phosphor particles causes thermal and optical problems, the novel idea of coating technology with immersion liquid cooling technique targeted towards abating hot spots and increasing the optics via a dielectric liquid and utilizing various phosphor coating techniques.

In Chapter 6, the key findings of the thesis are summarized. Furthermore, future directions, contributions and the broader impact of this work are outlined.

## CHAPTER III

### DESCRIPTION OF THE PROBLEM

Significant self-heating occurs during an LED operation causing the glass-like epoxy to undergo large displacements due to its high thermal expansion coefficient. This displacement inside the LED package may fracture the gold wire bonds and ultimately lead to device failure [62]. Furthermore, at elevated junction temperatures, the optical efficiency of an LED is also reduced, decreasing the overall light conversion efficiency of the phosphor. A significant heat generation leads to local hot spots and darkening of the phosphor particles as shown in Figure 9 [20,27,63].



**Figure 9.** Examples of a) phosphor darkening b) local hot spots and chip failures [20]

To reduce the junction temperature and to improve device performance, understanding and evaluating the thermal resistance between the p-n junction and ambient is thus critical [63]. A major obstacle in estimating the thermal resistance for LEDs is the accuracy of determining junction temperature especially for high power LEDs [64,65]. Ideally, the junction temperature could be determined reliably by monitoring the device temperature as close as possible to the junction. That could be achieved with small temperature sensors that are placed very close to the junction. But there are still physical



limitations to this method due to the sensor itself would be larger than the junction, which would result with an additional error to the measurement and will not be very useful in most applications [66]. Thus, three main techniques; Forward Voltage, Raman Spectroscopy and Infrared Imaging (IR) methods for determining the junction temperature are applied as proposed measurement techniques in the literature [1]. While, Forward Voltage method uses the voltage drop with the varying temperature, Raman Spectroscopy is based on the temperature dependent phonon frequency shift of the material [67]. For infrared thermal imaging technology, basic temperature mapping technique detecting thermal radiation is applied over a chip surface by a thermal camera using a microscopic lens.

While, the drawbacks and the inadequacy of the existing solutions, mentioned in the previous section, regarding the subject matter, it is required to make a development in the related technical field. As, the general aim for most of the previously explained cooling methods is to prevent the problems that are likely to occur due to the high heat formed in the chips during operation, local heating in the phosphor used for changing color in LEDs has lead the current study to direct liquid cooling with special phosphor coating technologies by evaluating their impact on LED performance (e.g., light extraction at the chip and light conversion of phosphor particles). Three coating ideas (coated over chip, dispersed inside the liquid coolant as particles and remote coated under the dome) with dielectric liquid cooling are examined.

Thus, the introduction of topside liquid cooling with optically-transparent liquids with a special integration of new phosphor coating application ideas is the main focus of this study to reduce average chip temperatures and to improve the uniformity of chip and phosphor temperature, leading to higher light extraction efficiencies. Furthermore, the study is involving a number of key research areas such as;

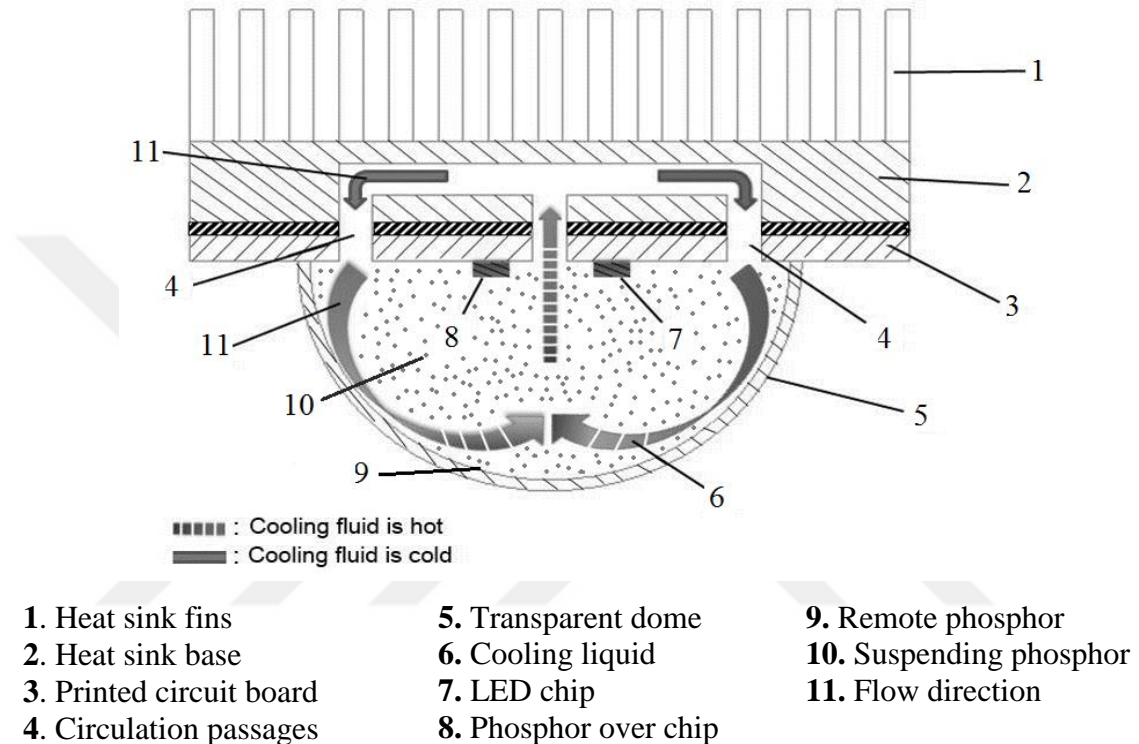
- Investigating the local hot spots in LED systems; chip and phosphor,
- Computational modeling of heat transfer and optical behavior,
- Optical losses due to phosphor white light conversion,
- Liquid cooling with nano-phosphor particle filled fluids,
- Developing an experimental study to validate modeling results.

Moreover, with the present immersion cooling technique, formation of local hot spots in the phosphor layer or in phosphor particles will be investigated with the help of computational studies. Another advantage of the technique is that it reduces the thermal resistance between the chip and heat sink to a great extent when compared to other cooling systems. The embodiment is suited for being used both in LEDs with high brightness producing white light and in LEDs with different colors (red, green, blue, etc.). In the state of the art, hot spots are also formed in the material adjusting/controlling the color of light, the so called phosphor, and this reduces quantum efficiency (light intensity). With the current cooling system, phosphor temperature will be controlled and light extraction (i.e. lumen extraction) efficiency will be increased.

Furthermore, in the present embodiment, a smaller heat sink will be sufficient, instead of using a bigger one, with the superior cooling effect thereof. Natural circulation of the cooling fluid in liquid form within the embodiment will continue in itself as long as the lamp operates, thereby achieving an efficient cooling without any extra power. Moreover, the heat will be taken from the chip and phosphor, and will be made to reach to the heat sink (i.e. heat rejecting block), with the effect of naturally formed movement.

### 3.1 Test Facility

The current proposed lighting system comprises heat sink fins, a heat sink base with vertically aligned flow channels, circulation passages, cooling fluid, printed circuit board LED chip, transparent dome and phosphor. The structural and characteristic aspects of the present design are shown in Figure 10.



**Figure 10.** Cross section view of the in-house made LED with an innovative single phase cooling concept.

The proposed lighting system particularly comprises a cooling system which comprises a heat sink and fins which are directly in contact with the cold environment and a heat sink base. Thus, the overall heat coming from the base is transferred to the ambient with the help of fins. Moreover, the current lighting system with the proposed cooling methodology comprises a dielectric cooling liquid which is in direct contact with the LED chip. Due to the high temperature formed in the LED chip, the density of the cooling liquid decreases. The liquid streams through a hole positioned in the center of the system towards the heat sink base where it transfers heat by passing through the

circulation passages. Until reaching the exit of the circulation passages, the temperature of the cooling liquid reduces and hence its density increases. At the exit of the circulation passages the low-temperature cooling liquid flows enters the dome again.

This natural cycle continues in itself as long as the LED lamp operates, and this occurrence which provides heat rejection, is achieved within the present system without using any extra power (pumps, fans, etc.). Moreover, a dielectric (i.e. not conducting electricity) cooling fluid which directly contacts with LED chips located on the metal circuit board having a better heat conductivity than other standard lamps is used. This, in turn, provides a better cooling when compared to the gases used for heat rejection in standard lamps.

Moreover, hot spots are formed in the phosphor, which is the material adjusting/controlling the color of light, and this reduces quantum efficiency (light intensity). In the embodiment, according to the design options, phosphor can be used in different variations as shown in Figure 10. It may be present in the lower surface of the transparent dome as remote phosphor in some embodiments, over the LED chip in some other embodiment, or inside the transparent dome as suspending particles in another embodiment in a dispersed manner. The idea mentioned in this application includes these three states of phosphor and the derivatives thereof. Phosphor may be present in the form of layer or particle. The cooling fluid cools down phosphor, which is in the form of layer or particle. Thus, the problem of local hot spot formation in phosphor is solved; and phosphor temperature can be controlled and light extraction efficiency can be increased. After the cooling fluid contacts with the heat sink base as mentioned in the above paragraph, the heat sink fins which are disposed on the heat sink base perform heat rejection since they directly contact with the cold environment. Thus, the heat sink base remains cold permanently.

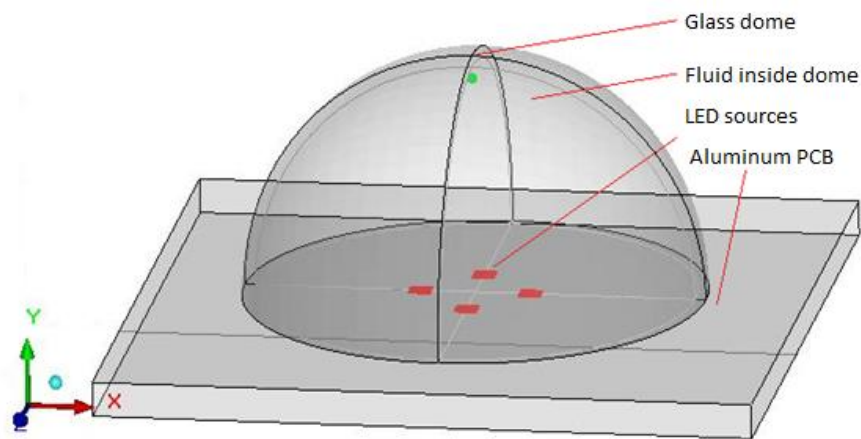
### **3.2 Operating Parameters and Boundary Conditions**

The boundary conditions for the current study are set under the consideration of fixed ambient temperature of 25°C and are given according to the expected operating parameters for the experimental activities which are performed at three different input power 150 mA, 300 mA, and 450 mA. Different types of dielectric liquids were also compared to each other in terms of thermal and optical performances. In the current study, the performance of a CREE EZ1000 455 nm 1.5 W blue LED chip has been evaluated using three different junction temperature measurement techniques. The related junction temperatures are first measured for uncoated 455 nm blue LED chip. The same samples are then coated with a phosphor-epoxy mixture (13 %, 4300 CCT) and measured again by means of the three methods explained before. The results are experimentally compared to each other to understand the advantages and limitations of each technique when used for estimating the LED junction temperature. Moreover, the experimental studies were compared with a set of numerical studies carried out with ANSYS Icepack. Besides, each case is individually experimented in integrating sphere for spectrometric results, since the main goal of the test device is to own optimal light extraction under a reasonable thermal management. As a result, the optical and thermal (Opto-thermal) performance changes were compared to each other.

## CHAPTER IV

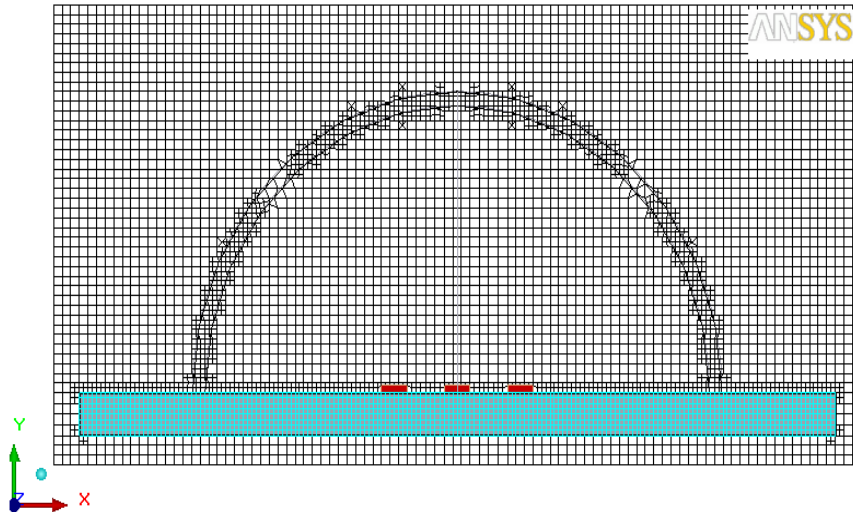
### COMPUTATIONAL STUDY ON THE THERMAL MANAGEMENT SCHEMES FOR HIGH POWER LEDs

To capture the local temperature distributions over the LED light engine with a dome in the domain, especially over the LED chip; numerical models have been built with commercial computational fluid dynamics (CFD) software, Ansys-Icepack [68]. Moreover, these studies have been applied for conduction, immersion cooled natural and forced convection individually. Later, attention has been turned into an opto-thermal evaluation for single and multi-phase heat transfer modes with dielectric fluids (LS5252, HFE7000, and silicone oil etc.).



**Figure 11.** Schematic of CFD domain for the light engine with dome

As shown in Figure 11, the computational domain for a multi-chip LED light engine consists several components; a printed circuit board (PCB), a solid glass dome and four LED sources. LEDs ( $1 \text{ mm}^2$ ) are placed on a square ( $3 \times 3 \text{ cm}^2$ ) metal core PCB with a thickness of 1.6 mm. LED chips are covered with a hemispherical glass dome with an outer diameter of 2 cm and height of 1 cm. Chip on board (COB) packaging approach is implemented in the current work. Similarly, the chosen grid structure according to the mesh independency test is illustrated in Figure 12.



**Figure 12.** Chosen grid for numerical analysis (mesh 1)

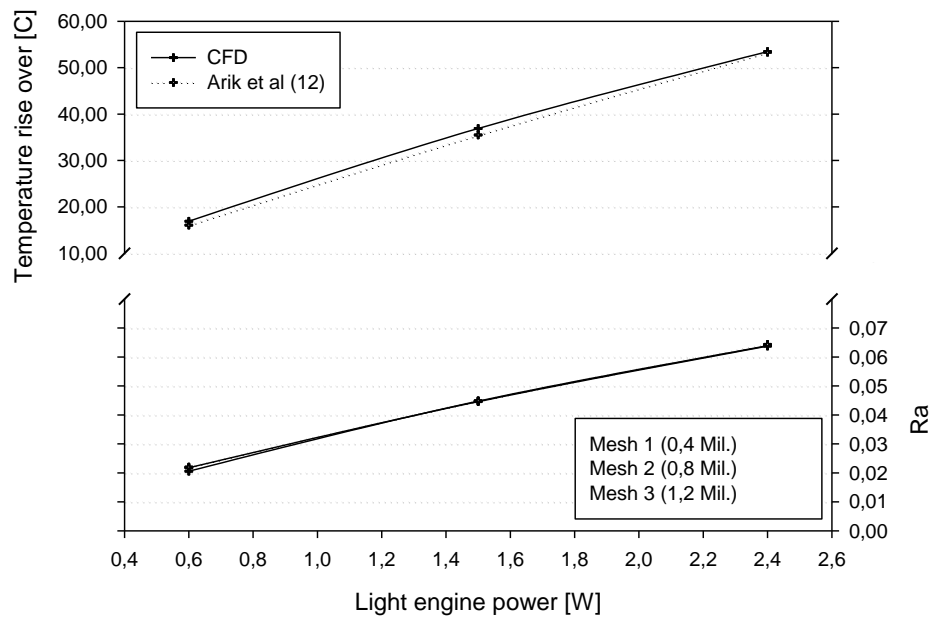
A number of comparisons have been made under a number of conditions of heat conduction and natural convection (single and multi-phase) in the tight space shaped by the hemispherical glass dome. While cured silicone inside the glass dome has been utilized for the conduction case, various dielectric liquids have been studied for the convection heat transfer modes. Moreover, to be able to compare the different cases, different driving power values (0.6 W, 1.6 W, and 2.4 W) were set. The external surfaces of the dome have been kept at room temperature (20°C) and radiation from external surfaces is also accounted in the computational models.

#### **4.1 Grid Sensitivity Analysis**

##### **4.1.1 Mesh Dependency Tests for Conduction and Natural Convection Cases**

Quality of the mesh is a crucial parameter to obtain reliable results in the CFD analysis. Hence, applying different levels of refinement is carried out for a series of cases to evaluate the impact of grid dependence on the results. A 3D computational domain is created with a commercial software package [68]. For meshing strategy, mainly hexahedral elements are chosen, while structured mesh elements are also utilized in order to reduce the instability behaviors in the flow due to the aspect ratio issues. Thus,

three different levels of mesh refinements are utilized in this study. The mesh resolutions are varied from coarse to fine grids with a total number of cells varying from 0.4 million to 1.2 million. To validate the mesh structure by comparing the grids accurately, instead of comparing just temperature values at special points over the geometry, the dimensionless numbers have also been compared. Thus, comparisons of Grashof ( $Gr$ ) and Prandtl ( $Pr$ ) numbers become important and the Rayleigh ( $Ra$ ) numbers are compared for different mesh structures and shown in Figure 13.



**Figure 13.** Grid refinements through three different mesh structures and comparison of present CFD analysis with experimental results published in Arik et. al. [20]

$Gr$  and  $Pr$  numbers are given in Eq. 1 and 2 as;

$$Gr = \frac{g\beta(T_s - T_\infty)L^3}{\nu^2} \quad (1)$$

$$Pr = \frac{\nu}{\alpha} = \frac{c_p \mu}{k} \quad (2)$$



The geometry, material, ambient temperature and boundary conditions were kept same for each test except for varying numbers of nodes between 0.4 million and 1.2 million nodes. However, the study has been repeated for three different power values passing through the LED chips to evaluate the impact of each mesh structure over the results. The results have shown that the increasing number of elements didn't make any significant differences (< 2 %). Thus, mesh-1 was chosen for the computational study. Moreover, the chosen mesh structure has also been compared with an experimental study shown in Figure 13 [20].

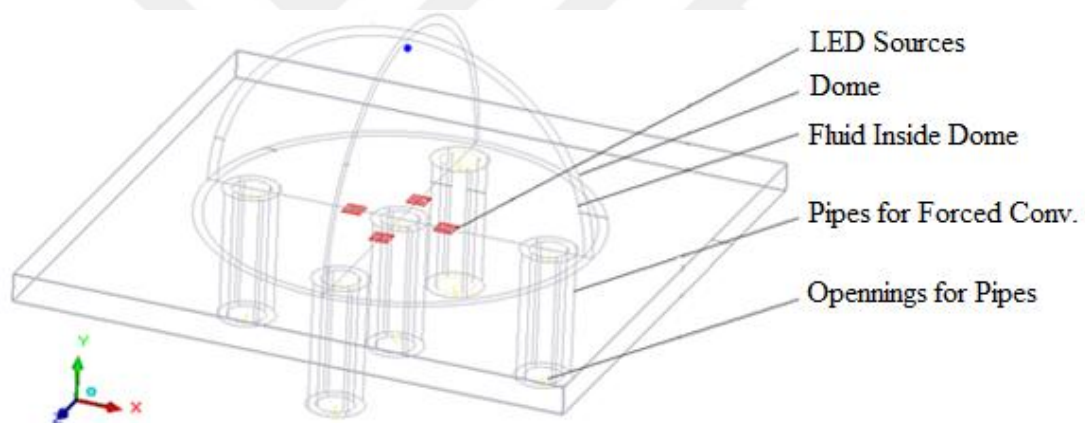
Thermal performances have been measured under three different power conditions. Then, the impact of various cooling systems on the temperature rise has been determined and they have been compared with percentage changes. Cooling performance comparisons have been made according to the temperature gradients obtained for each system separately. Moreover, a special term, called as thermal rate as seen in Eq. 3, is defined for comparison, where  $T_{MAX-Chip^*}$  stands for the maximum temperature over the chip in each case separately.

$$ThermalRate = \frac{\Delta T}{\Delta T^*} = \frac{T_S - T_\infty}{T_{Max,Chip^*} - T_\infty} \quad (3)$$

The maximum temperature rise over the ambient obtained under 2.4 W with natural convection to the air, and it is defined as  $\Delta T^*$ . For all other different cooling and power conditions  $\Delta T$ , which stands for the temperature difference between the die and the dome surface, is used. To make an easy and understandable comparison  $\Delta T^*$  has been chosen as baseline for the comparison of all natural convection cases while the coolants were changed. All other boundary conditions such as ambient temperature, differentiating power conditions kept same with the chosen mesh.

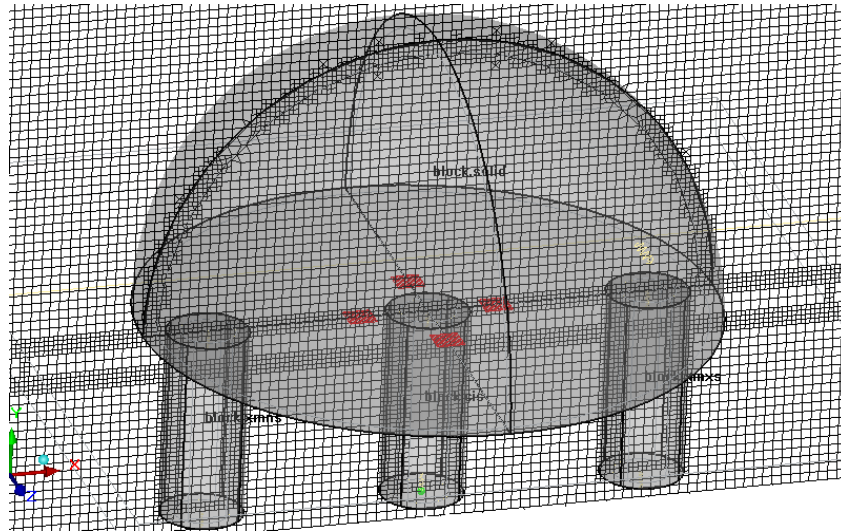
#### 4.1.2 Mesh Dependency Test for Forced Convection Cases

Another mesh dependency test has been applied also for forced convection cases. Figure 14 depicts the LED package of interest with a solid glass dome and 4 LED sources. LEDs (1 mm<sup>2</sup> in size) are placed on a metal core PCB and several cooling entrance and exhaust hole (1 mm radius) combinations for forced convection are established. In simulations considering only heat conduction, interior of the dome is taken as pure silicone and in all other cases it is HFE7200 dielectric coolant. An effort is made to evaluate the impact of grid dependence on the results by applying different levels of refinement. Beside of the refinement optimal grid size is tried to use for having reasonable computational timing.



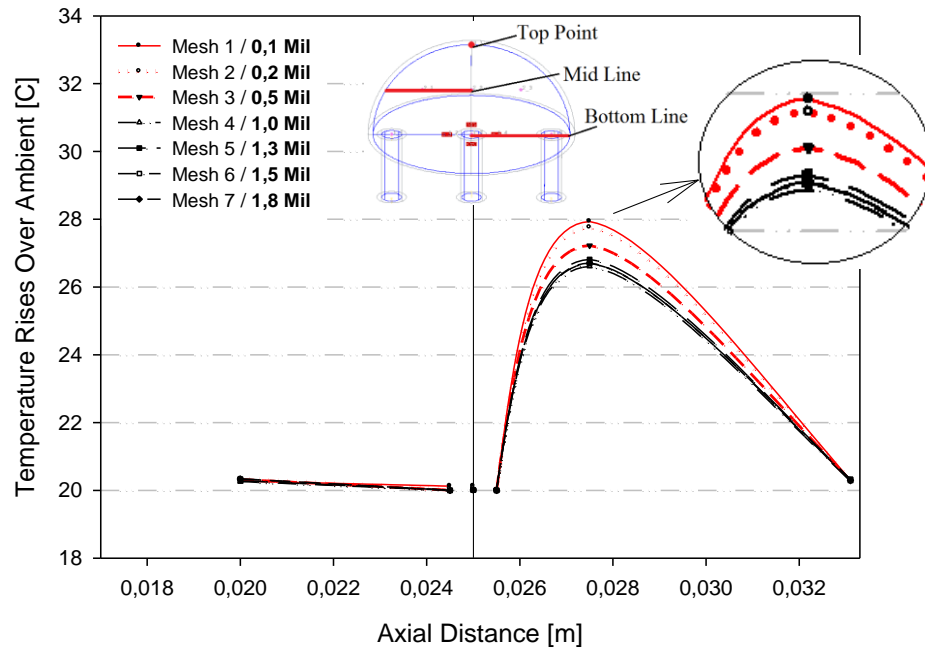
**Figure 14.** Schematic of the CFD domain

A three-dimensional geometry of the domain of analysis is again created with the help of a commercially available software ANSYS (Icepak) [68]. While, the strategy utilized in meshing is the usage of hexahedral elements in the overall geometry, free mesh type is also utilized in order to reduce the instability behaviors in the flow due to the aspect ratio problems. Inlet and outlet pipe number are varied according to the proposed ideas and related results are compared to each other.



**Figure 15.** Chosen grid for analysis (Mesh 4)

The grid (Mesh 4) that is used in the analysis is shown in Figure 15. Seven different levels of mesh refinements are utilized in this study. The results of temperature difference as a function of axial distance from the center on the bottom line of these various refinements are shown in Figure 16.

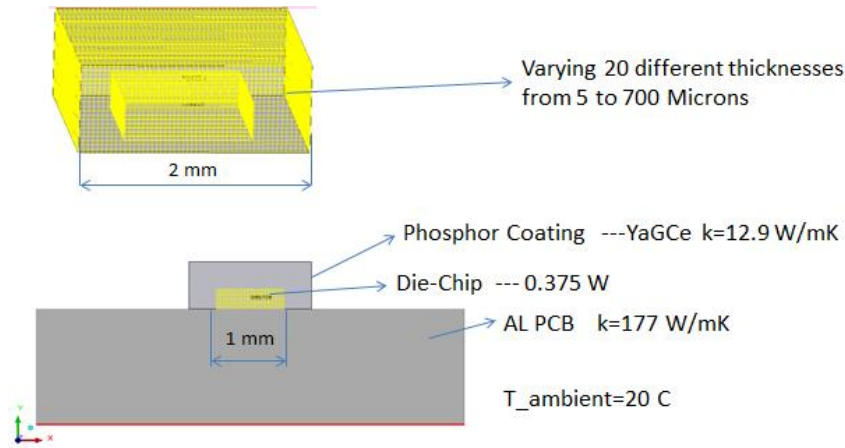


**Figure 16.** Grid refinements through 7 different meshes

The mesh resolutions are varied from coarser to finer grids with the total number of cells varying from 0.1 million to 1.8 million. Although a higher accuracy is expected in finer grids, the increased computational time is a limiting factor. To enhance the mesh quality, the grid refinement was utilized mainly on the sources, inside the dome, and also on the side part of the dome and the pipes. To be able to compare different grids accurately, temperature values have been obtained through 3 different lines as seen in Figure 16. The right half of the plot shows the temperature values on bottom line, on the left side the mid line values and also in the center (axial distance 0.025 m), the temperatures on the top of the dome are taken and compared according to the seven different grids. In Figure 16, it is clearly shown that most of the change happens over the bottom line, since over other lines there was not a significant temperature differences have been obtained. Mesh scheme 4 with a 1 million nodes is chosen as the grid for the CFD analysis.

#### **4.1.3 Energy Balance Tests**

Material and energy balances are other important criteria to check the accuracy of the mesh. Material quantities, as they pass through processing operations, can be described by material balances. Such balances are confirmation of the conservation of mass. Similarly, energy quantities can be described by energy balances. If there is no accumulation, what goes into a process must come out. This is true for batch operation. It is equally correct for continuous operation over any chosen time interval. Thus, in our study, energy balance for chosen phosphor material will be taken into account. Since the most important part is the chip and the phosphor slurry, the geometry has been simplified as seen in Figure 17. Different phosphor slurries have been added over the chip material and the energy balances have been investigated.

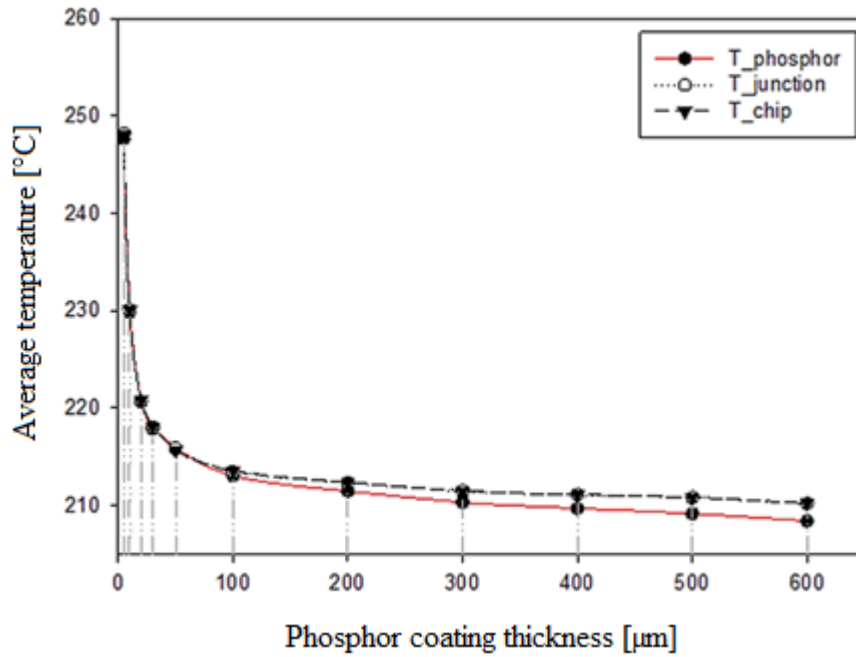


**Figure 17.** Geometry and compared boundary conditions

While the chip input power has been kept to 0.375 W, only the phosphor layer thicknesses have been changed from 5-700  $\mu\text{m}$ . The results are shown in Table 2. According to the observed data presented in Table 2, the fitting comparison for temperature values on junction, chip and phosphor can be seen in Figure 18.

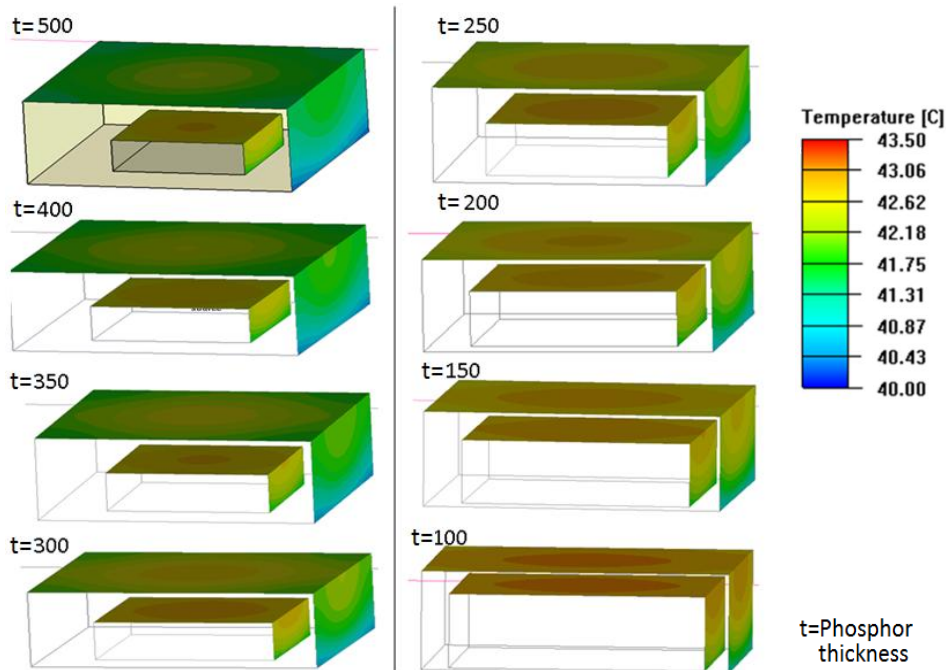
**Table 2.** Temperature values obtained from CFD for different phosphor thicknesses

Thickness ( $\mu\text{m}$ )	Average Temperature ( $^{\circ}\text{C}$ )			$Q_{\text{Phosphor}}$ (W)			
	$t_{\text{Phosphor}}$	$T_{\text{Phosphor}}$	$T_{\text{Junction}}$	$T_{\text{Chip}}$	All	Sides	Top
5		247.7	248.2	248.0	0.358625	0.358621	3.90E-06
10		229.9	230.1	230.1	0.365369	0.365366	3.20E-06
20		220.6	220.7	220.8	0.368868	0.368869	8.06E-07
30		217.9	218.0	218.1	0.369815	0.369818	2.31E-06
50		215.9	215.9	215.7	0.370409	0.370285	1.23E-04
100		213.0	213.5	213.5	0.370663	0.367976	2.69E-03
200		211.5	212.4	212.4	0.369718	0.352183	1.75E-02
300		210.3	211.5	211.5	0.368231	0.335542	3.27E-02
400		209.7	211.1	211.1	0.366305	0.322396	4.39E-02
500		209.2	210.8	210.8	0.363915	0.311825	5.21E-02
600		208.4	210.2	210.2	0.361081	0.303929	5.72E-02

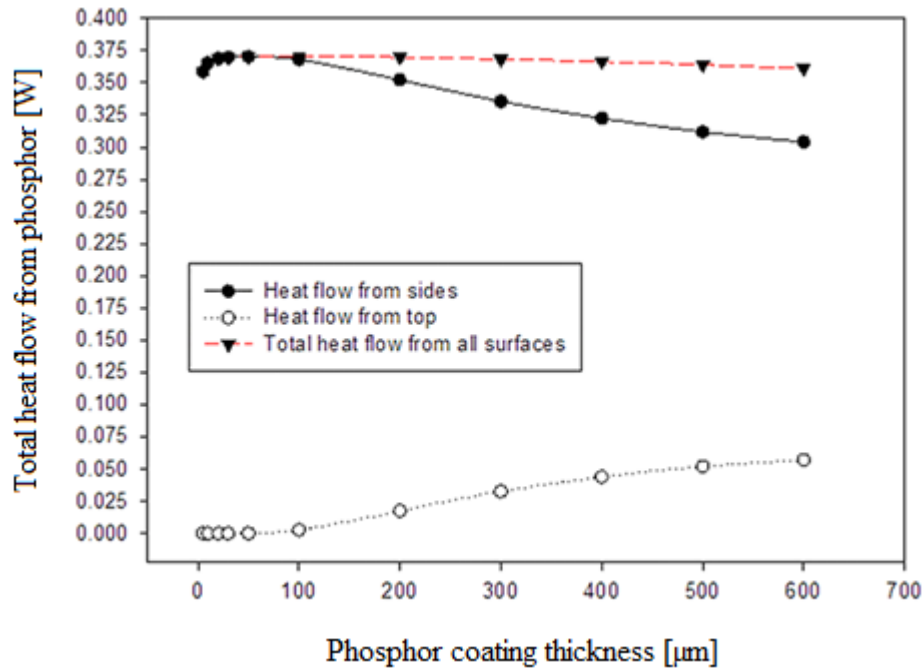


**Figure 18.** Average temperatures for different phosphor coating thicknesses

Moreover, the contour plots over the surfaces have been presented in Figure 19. It is clear that up to the thickness of 100 μm, temperature values are decreasing quite fast then the change by the increasing thickness is ignorable.



**Figure 19.** Contour plots for average temperatures for different phosphor coatings



**Figure 20.** Total heat flow through the phosphor layer

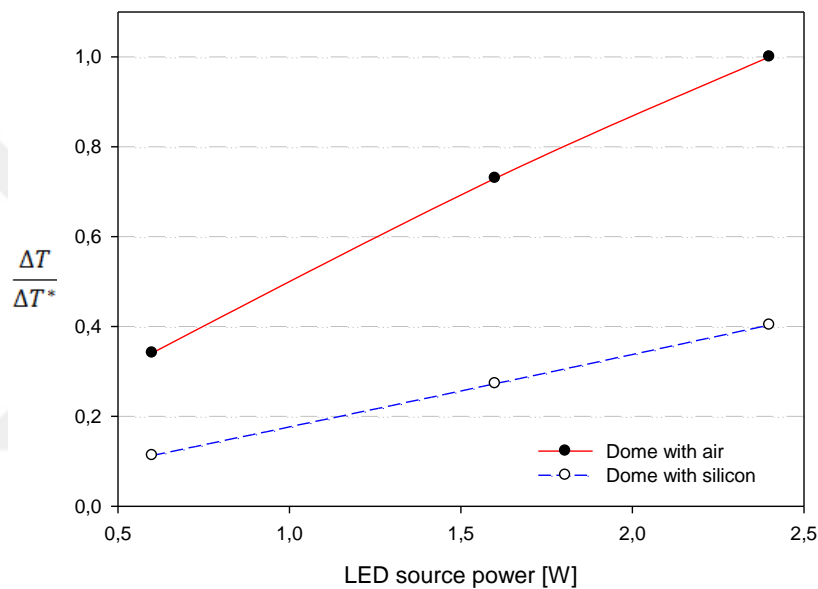
On the other hand, the amount of the heat is removed from the top and also the sides are important, thus we can establish an idea of different coating strategies. Hence, the heat flows from all surfaces and from the sides are compared and presented in Figure 20. It is clearly seen that the sum of the heat flows from sides and the top surfaces have given almost the same input power of 0.375 W. Thus, the achieved results both from mesh dependency and the energy balance tests have proved the suitability of the current computational model with the current mesh structure and enabled the overall study for making simulations for heat conduction and convection cases.

#### 4.2 Conduction Heat Transfer with Silicone

Typical LED systems utilize silicone for low optical losses. While silicone provides conduction heat transfer, convection may provide unique advantages. To compare various thermal performances, the thermal resistance ( $R$ ) is defined in Eq. 4 as follows:

$$R = \frac{T_{Maxchip} - T_{DomeTop}}{Q_{Sources}} \quad (4)$$

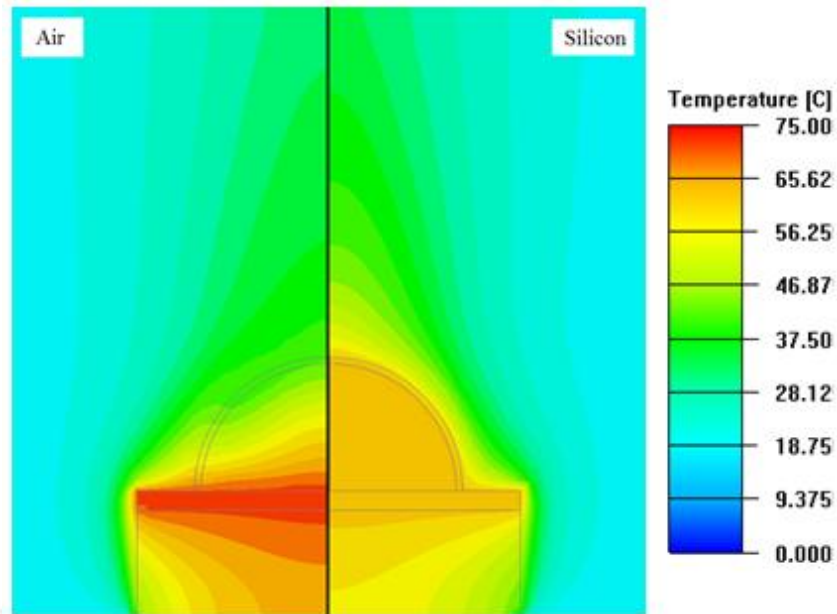
Cooling capability comparisons have been performed according to temperature gradient obtained for each system. Since the maximum thermal resistance value is obtained in case of air filled natural convection for 2.4 W, thermal resistances for other conditions are compared with air natural convection as the baseline condition.



**Figure 21.** Computational comparison of thermal capability for air and silicone

A closed system with air natural convection and a dome filled with a solid material (silicone) are compared in Figure 21. Silicone has shown a higher thermal performance between 20 % and 60 % for a range of driving conditions. Moreover, more homogenous temperature distribution is also achieved by silicone which is compared with air and presented in Figure 22. In comparison with air convection inside the dome, filling with silicone has shown a better thermal capability due to lower thermal conduction resistance with respect to natural convection from chip surfaces with air. However, the resulting high temperature in high brightness LED (HB LED) systems may cause vital problems.





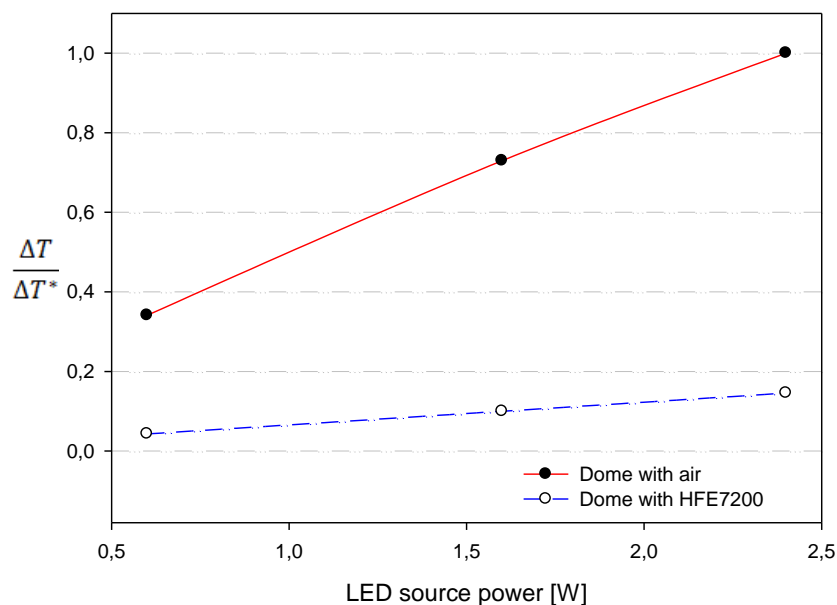
**Figure 22.** Temperature distributions for air (left) and silicone (right) filled domes

Since the coefficient of thermal expansions (CTE) are different for different materials inside the dome, temperature increase may cause CTE mismatch problem inside the dome which may result in delamination eventually air gaps in the contact surfaces. Thus, dielectric liquids will provide a better solution and avoid delamination problems. Therefore, direct liquid cooling cases also have been studied to evaluate and determine their exceptional thermal performance.

#### **4.3 Immersion Cooling of LEDs with Single Phase Natural Convection**

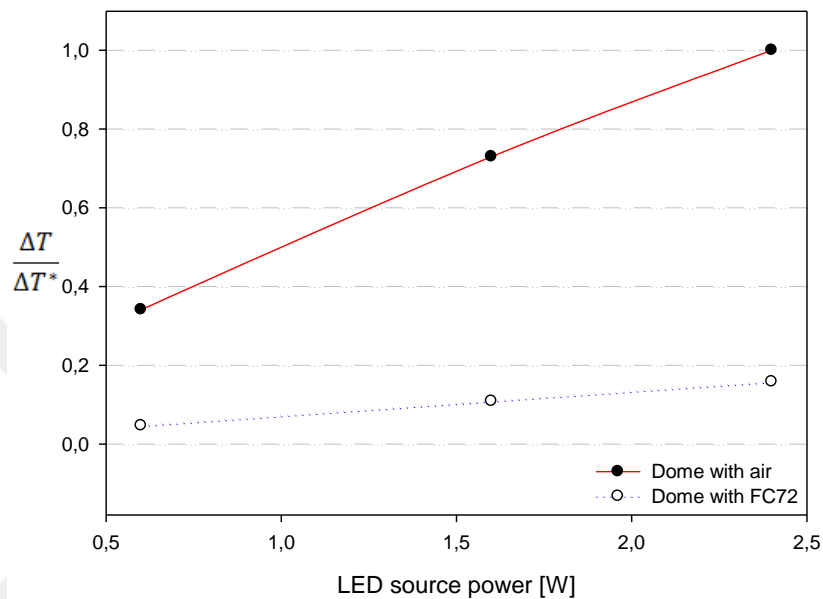
Liquid cooling requires the best contact possible between the metal and the liquid for most efficient heat transfer. Problems occur as the coolant approaches its boiling point, at which vapor bubbles start to form and decreases the cooling performance by behaving as blockage between the hot surface and liquid coolant. One of the main goals in assembling a useful cooling system is to ensure that the boiling point of the coolant is high in order to prevent damage due to local temperature rises. Water's boiling point is 100°C, which covers most of the electronics' working conditions. Moreover, water has

a particularly high specific heat capacity that makes it useful for storing and transporting heat. Thus, the computational convection cooling study for the same boundary conditions with water has provided an increase on heat transfer capability more than 80 % in comparison to air inside the dome. Besides, the wetting property of the liquid may have some influence also on the cooling mechanism. The less wetted the solid surface is, the higher are the chances that the air gases will be trapped in the cavities which will cause to increase the thermal resistances between two surfaces. On the other hand, water isn't suitable for electronics and can't be used as a coolant in immersion cooling, since it is electrically conductive, corrosive, and allows growth of bacteria. Although deionized water may overcome electrical issues, long life of LED systems may allow bacteria growth and lose DI characteristics overtime. Thus, per-fluorocarbons and Novec fluids such as LS5252, HFE7200, HFE7000, and FC72, etc. HFE7200 are of interest for thermal management of LEDs that are commonly studied in electronics cooling applications [69,70].



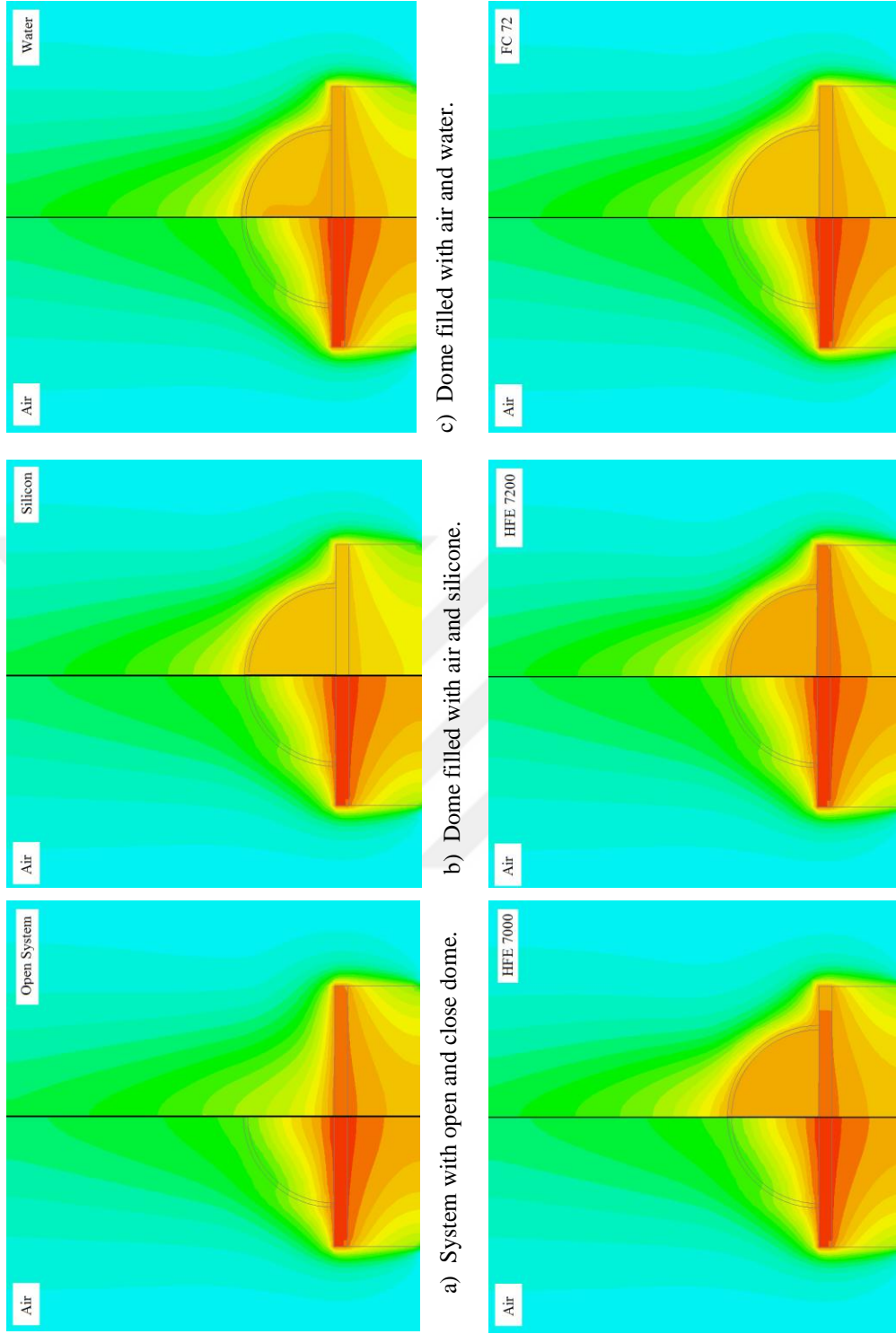
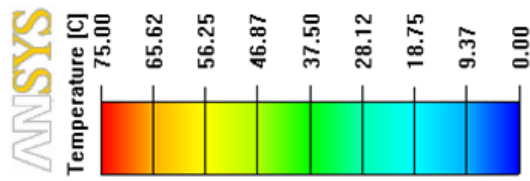
**Figure 23.** Computational comparison of thermal capability for air and HFE7200

Figure 23 shows the computational results with HFE7200. Although the thermal capability isn't as strong as water; under the condition of 1.6 W source power, the thermal enhancement over air convection cooling is found to be about a 60 % higher. FC72 was then evaluated as a coolant candidate.



**Figure 24.** Computational comparison of thermal capability for air and FC72

Although, other dielectric coolants have shown almost similar thermal performances within the range of  $\pm 10\%$ , their exceptional superiority over air convection cooling has clearly demonstrated. Under different chip power values, FC72 was simulated as a coolant inside the dome and the results are presented in Figure 24. It is clearly seen from the figure that the enhancement over air convection cooling is almost 50 %. Moreover, temperature distribution is also vital since the convection over the dome surface has also the highest part of thermal management. Distributing the temperature from chip surface to dome surface will increase the thermal performance of the total system. Thus, the resulted temperature distributions for different liquids in convection heat transfer inside the dome were compared in Figure 25.



**Figure 25.** Temperature contour plots for each liquids and also silicone in comparison to dome with air.

As it can be seen from Figure 25, heat transfer enhancement by dielectric liquids is much more than convection and conduction heat transfer due to better temperature distribution. Moreover, it is seen from the Figure 25, air has the lowest heat transfer. Thus, it leads researchers to focus on dielectric liquids.

Even though dielectric liquids have shown better cooling ability than air convection and silicone conduction, there are some performance differences among those liquids too. Thus, with a closer examination to the effects of physical properties, one may find fundamental reasons for the variation of heat transfer and perhaps determine an ideal candidate.

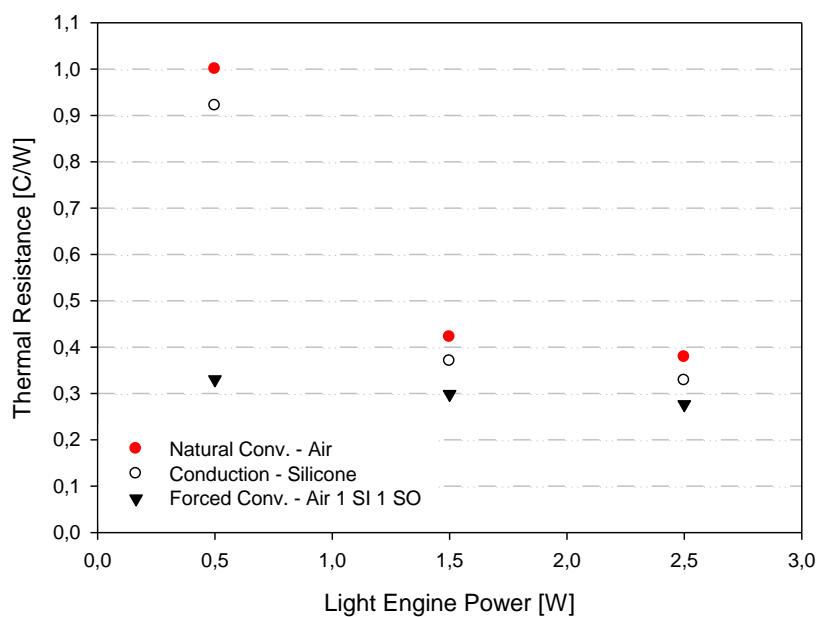
#### **4.4 Immersion Cooling of LEDs with Single Phase Forced Convection**

As noted already the performance including flux, forward voltage, color, reliability, and also the life of LED sources depend heavily on proper thermal management. This is a common characteristic for LEDs. While the temperature increases, several characteristics experience temporary and recoverable shifts such as decreasing light output, forward voltage and the color temperature shifts towards blue with the increase of temperature. Furthermore, absolute maximum rates, such as maximum temperatures must not be exceeded. Otherwise, one will observe irreversible damage on the product and cause permanent shifts in the performance. Any decrease on performance due to high temperature is not tolerable, since the primary goal is to extract maximum amount of lumens of a lighting device.

Thus, there are different methodologies in use for cooling purposes as explained in detail in chapter 2. Air still is the most preferred coolant due to its simplicity, low cost, easy maintenance and reliability. In many cooling scenarios, as electronics get smaller, heat transfer requirements increase; unfortunately air becomes inefficient at heat removal. It has low thermal capacitance with a large thermal resistance especially in

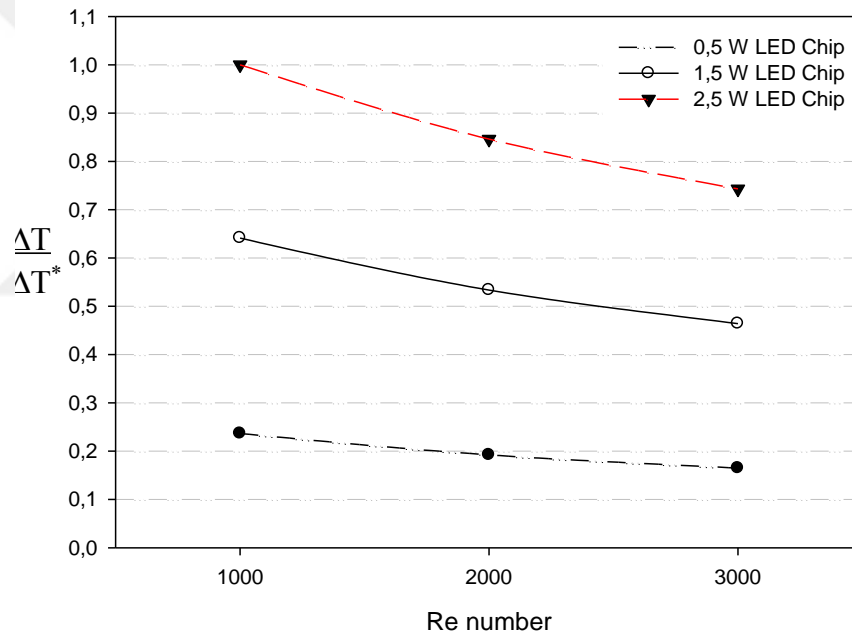
case of high current driven lighting technologies. As a cooling methodology, indirect liquid cooling mostly used with micro channels, which is disadvantageous for LED cooling due to unnecessary interfaces. Hence, direct liquid cooling strategy is chosen where the working fluid is directly in contact with the heat sources on the system.

In direct cooling, electronics are immersed into a dielectric liquid within a closed loop system. The electrical conductivity and optical properties (refractive index, transparency at the desired wavelength) are important criterion, since the fluid comes in direct contact with the light sources [3]. Furthermore, the selection of a dielectric coolant fluid for a particular application requires a proper match of characteristics and thermo-physical properties. Thus, some per-fluorocarbons (FC-72, HFE7100, and HFE7200 etc.) have already been used for cooling purposes of electronic components [40,65,69]. In this study, HFE 7200 as a dielectric coolant is compared with the performance of other coolants in terms of different designs and boundary conditions with thermal resistance.



**Figure 26.** Thermal resistances comparison for natural convection, forced convection and conduction heat transfer

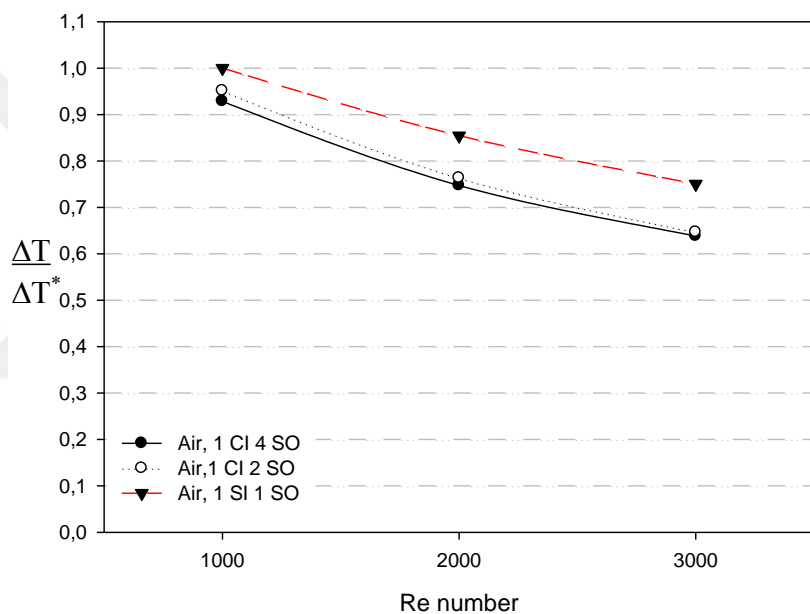
Accordingly, the thermal resistance comparison of different cooling techniques was presented in Figure 26. Since the maximum thermal resistance values are obtained in case of air filled natural convection case with a 0.5 W chip power, thermal resistances for other conduction and forced convection cooling cases are compared with air filled natural convection case with a 0.5 W chip power. For the conduction-only case, the dome is filled with pure silicone and the results are compared with those from convection when filled with air. Almost a 10 % decrease in the thermal resistance is seen in each chip for a range of driving conditions.



**Figure 27.** Variation of thermal rate as a function of  $Re$  number for different chip powers with 1SI-1SO

Thereafter, forced convection cases were tried. Different number of pipes was assigned as inlet and outlet that helps to push in or eject the liquid from the glass dome. Once two pipe were utilized from two edges, one is set as inlet while other as outlet. In case of 1SI (1 Side In) - 1SO (1 Side Out) forced convection with air, the thermal resistance is decreased almost 65 % for the 0.5 W chip power. Therefore, forced convection cases

provided better cooling capability even in terms of higher chip powers as compared to natural convection, as expected. The enhancement of forced convection over natural convection is clearly shown for different power levels and inlet velocities in Figure 26. According to the varying inlet velocities, force convection cases consist of pure air with 1SI-1SO have been studied for a range of  $Re$  numbers and a number of outlets as seen in Figure 27 and Figure 28. The heat transfer enhancement with the increase of the fluid flow per second has been observed.



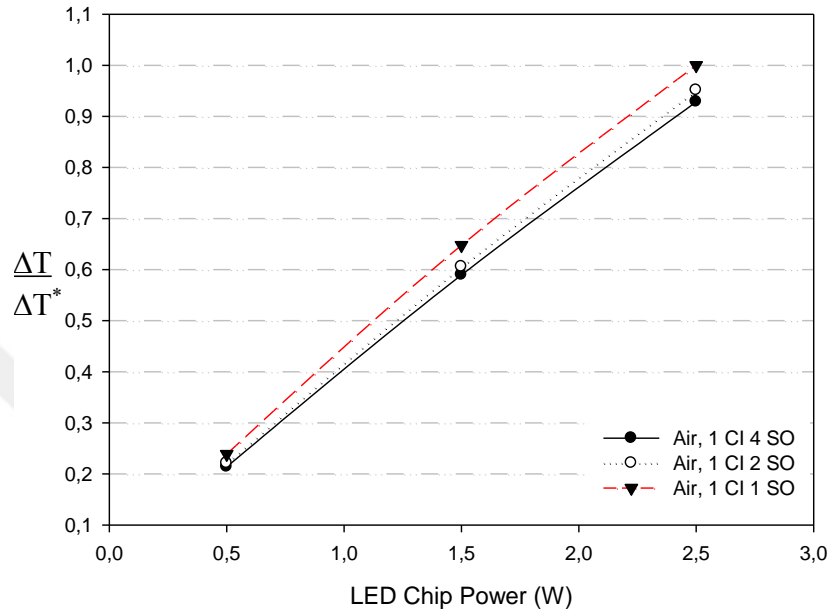
**Figure 28.** Variation of thermal rate as a function of  $Re$  number for varying number of outlets

Since, the maximum temperature in overall forced convection cases are obtained at  $Re$  number of 1000 and at 2.5 W light engine power, related thermal rate has been defined for an easy comparison. Thereafter, its thermal rate is set as 100 % and rest of all forced convection cases will be compared accordingly.

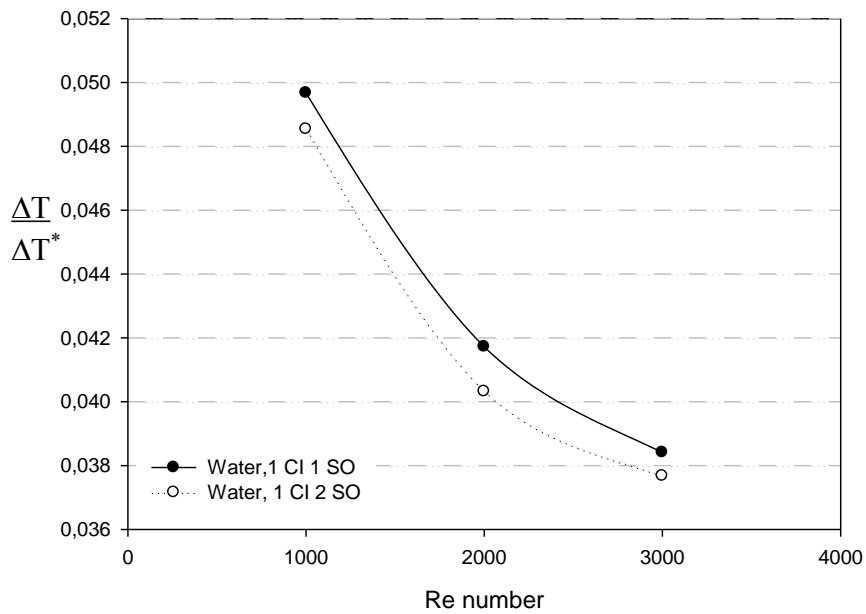
The comparison is made for different  $Re$  numbers at 2.5 W LED chips in Figure 28; where, the heat transfer enhancement with increasing number of outlets is presented as almost 8 %. In case of, 1CI (Center In) – 4SO (Side Out), the obtained data also shows



that the temperature is also decrease a bit more as compared to 1CI-2SO case. When the same geometries are compared under different chip powers but for Re number of 1000, similar trends are observed (see Figure 29).

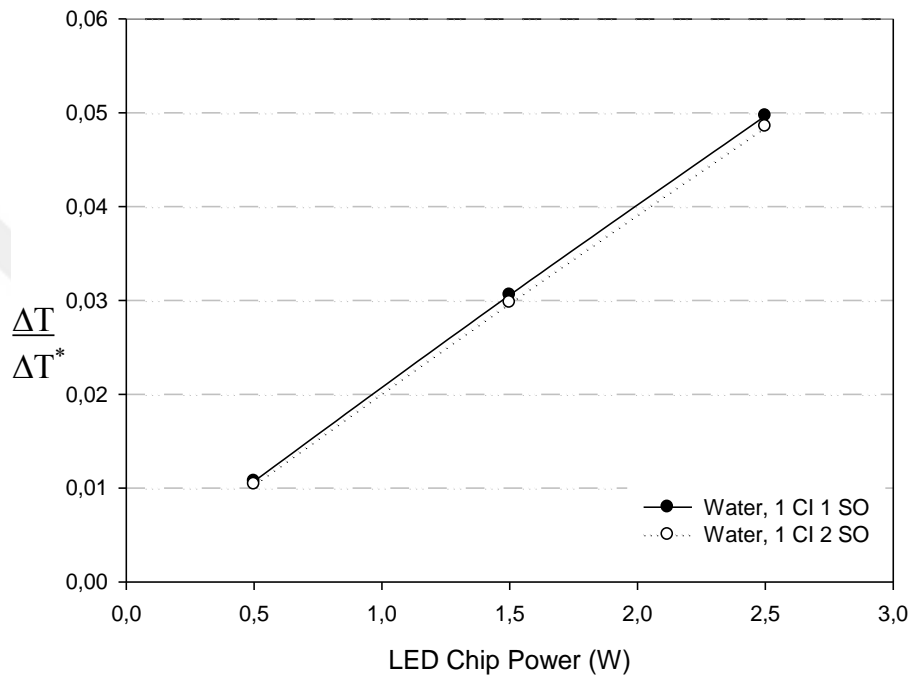


**Figure 29.** Variation of thermal rate with chip powers for air under forced convection



**Figure 30.** Variation of thermal rate with *Re* numbers for water under forced convection

While air is meeting some of the cooling challenges, when the flux is high, attention has to be turned to different liquids. Initially, water is used as the working fluid inside the dome. As seen in Figure 30 and Figure 31, the same boundary conditions are applied for forced convection with water as a coolant inside the dome.

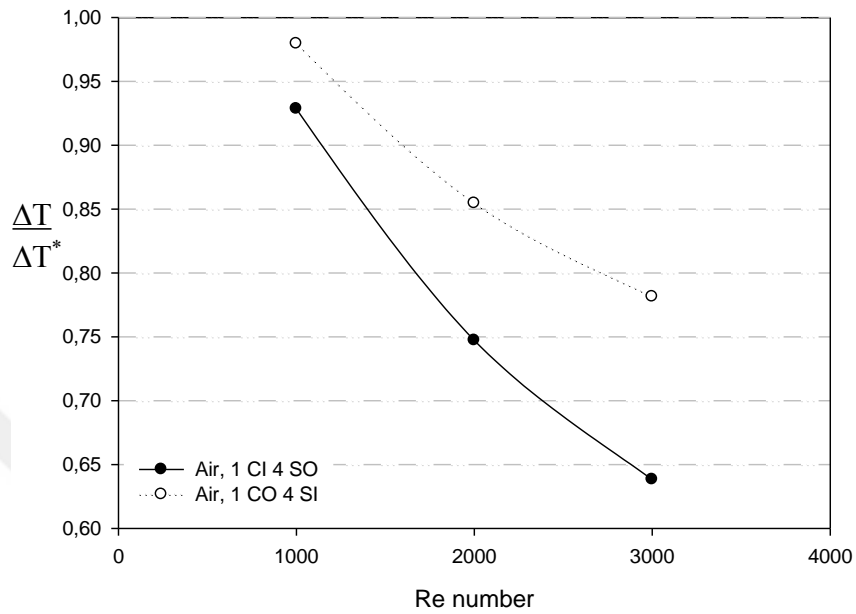


**Figure 31.** Variation of thermal rate with chip powers for water forced convection with new designs

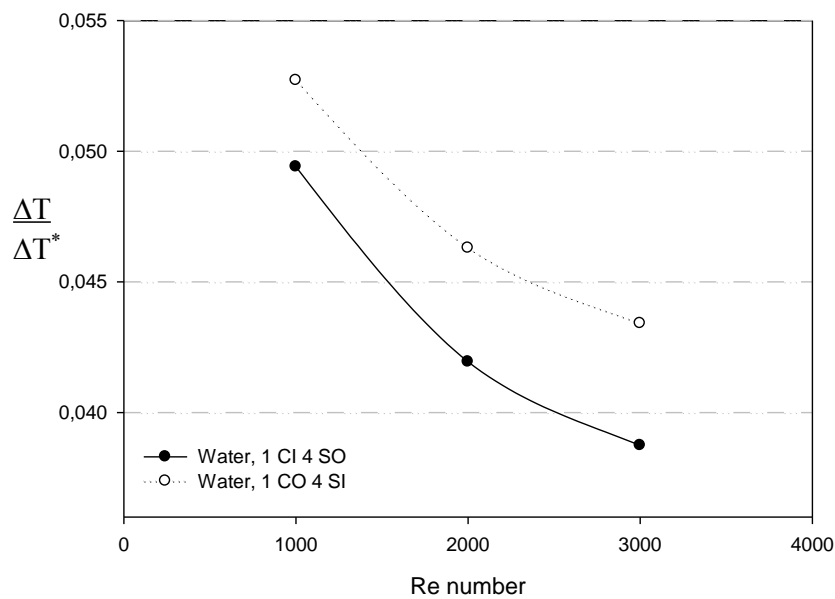
The figures present that the heat transfer enhancement with increasing number of outlets is not changing noticeably in contrast to forced convection air cases. An interesting finding is that in comparison to air 1SI-1SO case, with the application of water, almost a 95 % lower temperature value is observed. Thus, this can be also seen from Figure 31, where results are shown in terms of different chip powers.

Hence, the number of configuration has been studied and resulted heat transfer capabilities of new design approaches with switching the inlets and outlets between each other by changing the direction of the flow has been presented.

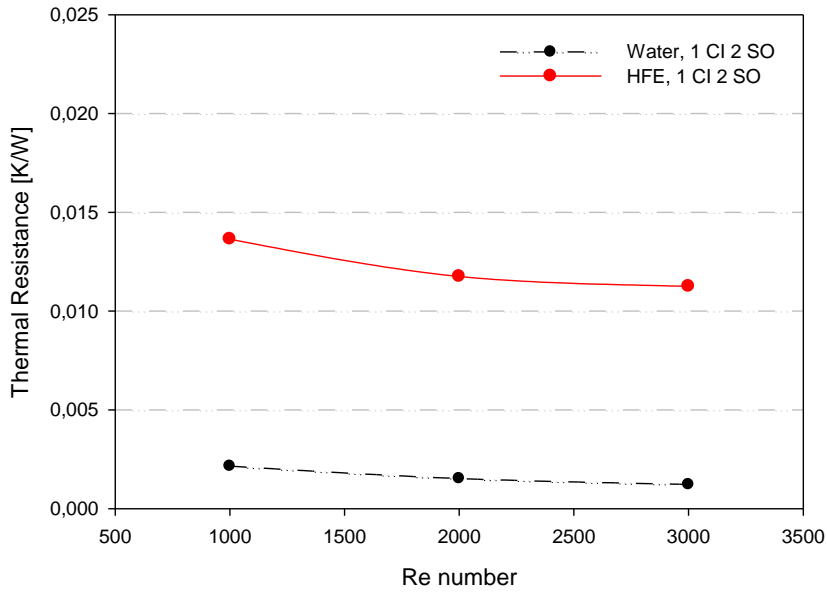
Finally, maximum heat transfer achieved geometry is (1CI-4SO) for air and water, and the results are shown in Figure 32 and Figure 33.



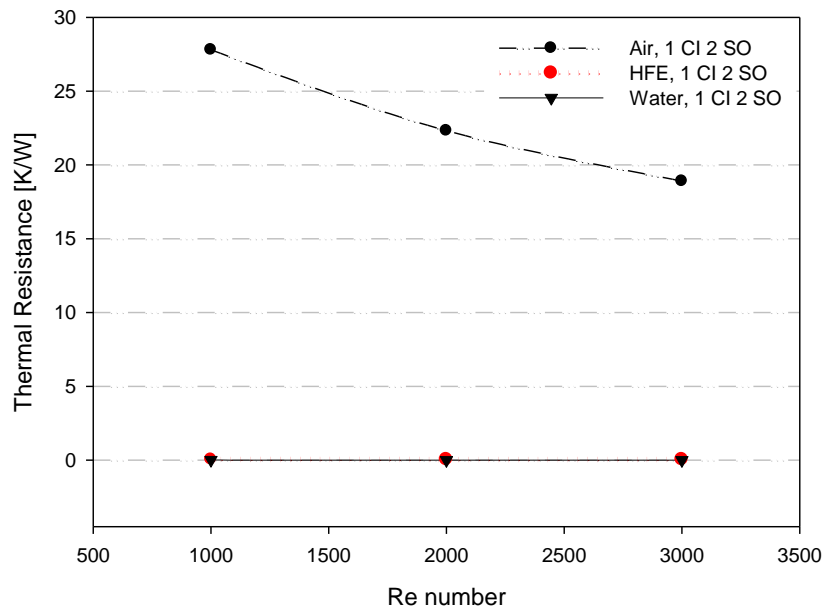
**Figure 32.** Variation of thermal rate comparisons for  $Re$  numbers with 1CI-4SO and 1CO-4SI designs with air under forced convection



**Figure 33.** Variation of thermal rate with  $Re$  numbers for new designs (1CI-4SO / 1CO-4SI) with water under forced convection



**Figure 34.** Variation of thermal resistance with  $Re$  numbers for water and HFE 7200

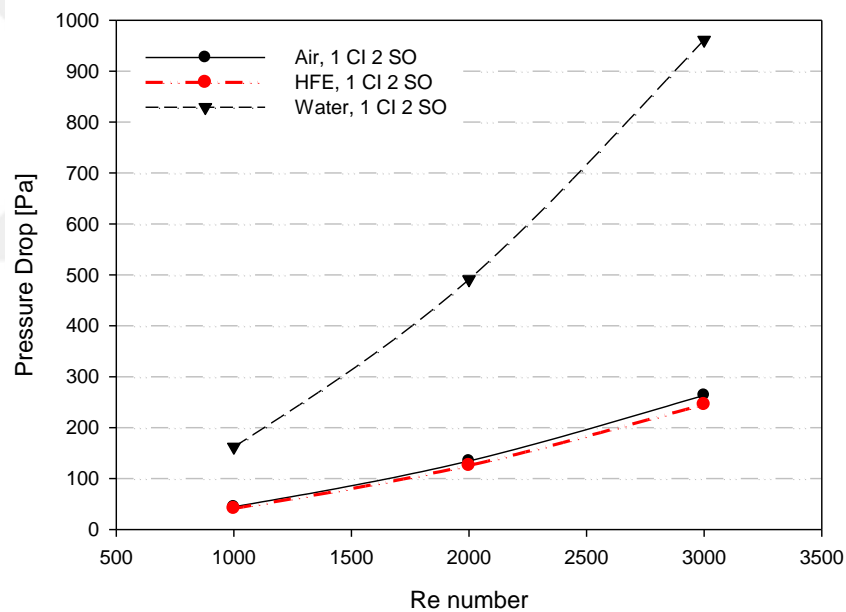


**Figure 35.** Variation of thermal resistance with  $Re$  numbers for air-water-HFE 7200

On the other hand, all of the forced convection cases that are used in this study are examples of direct liquid cooling. Due to better cooling capabilities of per-fluorocarbons (FC-72, HFE7200 etc.), here we also studied HFE7200 and compared with water [78]. As seen from Figure 34, there is a significant difference in terms of

thermal resistance between water and HFE7200. However, when the difference is compared to air as coolant, the significant difference between air and liquid cooled systems can be clearly seen in Figure 34; while, negligible levels of water and HFE7200 coolants results are presented in Figure 35.

Another important criterion needs to be taken into account is the pumping power required with the increasing number of outlet pipes; while increasing number of outlets served better heat transfer capability. Therefore, to be able to obtain the same thermal performance with the same mass flow rates, more pumping power is required in case of higher number of pipes.



**Figure 36.** Variation of pressure drops with  $Re$  numbers for Air-Water-HFE 7200

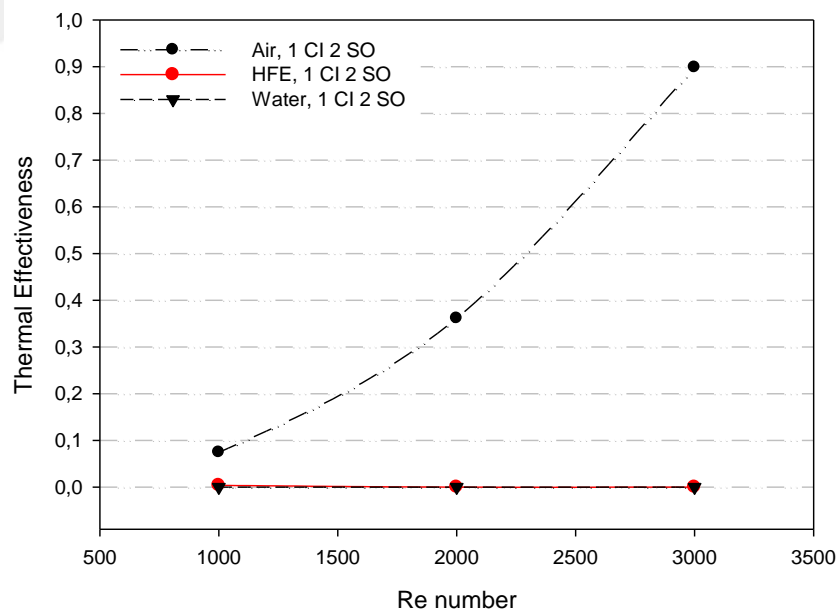
It also has an increasing trend with higher  $Re$  numbers. Both computational findings for air and HFE 7200 present almost the same values, which have the lowest losses in comparison to water case.

However, better heat removal capabilities of those systems, which are resulted in higher-pressure drops, are already shown in Figure 36 and Figure 37. Therefore, both

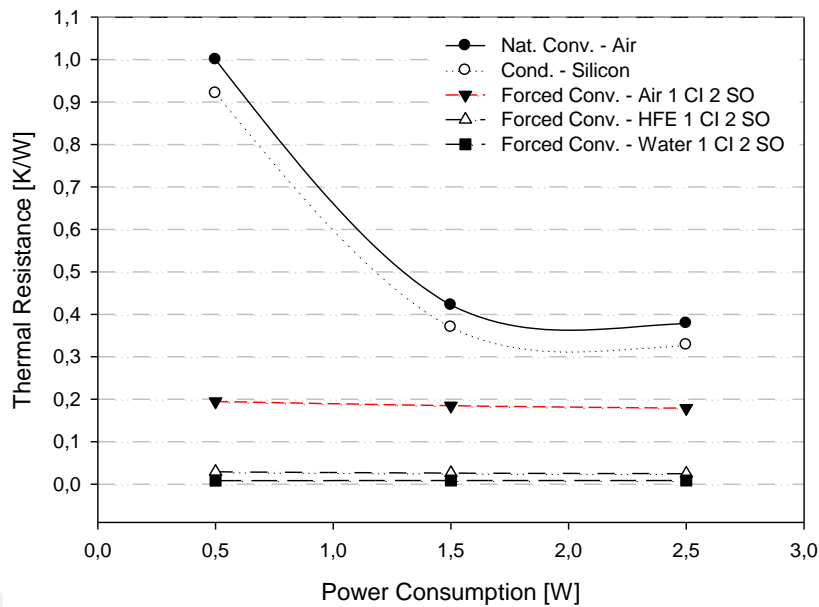
thermal enhancement and pumping powers should be evaluated together to find out the total thermal effectiveness of a system. Thus, we define a term, where the effect of both can be seen in Eq. 5.

$$Thermal\ Effectiveness = (\Delta P * \dot{V}) * \Delta T \quad (5)$$

Since air has lower pressure losses in the pipes when the comparison is coupled with the heat removal capability, Figure 37 shows temperature rise over ambient times pumping power. Due to high temperature rises over ambient and high pressure losses with increasing inlet velocities in case of air has been confirmed as the lowest capable coolant compared to water and HFE 7200 in forced convection cooling systems, which are shown lower temperature values over the chips.



**Figure 37.** Thermal effectiveness for Air-Water-HFE 7200 with increasing  $Re$  numbers

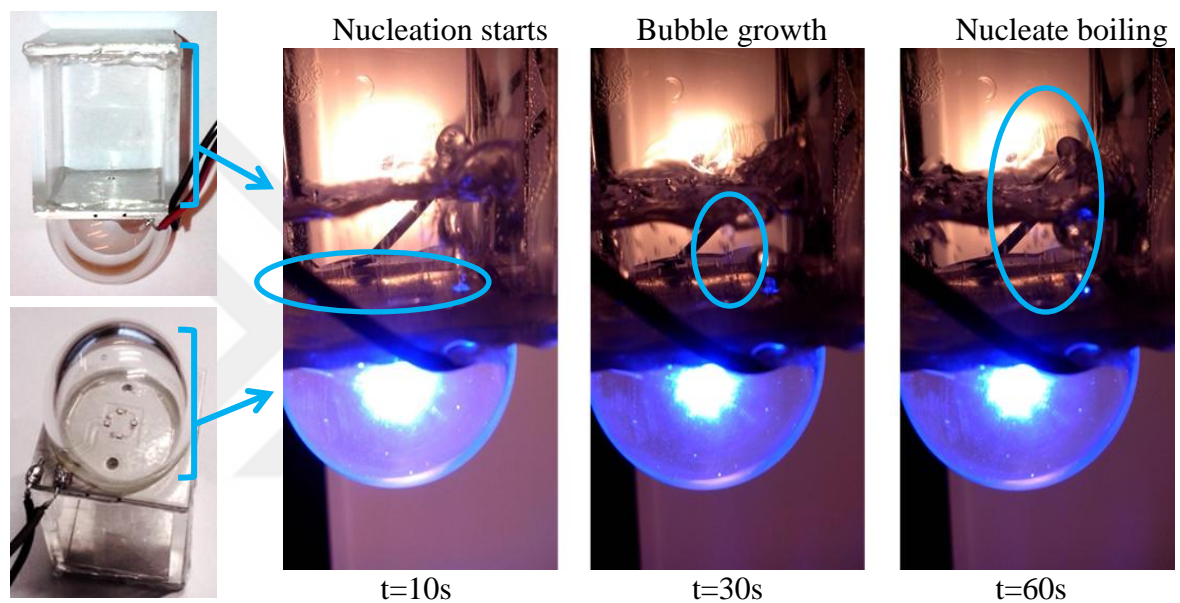


**Figure 38.** Comparison of thermal resistances for natural convection, forced convection and conduction

For a comparison purpose, the reference value of maximum temperature is set to a value that is obtained from natural convection case with 0.5 W chip power and a dome filled with air. After that, thermal resistances were compared according to a reference value. In the conduction case, 10 % less temperature values were observed, while, air forced convection has shown almost 80 % lower thermal resistance values (see Figure 38). On the other hand, liquid cooled forced convection cases with water and HFE 7200 has shown the highest thermal performances but pressure losses should be taken into account. After, a special evaluation process, HFE 7200 has shown suitable results for the current study, in terms of thermal enhancement capability with reasonable pumping power values. Beside of the extra pumping power requirements, the life time of this pumping system will also affect the overall life time of the lighting system. Thus, it still does not fully cover the required cooling capability under reasonable working conditions for longer time periods.

#### 4.5 Immersion Cooling of LEDs with Boiling Heat Transfer

After, evaluating the forced convection heat transfer mechanism for lighting systems, phase change heat transfer was in consideration due to the drawbacks have been mentioned in the previous section. Phase change heat transfer is very powerful method due to latent heat effect of the working fluids and provides several orders of magnitude higher performance than single phase heat transfer. A number of studies have already been published for immersion cooling of electronics [40,65,69].

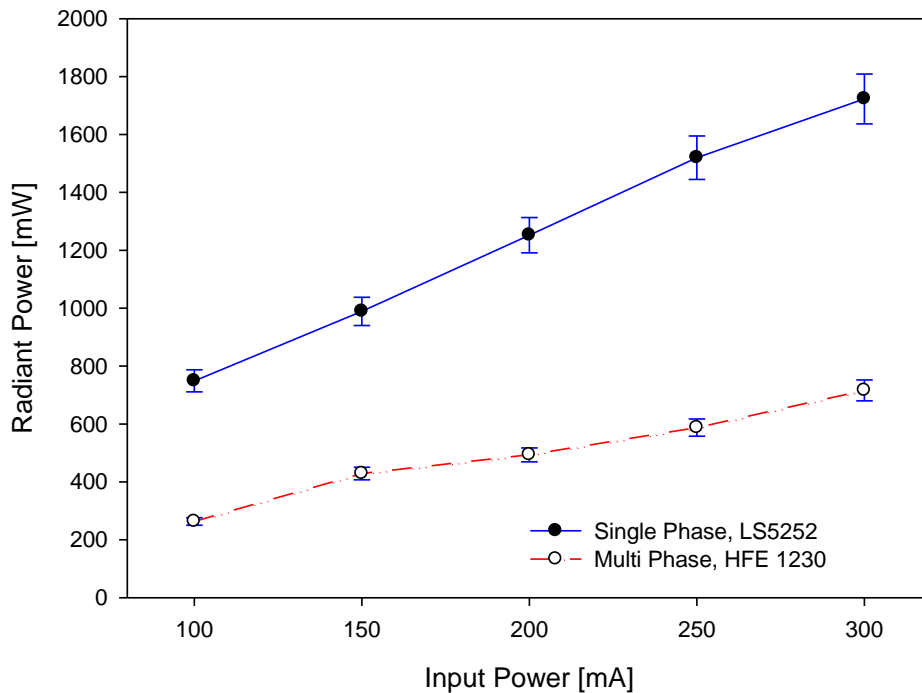


**Figure 39.** Optical degradation with boiling

Boiling heat transfer can also provide unique solutions for LED local hot spot problems. However, in order to benefit from thermal superiority of multi-phase cooling in LEDs, the evaluation of the impact on light extraction is more crucial than the thermal performance enhancement of multi-phase convection since bubbles occur on the light path while functioning as seen in Figure 39. Thus, a set of optical experiments was performed first to evaluate the impact on light extraction before computational thermal performance analysis, and also added to the computational analysis part of the current thesis to complete the overall picture. In the experimental study, LS5252, HFE 1230 and also silicone oil are used simultaneously as single and multi-phase cooling.



Although a higher heat transfer performance is expected in multi-phase convection, the negative impact of boiling on light extraction due to bubbles over the light path is clearly shown in Figure 40. As a result, single phase liquid cooling has shown better optical light extraction with a reasonable thermal performance in comparison to boiling.

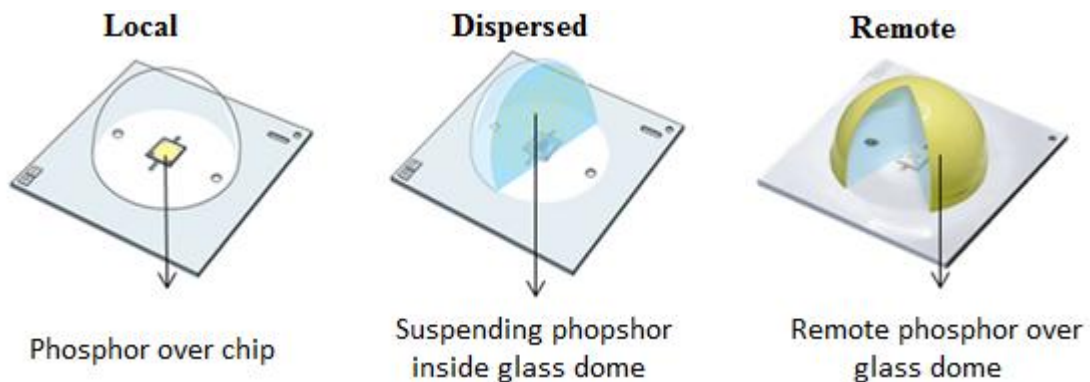


**Figure 40.** Effect of boiling over radiant power

#### 4.6 Immersion Cooling of Suspended and Coated Nano-Phosphor LEDs

LED systems are primarily limited in terms of their efficacy due to optical, electrical and thermal losses. There are a considerable amount of optical losses in a typical LED system. Although they have been mentioned in a number of publications partially, there is no published study presents the total optical-loss scheme in SSL systems. Therefore, there is a need for a research that can grasp all of the optical losses in the LED systems. However, the resultant inefficiency in the phosphor manifests itself in terms of heat generation and can further reduce the phosphor efficiency as suggested by Arik et al [27]. All these factors in an LED optical package design can be quite challenging and

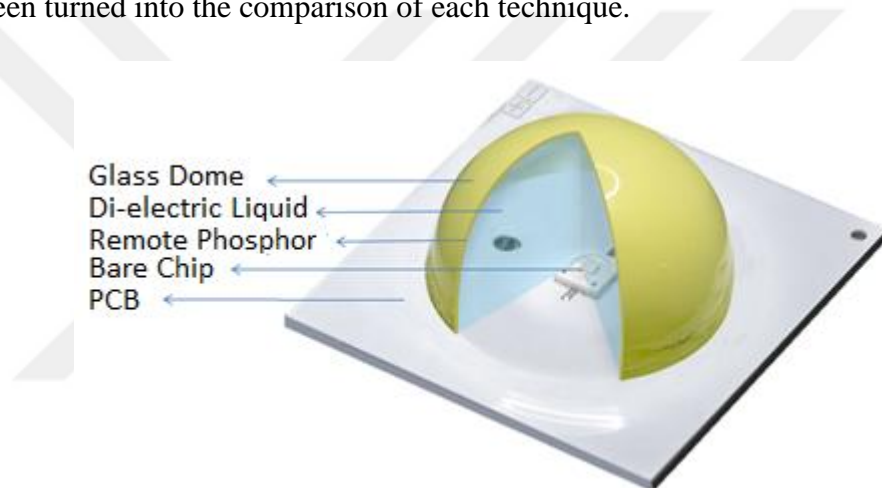
must be coupled with all the other factors including thermal design and reliability. Even though optical design may reach an optimum value, local hot spots cannot be avoided and temperature non-uniformities can only be addressed by topside immersion cooling. The inclusion of phosphor into an HB LED package is a complex task. In a typical 450 or 470 nm blue LED, YAG phosphor is introduced and combined with the blue emission to create what appears to the eye as white light. There are several factors that must be considered when adding the phosphor, such as particle size, concentration, geometry and carrier medium. The common practice for phosphor carrier medium is the use of typically a high index of refraction silicone but the geometry of the phosphor is a primary design variable and can be classified as local, dispersed, and remote (see Figure 41). In each case, the geometry greatly affects the ultimate optical output of the LED color qualities and conversion efficiency. Since there is limited information about individual losses in an LED system and there is no available correlation to predict the total losses, the proposed research is about developing a theory for this fundamental problem. In addition, after identifying the losses, LED topside liquid cooling will tackle a major challenge “hot phosphor losses”, that provides unique information for both fundamental nano-fluid (phosphor based) single phase heat transfer and improved efficacy.



**Figure 41.** Application approaches for phosphor in high brightness LED packages

Thus, the introduction of immersion liquid cooling with optically-transparent liquids integrated with different coating ideas is the main focus of this part of the thesis. It is aimed to reduce average chip temperatures and to improve the uniformity of chip and phosphor temperature, which leads to higher light extraction efficiencies.

To capture the local temperature distributions over the LED light engine while phosphor is at different positions, numerical models have been built with commercial computational fluid dynamics (CFD) software. Moreover, these coating techniques have been integrated with immersion cooled natural convection individually. Later, attention has been turned into the comparison of each technique.

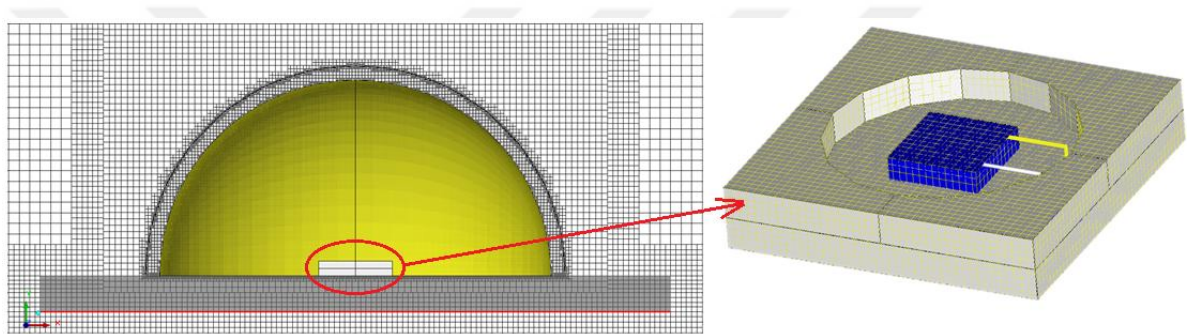


**Figure 42.** Schematic of CFD domain for the light engine with remote phosphor under dome

As already described in Chapter 3, the computational domain for a single-chip LED light engine has been built in Ansys-Icepak [68]. The light engine with remote phosphor dome is presented in Figure 42 as domain of one of the proposed coating ideas. It consists of several components; a printed circuit board (PCB), a solid glass dome and an LED package. LED ( $1 \text{ mm}^2$ ) chip is placed inside the ceramic enclosure including the wire bondings from two corner of the chip to enclosure path to complete the circuit, all of which is placed on a square ( $3 \times 3 \text{ cm}^2$ ) a metal core PCB (printed circuit board) with 1.6 mm thick. LED chip is then covered with a hemispherical dome

with a 2 cm outer diameter and 1 cm height. For the same study, three different phosphor positions have been applied as shown in Figure 41. Chip on board (COB) packaging approach is implemented in the current study. Similarly, the chosen grid structure according to the mesh independency test is given in Figure 43.

A number of comparisons have been made for a range of coating positions and input powers. While the silicone-phosphor mixture has been utilized over bare LED chip for local coating case, the mixture has been applied at the inner surface of the glass dome placed on PCB for remote phosphor case.



**Figure 43.** Chosen grid for analysis (Mesh 1)

For the third case shown as dispersed in Figure 41, phosphor particles have been dispersed inside the glass dome as a suspending inside the dielectric liquid coolant. Moreover, varying driving current values which are 150, 300 and 450 mA were set respectively to be able to compare the different cases. The external surfaces of the dome are kept at the room temperature (25°C) and radiation from external surfaces is accounted for the computational models.

On the other hand, the quality of the mesh is a crucial parameter to obtain reliable results in a CFD analysis. Hence, applying different levels of refinement is carried out for a series of cases to evaluate the impact of grid dependence on the results. As hexahedral elements are mainly chosen for meshing strategy, structured mesh elements

are also utilized in order to reduce the instability behaviors in the flow due to the aspect ratio issues. The mesh resolutions are varied from coarse to fine grids with a special interest on computational time. Moreover, the grid refinement was utilized mainly on the source and dome to enhance the mesh quality.

The boundary conditions for the current isothermal study are set under the consideration of fixed temperature 25°C, and according to the expected operating parameters for the experimental activities for which all experimental input value including radiant power are listed in Table 3 below. As described previously, first bare chip cases were applied. The input power for LED chip has been defined according to the experimental findings. Since the thermal simulation software, Icepack, is not able to solve optical extraction, the total input power to the LED chip has been assigned as the difference between the electrical input power and optical radiant power extraction obtained from experimental study. Then, the bare LED chip has been coated with silicone for remote and suspending phosphor cases. Thereafter, the chip on board system has been covered with a glass dome in which dielectric liquid has been filled.

One case has been designed according to the remote phosphor under the glass dome, while second system has phosphor particles suspending inside the glass dome. According to the new system the difference between the electrical input power and radiant power (light extraction) has been changed. The power difference between two systems has been assigned as an extra heat generating power in phosphor layers or particles. While the light conversion efficiency in bare LED chip has been assumed as constant, the rest of the difference has been assigned as an extra heat generation in phosphor layer or particles. The detailed parameters and boundary conditions are listed in Table 3.

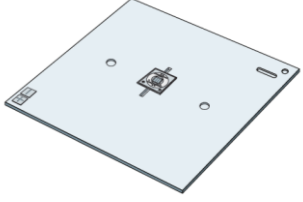
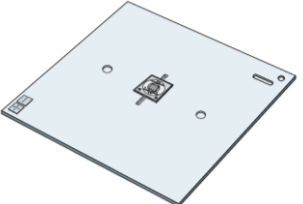
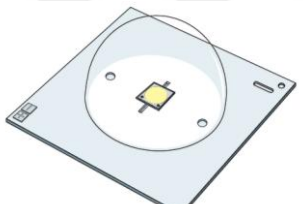
**Table 3.** Operating parameters and boundary conditions

Measured Power Quantity				Calculated Power Quantity	
$I_F$ (mA)	$V_F$ (V)	Electrical (W)	Radiant (W)	Chip (W)	Phosphor (W)
<b>Bare Chip</b>					
450	2,4265	1,44	0,493	0,947	-
300	2,4501	0,92	0,363	0,557	-
150	2,4700	0,44	0,201	0,239	-
<b>Phosphor Coating over Chip</b>					
450	2,4152	1,44	0,164	0,944	0,332
300	2,4310	0,92	0,125	0,554	0,241
150	2,4559	0,44	0,072	0,238	0,130
<b>Phosphor Coated Chip + Glass Dome + Air</b>					
450	2,4098	1,45	0,167	0,944	0,339
300	2,4317	0,92	0,125	0,554	0,241
150	2,4563	0,44	0,070	0,238	0,132
<b>Phosphor Coated Chip + Glass Dome + Dielectric Liquid</b>					
450	2,4097	1,43	0,184	0,944	0,292
300	2,4330	0,91	0,139	0,554	0,217
150	2,4541	0,43	0,079	0,238	0,113
<b>Silicone Coating over Chip</b>					
450	2,4242	1,45	0,493	0,957	-
300	2,4486	0,93	0,363	0,567	-
150	2,4696	0,44	0,201	0,239	-
<b>Silicone Coated Chip + Glass Dome + Air</b>					
450	2,4174	1,46	0,454	1,006	-
300	2,4390	0,93	0,333	0,597	-
150	2,4566	0,44	0,181	0,259	-
<b>Silicone Coated Chip + Glass Dome + Dielectric Liquid with Suspended Phosphor</b>					
450	2,4094	1,43	0,155	1,006	0,269
300	2,4330	0,92	0,110	0,597	0,213
150	2,4541	0,43	0,061	0,259	0,110
<b>Silicone Coated Chip + Remote Phosphor under Glass Dome + Air</b>					
450	2,4196	1,45	0,201	0,957	0,292
300	2,4476	0,93	0,148	0,567	0,215
150	2,4693	0,44	0,080	0,239	0,121
<b>Silicone Coated Chip + Remote Phosphor under Glass Dome + Dielectric Liquid</b>					
450	2,4259	1,44	0,254	0,957	0,229
300	2,4524	0,92	0,189	0,567	0,164
150	2,4731	0,44	0,104	0,239	0,097

Then, cooling capability comparisons have been performed according to temperature gradient obtained for each coating method. Since the phosphor temperature is affecting the conversion efficiency of phosphor, its temperature is expected to decrease by changing the coating position under the special interest of light extraction. First, a bare chip study has been simulated. There, the power input values in simulation were given from the experimental findings obtained at junction temperature and radiant power measurements. The net heat generation inside the package has been assigned as the difference between the total power applied to the package and the radiant power emitted as light out of the package. The extracted portion of total power was called undesired heat generation inside the LED chip due to lower conversion efficiency. After the coating, excited photons will pass through the phosphor particles where the 465 nm blue light is being converted to white light. While the phosphor is only capable of converting some portion of blue light to white light, rest of the radiant power remains inside the phosphor as well.

Thus, in case of phosphor coated packages, measured heat generation is also added to phosphor layers. Boundary conditions for a range of input powers and corresponding CFD results have also been presented in Table 4. The junction temperatures after coating both with silicone and phosphor individually, have increased. Moreover, the phosphor coated package (C) has shown the highest junction temperature in Table 4, while the phosphor layer has shown slightly higher temperature than LED junction due to the extra heat generation because of lower phosphor conversion efficiency. Table 5 shows the immersion cooling technologies with dielectric liquid filled glass dome including suspending phosphor, phosphor over chip and remote phosphor. It is clearly seen that moving away the phosphor layer from the LED chip decreases the junction temperatures.

**Table 4.** Computational junction temperature results for corresponding technologies


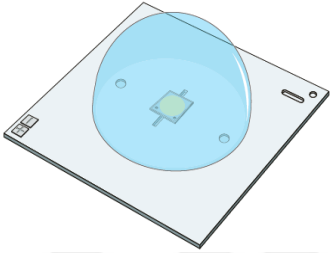
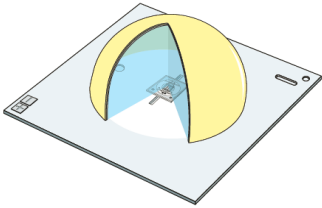
Boundary Conditions			Test Vehicle	CFD Temperature Results		
<b>I (mA)</b>	<b>Chip Power (W)</b>	<b>Phosphor Power (W)</b>	 Bare Chip	$T_{Base}$ (°C)	$T_{Junction}$ (°C)	$T_{Phosphor}$ (°C)
450	0.947	N/A		40	57,95	N/A
300	0.557	N/A		40	50,57	N/A
150	0.239	N/A		40	44,53	N/A
(A)						
<b>I (mA)</b>	<b>Chip Power (W)</b>	<b>Phosphor Power (W)</b>	 Silicone Coated Chip	$T_{Base}$ (°C)	$T_{Junction}$ (°C)	$T_{Phosphor}$ (°C)
450	0.957	N/A		40	58,01	N/A
300	0.567	N/A		40	50,61	N/A
150	0.239	N/A		40	44,47	N/A
(B)						
<b>I (mA)</b>	<b>Chip Power (W)</b>	<b>Phosphor Power (W)</b>	 Phosphor over Chip	$T_{Base}$ (°C)	$T_{Junction}$ (°C)	$T_{Phosphor}$ (°C)
450	0,944	0,332		40	60,05	60,08
300	0,554	0,241		40	52,45	52,48
150	0,238	0,130		40	45,71	45,74
(C)						

Moreover, the deported phosphor layer has resulted a lower temperature in comparison to direct coating over the chip. While remote phosphor coating under the glass dome with dielectric coolant has shown the lowest junction temperature, suspending phosphor case has shown slightly higher temperature as seen in Table 5.

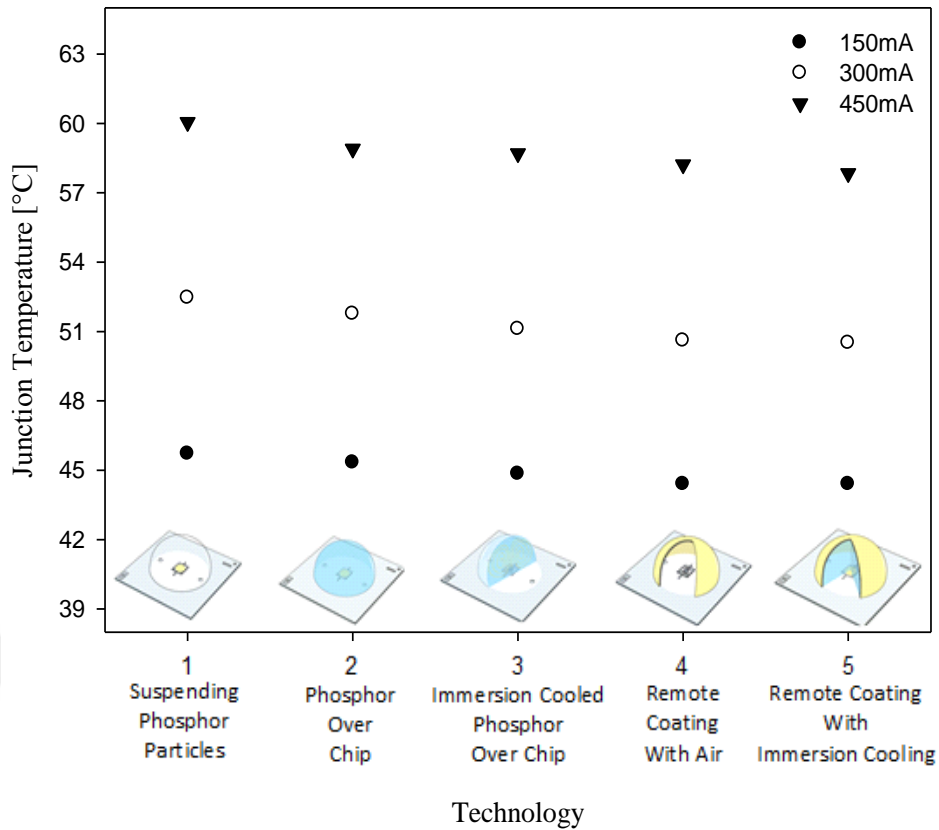
Even though immersion liquids have shown better cooling ability than air convection and silicone conduction, there are some performance differences among those coating technologies too as clearly seen in Figure 44. While, phosphor over chip coating with pure air convection, technology 1, has shown the highest junction temperature, dielectric liquid filling inside the dome still did not decrease the junction temperature as shown as technology 2 in Figure 44.



**Table 5.** Computational junction temperature results for corresponding technologies

Boundary Conditions			Test Vehicle	CFD Temperature Results		
<b>I (mA)</b>	<b>Chip Power (W)</b>	<b>Phosphor Power (W)</b>	 <p>Suspended phosphor inside the glass dome with dielectric coolant</p>	<b>T<sub>Base</sub> (°C)</b>	<b>T<sub>Junction</sub> (°C)</b>	<b>T<sub>Phosphor</sub> (°C)</b>
450	0.947	N/A		40	58,70	N/A
300	0.557	N/A		40	51,10	N/A
150	0.239	N/A		40	44,84	N/A
(D)						
<b>I (mA)</b>	<b>Chip Power (W)</b>	<b>Phosphor Power (W)</b>	 <p>Immersion cooled phosphor over chip</p>	<b>T<sub>Base</sub> (°C)</b>	<b>T<sub>Junction</sub> (°C)</b>	<b>T<sub>Phosphor</sub> (°C)</b>
450	0.947	N/A		40	58,90	58,95
300	0.557	N/A		40	51,76	51,78
150	0.239	N/A		40	45,33	45,36
(E)						
<b>I (mA)</b>	<b>Chip Power (W)</b>	<b>Phosphor Power (W)</b>	 <p>Remote phosphor coated glass dome with dielectric coolant</p>	<b>T<sub>Base</sub> (°C)</b>	<b>T<sub>Junction</sub> (°C)</b>	<b>T<sub>Phosphor</sub> (°C)</b>
450	0.947	N/A		40	57,84	N/A
300	0.557	N/A		40	50,50	N/A
150	0.239	N/A		40	44,40	N/A
(F)						

On the other hand, technology 3, which is dispersed phosphor particles inside the dome, did not perform as expected. Technology 4, stands for the remote phosphor coating with air convection inside the dome, also experienced higher junction temperature in comparison to the technology 5, which is remote phosphor coating with immersion liquid cooling. Thus, the best thermal performance has been observed with remote coated immersion liquid cooled system that is presented as technology 5.



**Figure 44.** Computational comparison of thermal capability for air and silicone

As an overall summary for computational studies, thermal behaviors of high power LED light engines using different cooling techniques with different coolants and coatings have been tested computationally. First of all, air natural convection has been studied and the results are validated with an experimental study from open literature. Then the cooling strategy via silicone has been presented. In case of high chip powers, poor thermal management capability of conduction is shown; then the focus is changed to liquid cooling. Currently existing coolants have been analyzed with an objective of achieving a lower thermal resistance with newly proposed candidate coolants. Computational results have shown that the proposed coolant, NS15, has a higher thermal performance in comparison to other tested dielectric coolants. However, any randomly selected fluid cannot be directly chosen just because of better thermal capability.

Although, the heat transfer performance enhancement with a fluid may be attractive, the optical performance should also be evaluated. Besides the thermal performance of conduction and natural convection cases, multi-phase convection for abating local hot spots on LEDs have been also performed. Although, higher thermal performance has been achieved in multi-phase liquid cooling system, it has shown a degraded light extraction due to the bubbles over the chips. However, single phase liquid cooling has shown better optical light extraction capability with a reasonable thermal performance in comparison to boiling. While the unsuitability of water for electronics was explained before, per-fluorocarbons and Novec fluids such as LS5252, HFE7200, HFE7000, and FC72, etc. were tested for thermal management of LEDs. In coating comparative study, Nusil liquids LS5252 and LS5238 have been used as a coolant in immersion cooling due to the enhancement on the optical enhancements beside of thermal performance.

#### **4.7 Ideal Dielectric Coolant for LED Immersion Cooling**

In the current study, conduction heat transfer, natural and forced convection heat transfer and multi-phase heat transfer mechanisms were tested, respectively. After all, single phase immersion cooling technique was shown as the best possible cooling method for high power LEDs under a set of comparative studies. However, in the simulations current available dielectric coolants were utilized. While there are a number of alternative coolants inherited from electronics cooling industry, SSL requires a new unique coolants with superior thermal and optical properties. Therefore, a further study to identify possible candidates has been studied computationally with superior properties. Thermal performances of computational results have been compared with the current available liquids with respect to average Nusselt numbers over the chip.

Since the major part of the heat is removed from the chip with natural convection, understanding the heat transfer mechanism of LED chips will enable better cooling and higher lumen extraction goals. The driving equations for convection and convection resistance are given in Eq. 6 and Eq. 7.

$$Q_{conv} = \frac{\Delta T}{R_{conv}} = hA(T_S - T_\infty) \quad (6)$$

$$R = \frac{1}{hA} \quad (7)$$

These functional variables can be reduced by forming dimensionless groups consisting of a relevant heat transfer coefficient which depends on fluid properties, geometry, boundary and flow conditions.  $Ra$  number is a function of both  $Gr$  and  $Pr$  numbers as seen in Eq.8.

$$Ra = Gr \cdot Pr \quad (8)$$

$$Nu = C \left( \frac{g\beta(T_w - T_\infty)L^3}{\vartheta^2} \right)^m \times \left( \frac{\vartheta\rho c_p}{k} \right)^n \quad (9)$$

$$h = C \cdot \frac{\left( \frac{g\beta(T_w - T_\infty)L^3}{\vartheta^2} \right)^m \cdot \left( \frac{\vartheta\rho c_p}{k} \right)^n \cdot k}{L} \quad (10)$$

A new correlation for  $Nu$  number for the convection heat transfer from a flat chip surface is presented in Eq. 9. By grouping parameters for different fluids and geometries,  $c$ ,  $m$ , and  $n$  constants may change (see Eq. 9 and Eq. 10).

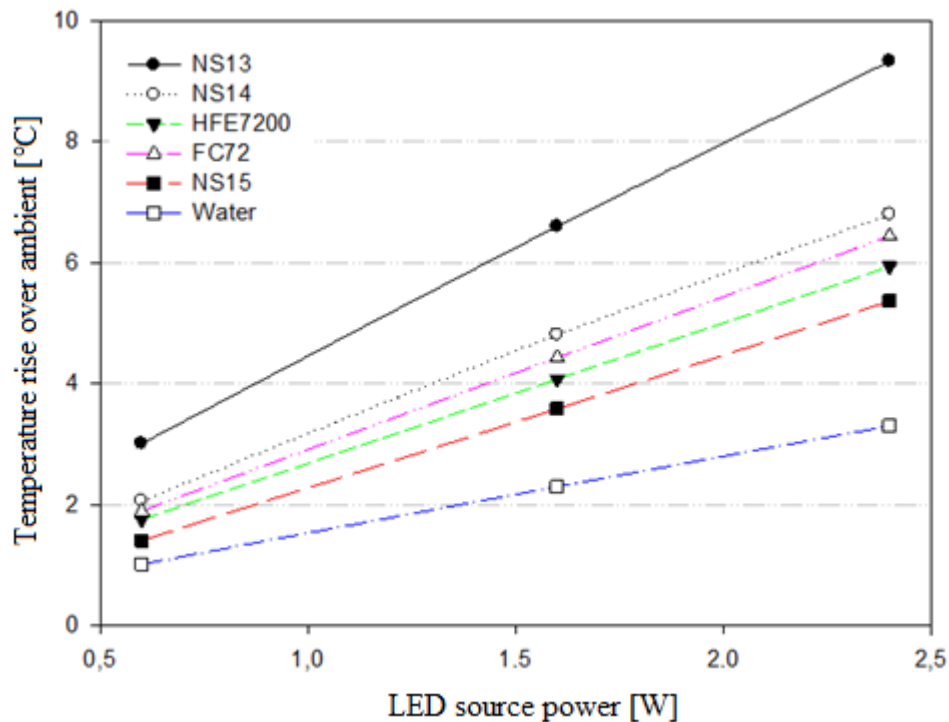
As seen from Eq. 10,  $h$  is dependent on the fluid properties of materials, since other variables such as geometry, and boundary conditions are fixed.

While dielectric liquids used in the current study have different fluid properties on heat transfer under natural convection, it is aimed to identify properties that will lead to a

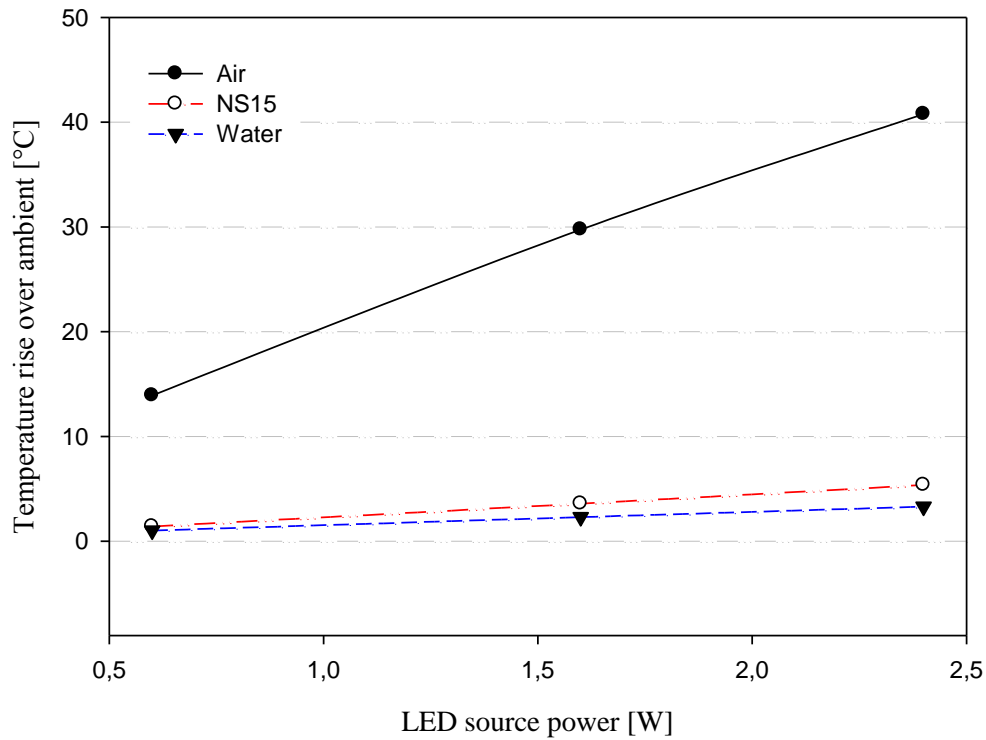
novel liquid with a higher convection coefficient. Three different configured fluids are listed and named as NS13, NS14, and NS15. They all have same physical properties but different thermal expansion coefficients and densities as shown in Table 6.

**Table 6.** Proposed dielectric coolants with their differentiated properties

Property		Water	FC-72	FC-40	HFE7000	HFE7200	NS-13	NS-14	NS-15
$T_{\text{sat}}$	[C]	100	56	165	34	76	N/A	N/A	N/A
$M_{\text{molweight}}$	[g/mol]	18.015	338	650	200	264	200	200	200
$\rho$	[kg/m <sup>3</sup> ]	989	1680	1855	1400	1430	800	1500	1500
$\vartheta$	[centistokes]	1	0.38	2.2	17	0.61	N/A	N/A	N/A
$c_p$	[J/kg.K]	4177	1100	1100	1300	1210	1300	1300	1300
$\beta$	[1/K]	0.000435	0.00156	0.0012	0.00219	0.002	0,00016	0,0016	0,016
$k$	[W/m-K]	0.61	0.057	0.065	0.075	0.075	0.075	0.075	0.075

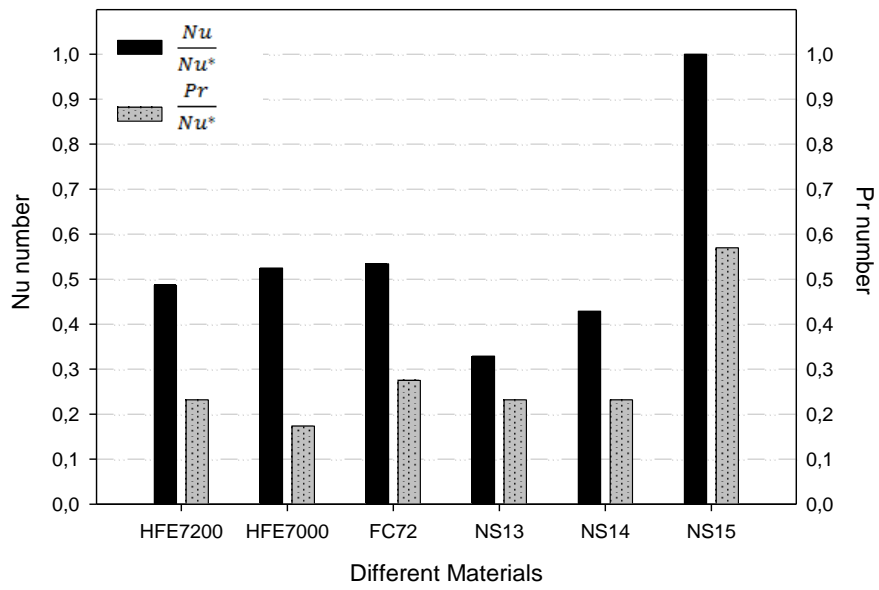


**Figure 45.** Temperature rise over ambient for different liquids at various driving conditions.

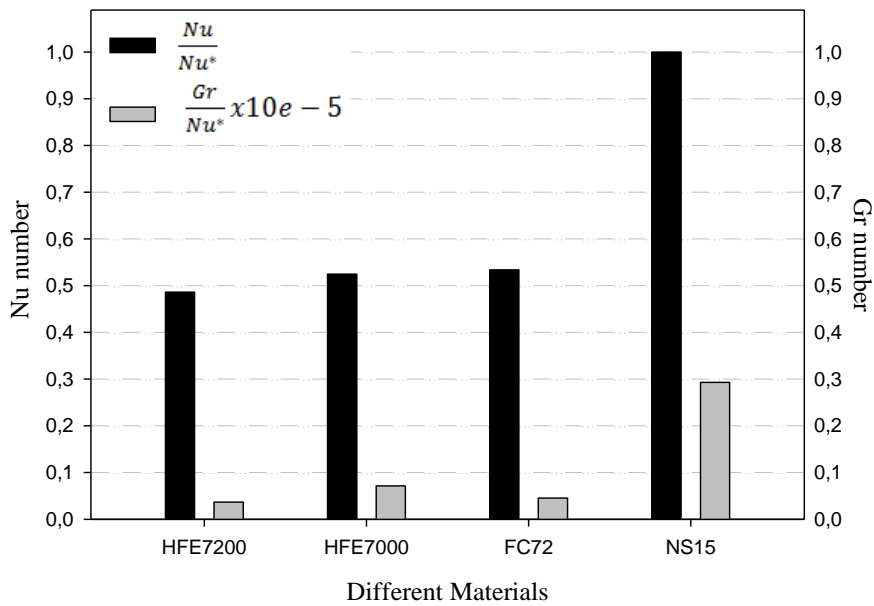


**Figure 46.** Temperature rise over ambient for air, water and NS15 at various driving conditions.

The results related to those newly proposed liquids shown in Figure 45 and Figure 46 are compared with other dielectric liquids. While NS13 and NS14 present a lower heat removal behavior than the existing dielectric liquids, NS15 has shown higher temperature difference over ambient. Since some properties such as density, specific heat capacity and volumetric expansion coefficient have positive impact on the convection coefficient, NS15 has shown the best thermal performance. When it is compared to water and air, the possible increase over air convection is also clearly shown in Figure 46. It is seen that  $Gr$ ,  $Pr$ , and  $Nu$  numbers provided a better path in understanding heat transfer performance. Since the maximum  $Nu$  number values are obtained from NS15, they are used as a reference value for comparing results. Various fluids are compared with respect to  $Nu$  with  $Pr$  numbers in Figure 47 and again  $Nu$  with  $Gr$  numbers in Figure 48.



**Figure 47.** *Nu* and *Pr* numbers for dielectric liquids with NS fluids



**Figure 48.** *Nu* and *Gr* numbers for dielectric liquids with NS15

As a result, candidate new liquids have been analytically studied. However, the superiority of new liquid NS15 was computationally presented, while experimental validation is required. Moreover, an optical study will make it much clear about the overall performance for such a lighting system.

## CHAPTER V

### EXPERIMENTAL STUDY ON JUNCTION TEMPERATURE MEASUREMENT TECHNIQUES

To convert blue to white light, GaN LEDs are encapsulated with a clear epoxy resin that cures into a soft material at high temperatures. During the typical operation of an LED, significant self-heating at the LED and the phosphor particles occurs causing the glass-like epoxy to undergo large displacements due to its high thermal expansion coefficient at a critical temperature. This enhanced displacement inside the LED package may fracture the gold wire bonds and ultimately lead to device failure [62]. This undesired heat generation leads to local hotspots and darkening of the phosphor particles [20,27,63]. Furthermore, an elevated junction temperature decreases overall light conversion efficiency of the phosphor and reduces the optical efficiency of an LED. To reduce the junction temperature and improve device performance, understanding the junction to ambient thermal resistance for an LED is thus critical [63].

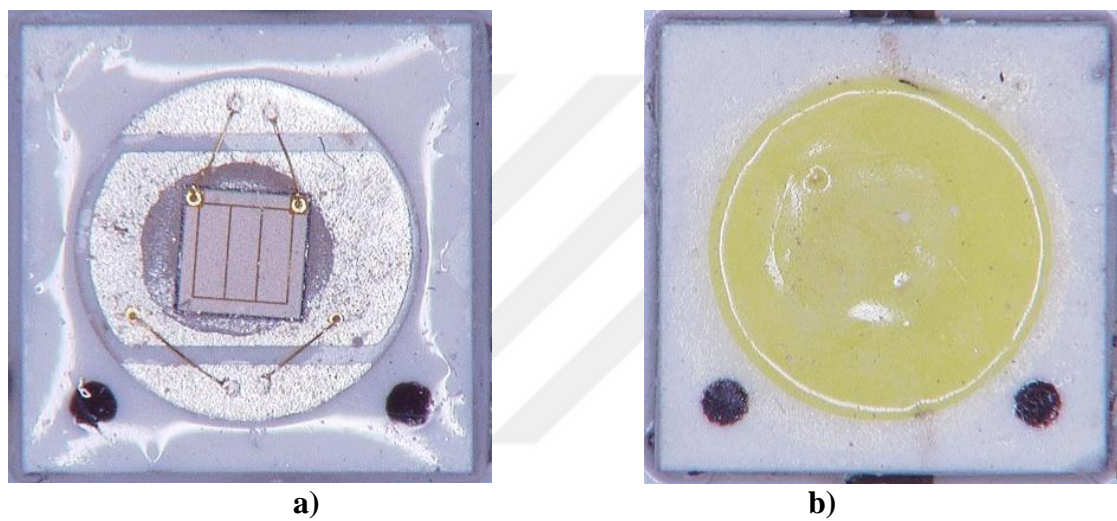
A major obstacle in estimating the thermal resistance for LEDs is the accuracy of determining the junction temperature especially for high power LEDs [64,65]. Ideally, the junction temperature is determined reliably by monitoring the device temperature at the junction, but it is an invasive technique which is not desirable. Although, this could be achieved with tiny temperature sensors that are placed very close to the junction, there are still physical limitations to this method due to the sensor itself would be larger than the junction, which would result in an additional error to the measurement and will not be very useful in most applications [66].

In this study, three experimental techniques are used to determine the junction temperature: Forward Voltage, Raman Spectroscopy and Infrared (IR) Imaging methods [1]. While Forward Voltage method uses the voltage drop with the varying temperature,



Raman Spectroscopy is based on the temperature dependent phonon frequency shift of the material [67]. For infrared imaging technology, the measurement of thermal emission from the device is used to assess the temperature distribution [11].

In the present study, the performance of a CREE EZ1000 465 nm, 1.5W blue LED chip has been evaluated by using these techniques. A bare blue chip without any phosphor coating (see Figure 49a), and a chip coated with a phosphor (YAG:Ce) - epoxy mixture (see Figure 49b) have been tested respectively.

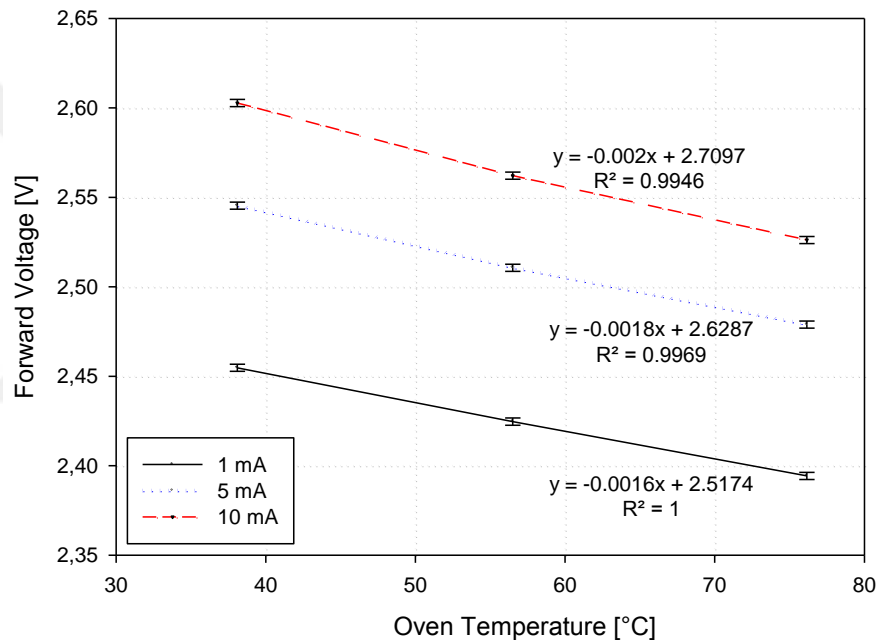


**Figure 49.** Devices under test a) Bare chip and b) Phosphor coated chip

For the coating, 3  $\mu\text{l}$  of a phosphor-epoxy mixture has been filled and cured over the bare chip placed inside a ceramic enclosure. The approximate phosphor coating thickness over the chip was 100  $\mu\text{m}$ . The percentage of phosphor inside the mixture was set in order to obtain the desired color temperature of the light emitted from the package. After all coatings were fully applied to the chip, thermal and optical experiments were performed at three different inlet power conditions. The corresponding results are experimentally compared with each other to understand the advantages and limitations of each technique when used for estimating the LED junction temperature.

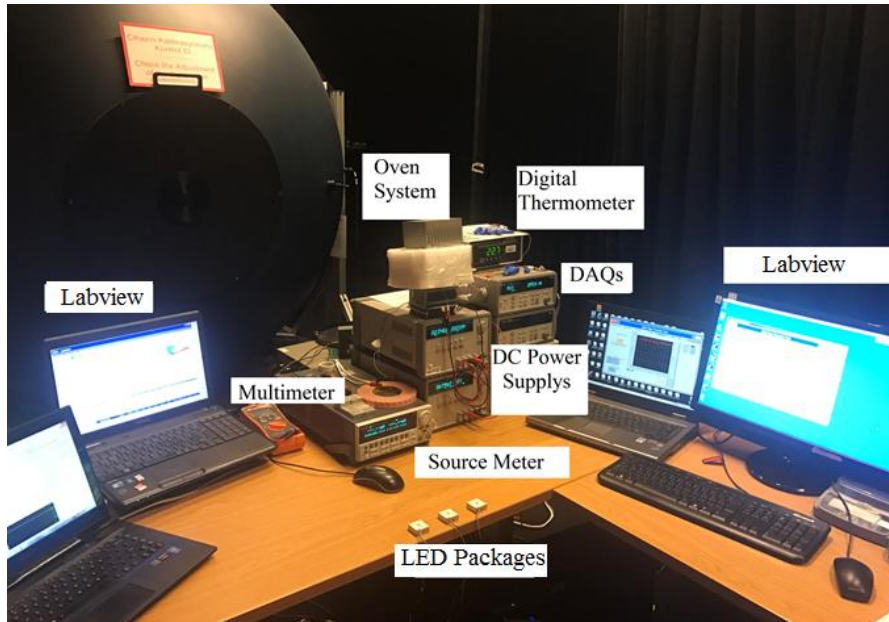
## 5.1 Forward Voltage (FVM)

Estimating the junction temperature via electrical characterization of the forward voltage has shown to be a fast and simple technique that can be implemented for in-situ monitoring [1,72-74]. Using a linear regression analysis, the specific forward voltage drop,  $V_f$ , can be related to its junction temperature as shown in Figure 50. The linear slope constant extracted from this calibration can then be used to directly estimate the junction temperature at any given forward voltage.



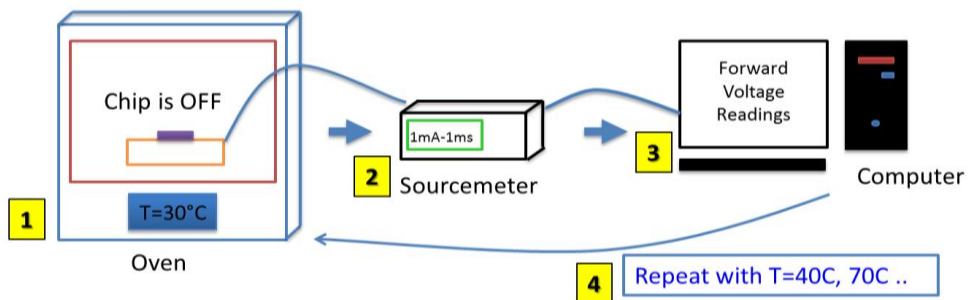
**Figure 50.** Experimental results depicting the linear behavior of  $V_f$  with the junction temperature

To perform the calibration, the LED package is placed inside a temperature controlled chamber and connected to the powering and measurement equipment as shown in Figure 51. A programmable source meter unit (Keithley 2602B Source Meter) has been used to provide power and measure voltage and current simultaneously. The temperature inside the chamber is adjusted by a thermoelectric module placed at the outer walls of the chamber. The thermoelectric system is powered by a DC power supply that is controlled with a LabVIEW program.



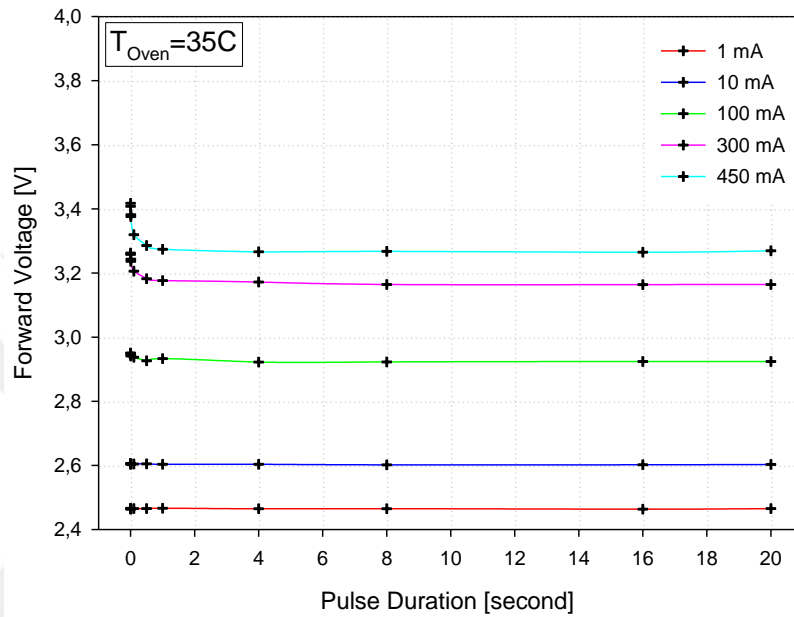
**Figure 51.** Schematic of the experimental apparatus for Forward Voltage experiments

To reduce the error in the measurement for electrical resistance, a four-wire measurement was performed. The steps followed for each calibration is shown in Figure 52. The device under test (DUT) is first placed into the heating chamber that is set to an initial temperature. Once thermal equilibrium is achieved, a 1 mA current pulse for duration of 1 ms is sourced and the corresponding forward voltage is measured. The steps are then repeated at different oven temperatures between 20 °C and 100 °C. To estimate the uncertainty in the temperature measurements, each sample and each separate condition was tested individually 10 times and the average of them was reported with a 95% confidence level.

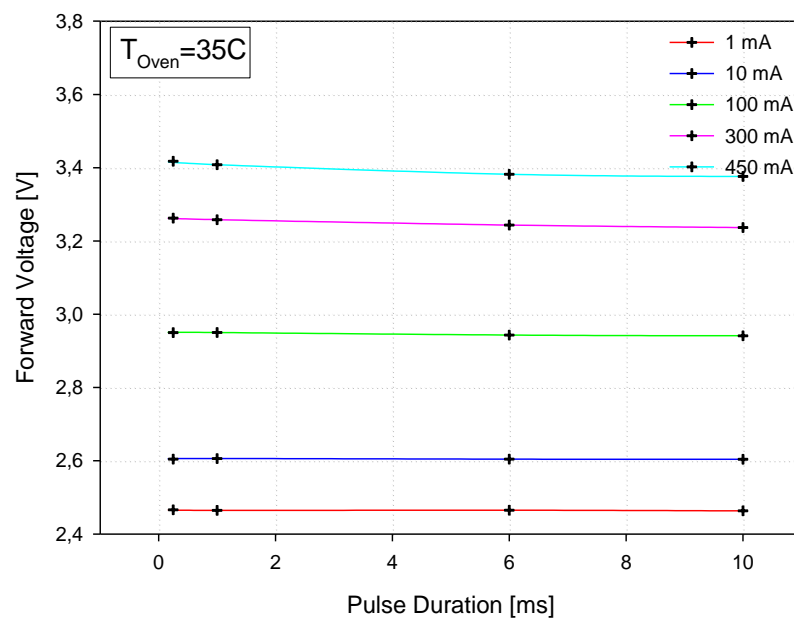


**Figure 52.** Block diagram for the experimental procedure

To gain more insight into the accuracy of the calibration procedure the probe current pulse width and amplitude were varied to determine their effect on the measurement. Sourcing a large current or a pulse with too long of a duration may skew the results by heating the junction.



a)



b)

**Figure 53.** Variation of forward voltages a) Coarse scale b) Fine scale pulse duration and current

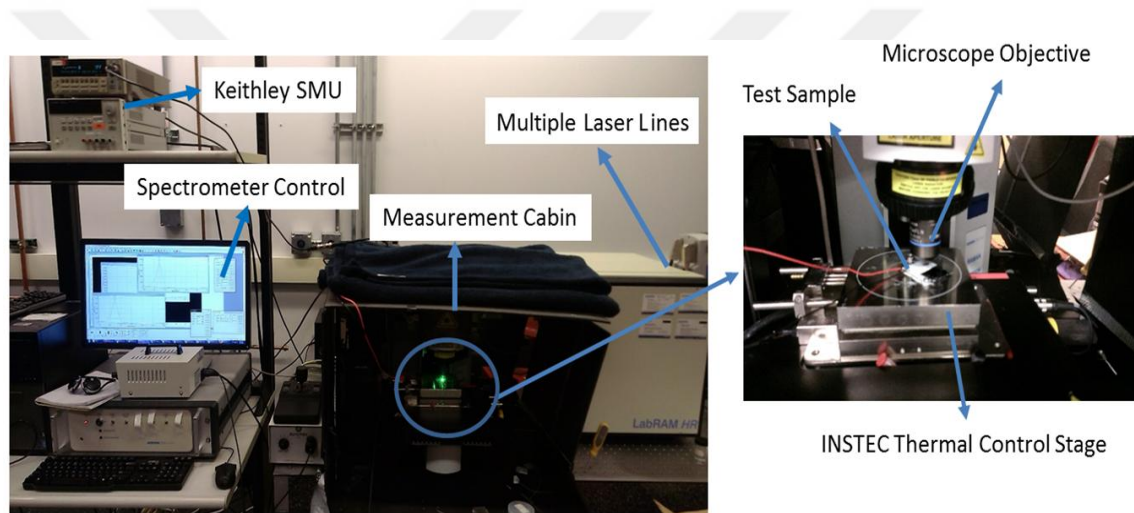
As shown in Figure 53a and Figure 53b, the forward voltages were measured at constant probe currents varying from 1 mA to 450 mA with varying pulse width between 1 ms and 20 seconds. The voltage drop curves presented in Figure 5a show that the highest change in voltage happens in the first couple of seconds followed by minor changes. To understand the effect of pulse width on the millisecond scale, Figure 5b shows the variation of the pulse width between 1 and 10 ms. Since any self-heat generation at the junction is observed as also proposed in JEDEC standards [75,76], 1 mA pulsing current at a pulse duration of 1 ms is chosen for measurements and all experiments have been completed under these conditions. After the calibration process is completed, the package is powered with the selected working currents (450-300-150 mA) and the corresponding forward voltages are measured. The DUT is considered to have reached steady state when the temperature change inside the oven is observed to be less than 0.1 °C for 10 minutes, the current is also pulsed down to 1 mA for 1 ms and pulsed back to its running current for measuring the forward voltage accurately. Then, the same process was repeated individually and also with other selected currents. The corresponding voltages are recorded and compared with previously collected calibration data. Finally, related junction temperatures are found at 150-300 and 450 mA individually with an easy interpolation.

## **5.2 Raman Spectroscopy**

Raman Spectroscopy is used to capture the vibrational energies of the optical phonons in Raman active materials. Due to the strong Raman scattering detected from AlGa<sub>N</sub>, a volumetric averaged temperature across the AlGa<sub>N</sub> thickness can be estimated to determine the junction temperature. Previous studies have shown the temperature dependence of the A1 LO and E2 HI peak in GaN [77,78]. Since a large temperature

gradient may exist across the AlGa<sub>N</sub> thickness, Raman active nano-particles, such as TiO<sub>2</sub>, can be deposited on the top of the device to estimate the surface temperature and thus give a better representation of the peak temperature [75].

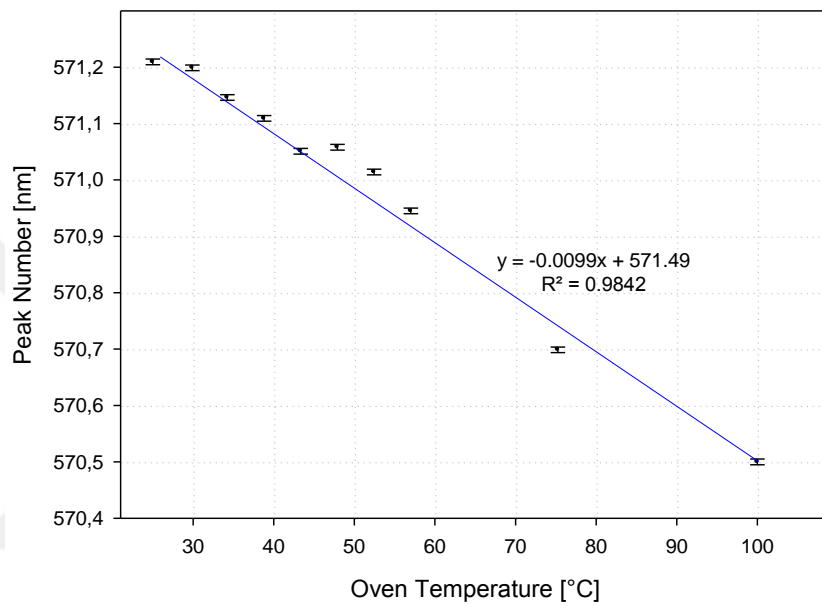
Raman Spectroscopy was performed using a Horiba Jobin Yvon LabRAM HR800 as shown in Figure 54. Three different excitation sources (532 nm, 440 nm and 325 nm lasers) were exposed perpendicular to the sample plane of GaN (LED chip) in an 180° backscattering configuration. The laser beam diameter was approximated to be 1 μm with a 50X objective.



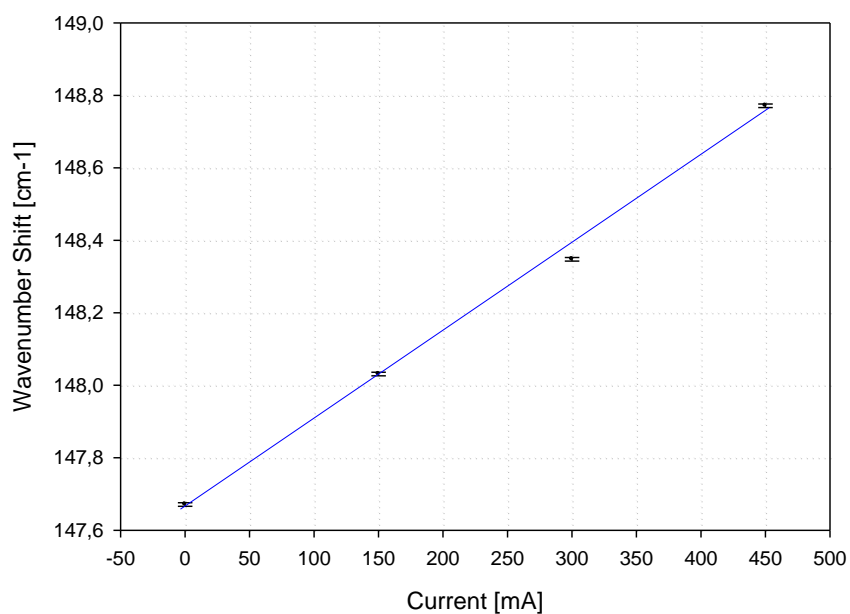
**Figure 54.** Schematic of the experimental apparatus for Raman Spectroscopy

A liquid nitrogen cooled charge coupled device (CCD) camera was integrated into the system to image the collected Raman signals. An 1800 l/mm grating was used with a slit width of 100 μm for the measurements. To prevent substrate heating, the laser power was controlled via neutral density filters. Since changing the filter density will decrease the laser intensity, the acquisition times were adjusted every time to keep the peak intensities uniform throughout the experimental study and reduce the uncertainty in the measurements. To estimate the uncertainty in the temperature measurements with a 95% confidence interval, an average of 10 measurements was performed at selected

power conditions. Experimental measurements for the calibration process were completed with a temperature controlled stage set between 30°C and 90°C to control the repeatability of the method as seen in Figure 55. Then, the Raman spectra was measured and corresponding junction temperatures were calculated with the peak parameters of the Stokes peaks of AlGaIn at fixed base temperature of 40°C.



**Figure 55.** Variation of Raman peak wave number with temperature for uncoated LED chip



**Figure 56.** Variation of wavenumber shift for TiO<sub>2</sub> particles over uncoated LED chips

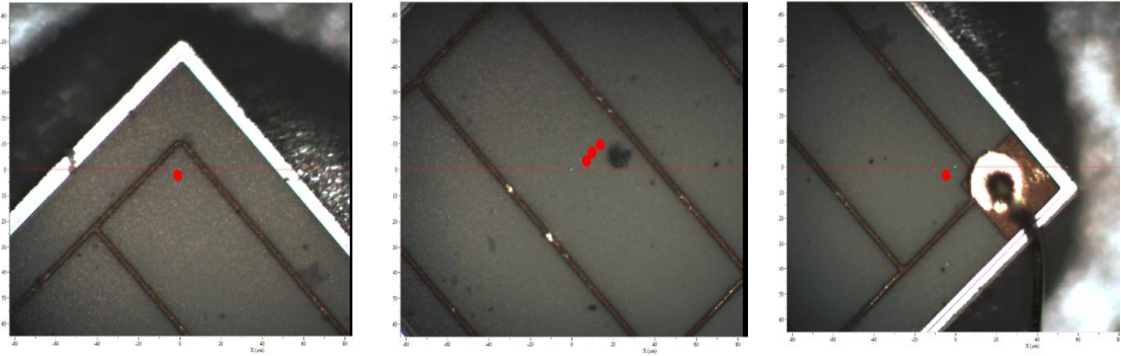
While junction temperature measurements for uncoated chip were successful with Raman thermometry; once it was coated with the phosphor-epoxy mixture, the laser for the Raman excited broad emissions from the phosphor layer which overlapped with the Raman emission from the underlying AlGaIn chip. Thus, capturing the GaN Raman signature for phosphor coated chips became challenging with Raman Spectroscopy. To overcome this problem, Raman active TiO<sub>2</sub> particles were dispersed over the surface of uncoated GaN die. Since anatase TiO<sub>2</sub> particles have a Raman peak wavenumber shift (145 cm<sup>-1</sup>) that is outside of the light emission range of the LED, it was possible to make these measurements during device operation.

Accordingly, the experiments were repeated and wavenumber shift versus operating current was obtained for coated packages as shown in Figure 56. However, the obtained data from the anatase TiO<sub>2</sub> particles represented the temperature at the surface of the LED which may be different than the actual junction temperature which was needed to estimate the thermal resistance.

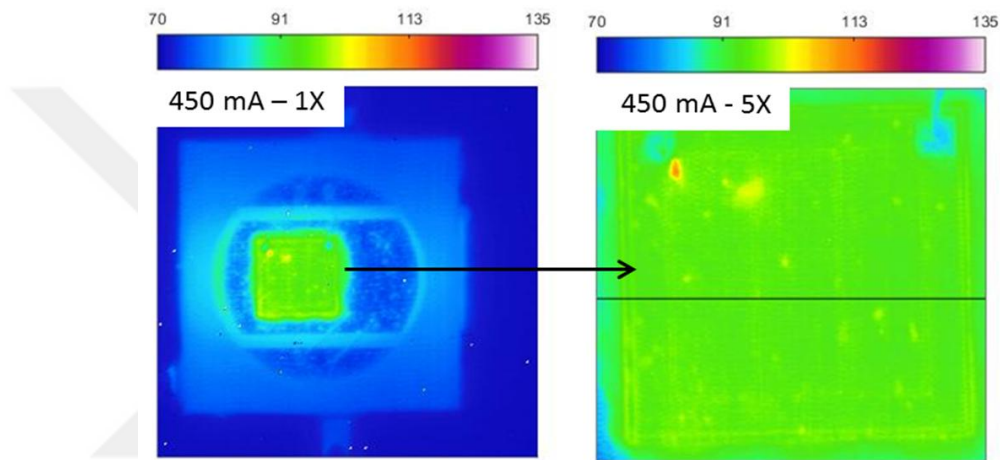
On the other hand, the temperature uniformity across the chip surface is also important for the Raman method, since the laser beam is adjusted to a tiny area at the chip surface. In case of the existence a non-uniform temperature distribution across the surface, the results would change if the location of the Raman laser was slightly moved between different measurements.

Hence, calibration curves were obtained for several locations in order to ensure uniformity of slope and measurements as it can be seen in Figure 57. The laser beam is adjusted to 5 different locations over the chip as seen in Figure 57, and the surface temperature uniformity is being ensured with the corresponding evaluated wavenumber shift from each point.





**Figure 57.** Raman test measurements through the surface at different positions



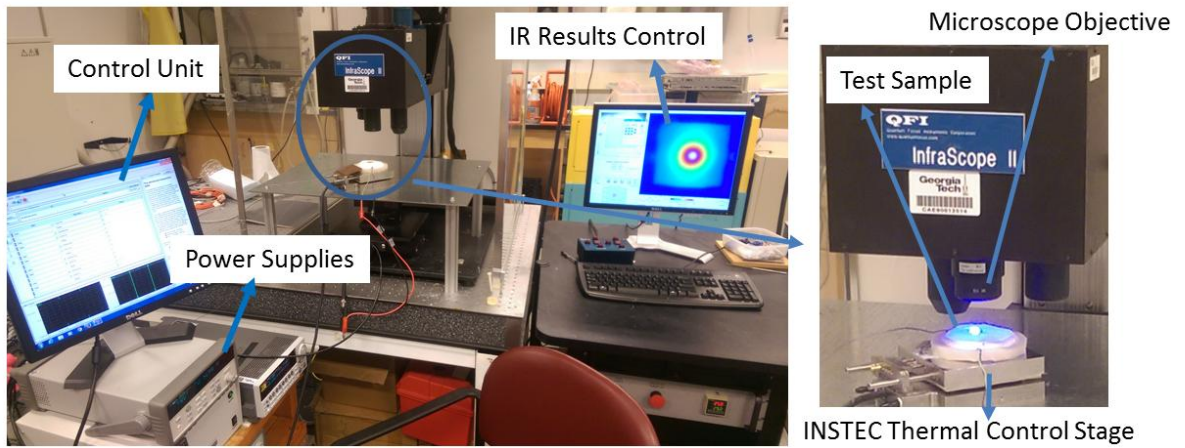
**Figure 58.** IR Imaging through the surface at different positions

Moreover, the whole surface temperature image was also taken and compared with IR Imaging technology as shown in Figure 58. It is clearly seen from the IR images that, both Raman Spectroscopy peaks and IR measurements results have proved that the temperature gradient over the surface negligible.

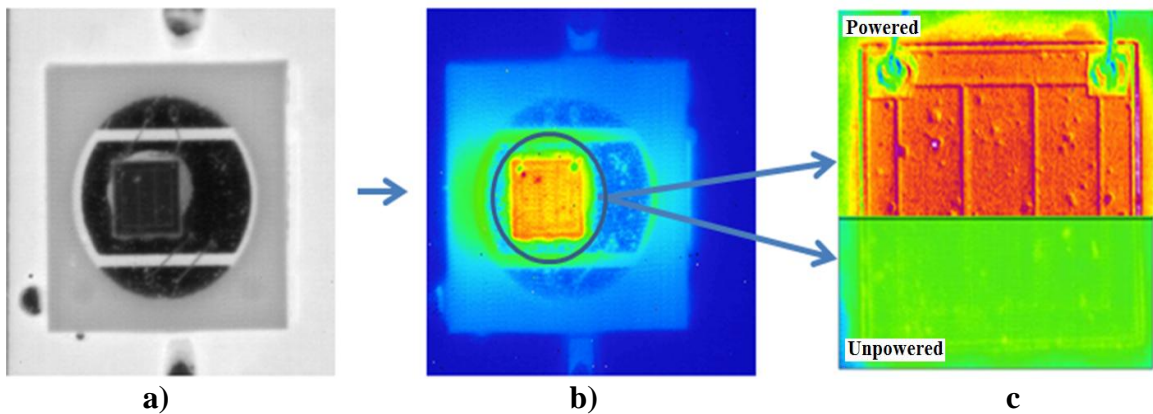
### 5.3 Infrared (IR) Thermal Imaging

While, infrared radiation is able to transmit through a number of materials; this method is used to determine the junction temperature of LEDs, since the emitted infrared energy increases with increasing object temperature [79].

According to this technique, experiments were performed by using a QFI (Quantum Focus Instruments) Infra-Scope II system as shown in Figure 59. Before beginning an experiment, a 1X magnification objective was employed to focus on the LED chip. Then, a 5X magnification objective was used during the measurements.



**Figure 59.** Schematic of experimental apparatus used for Infrared Imaging (IR) test station



**Figure 60.** Emissivity correction process via QFI Infra Scope system, a) Unpowered LED chip, b) Emissivity correction, c) 5X magnified correction result; uniform temperature

Before starting each measurement, a radiance image was captured over un-powered LED chip at an elevated temperature ( $70^{\circ}\text{C}$ ). The emissivity variation of different materials on the semiconductor device is shown in Figure 60a. The QFI system makes

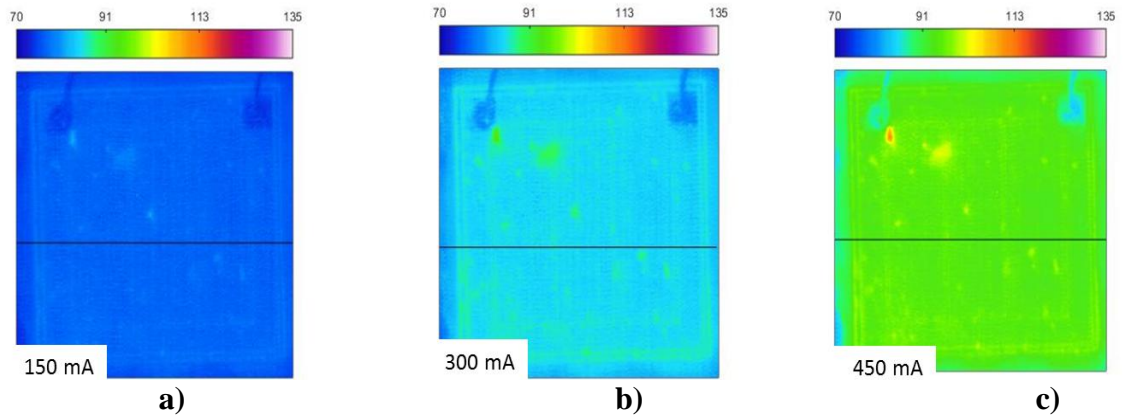
emissivity correction accordingly (see Figure 60b). After the emissivity correction, an un-powered image shows a uniform temperature map, while powered case shows the real temperature readings as seen in Figure 60c. To lower the uncertainty, the device does a number of measurements by itself accordingly and gives a single average temperature reading for each separate case as a result. Finally, the corresponding temperatures were obtained for the selected working conditions (150-300-450 mA).

#### **5.4 Comparison of Measurement Techniques**

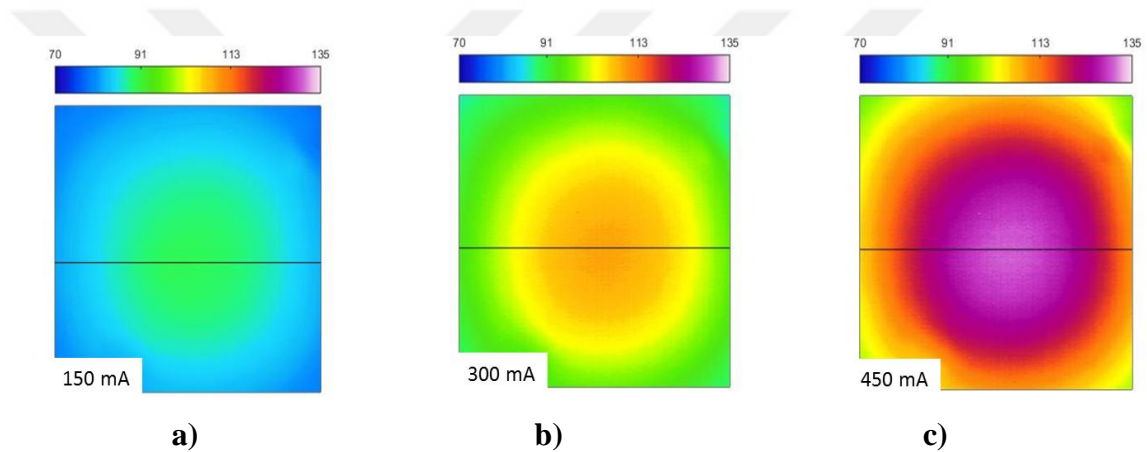
To have an accurate comparison between three methods, Forward Voltage approach is applied simultaneously with Raman and IR techniques (FVM-Raman, FVM-IR) individually. Moreover, the experiments were conducted at three different oven temperatures (40°C, 60°C and 80°C) to check the repeatability of each method. To validate the results, experiments were conducted at three input currents (150mA, 300mA, and 450mA), individually. While, the junction temperatures for uncoated LED chip were measured successfully with all methods in good agreement, the IR and Raman techniques, however, have shown some deviation for coated chips.

More intense light emission with over broad a wavelength range of the coated package interfered with the Raman peaks from the GaN material thus making the junction temperature measurements impossible. Although, the method accurately measured the temperature when TiO<sub>2</sub> particles were dispersed over the surface, the measured data is attributed to the surface temperature and not to the junction.

Alternatively, the same experiments were repeated with Infrared (IR) Imaging technology and Forward Voltage method simultaneously. While the maximum junction temperature for uncoated package is observed to be 95°C at 450 mA and 85°C and 77°C for the currents 300 mA and 150 mA respectively, as shown in Figure 61.



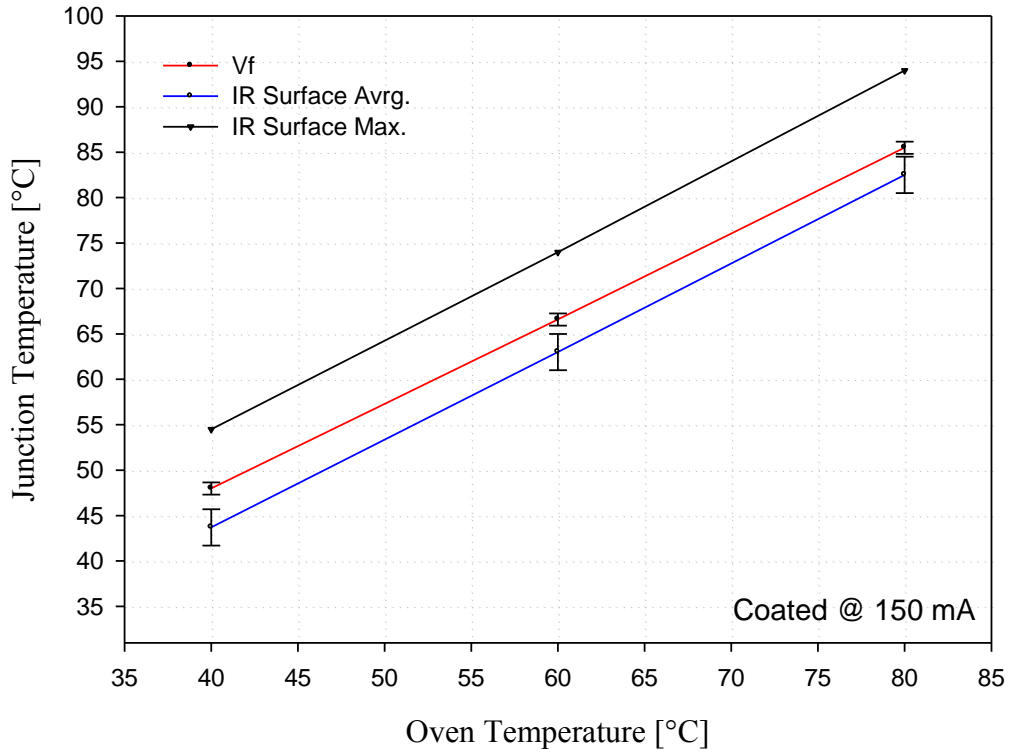
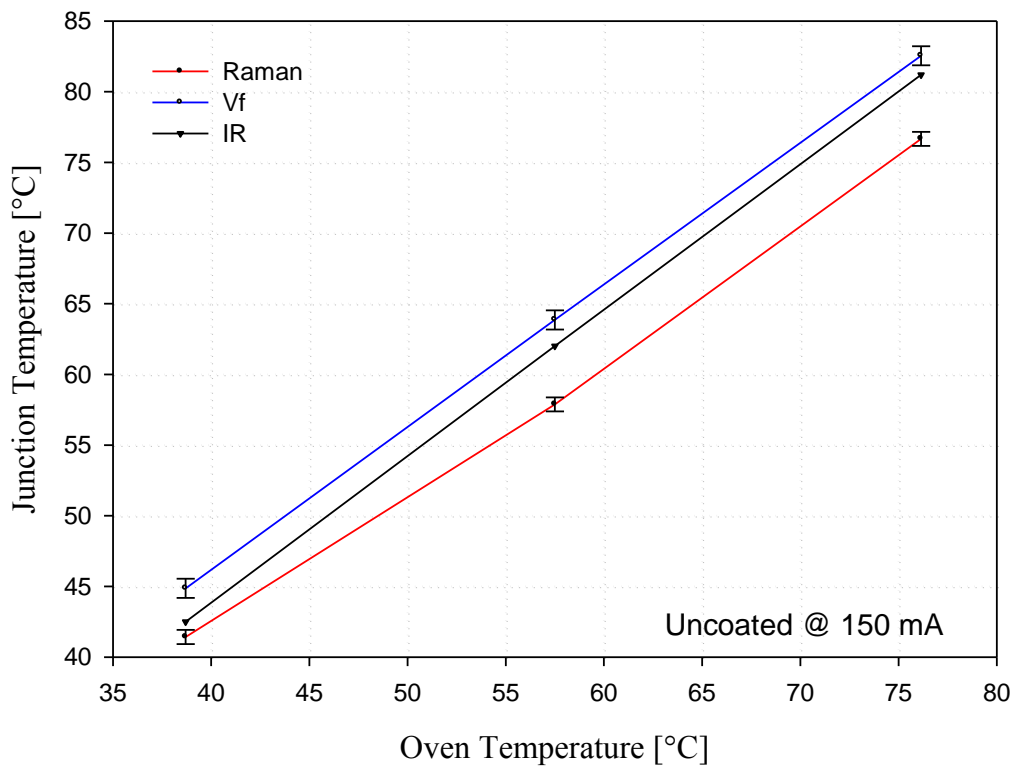
**Figure 61.** Infrared Imaging measurement results for uncoated chips a) 150mA b) 300mA c) 450 mA



**Figure 62.** Infrared Imaging measurement results for coated chips a) 150mA b)300mA c) 450mA

Unlike the uncoated chips, the coated chip measurements have shown a non-uniform temperature distribution over the chip surface. As presented in Figure 62, there is a rising temperature trend with increasing current. Moreover, the thermal distribution over the package has shown a big difference through the center to edges, due to the lower thermal conductivity of phosphor-epoxy mixture.

The results for Raman Spectroscopy and FVM can also be seen in the following figures with IR measurements. While uncoated chip measurements for varying current values (150mA, 300mA, and 450mA) were showing similar results; phosphor coated chips have shown some identical differences between each other.



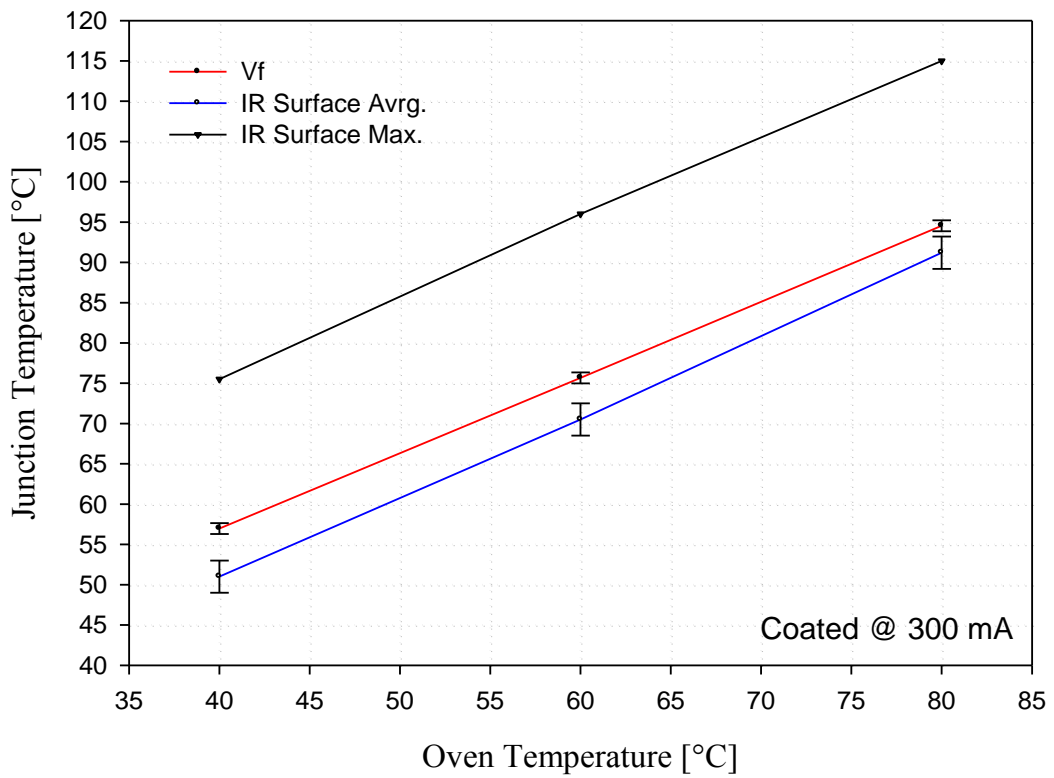
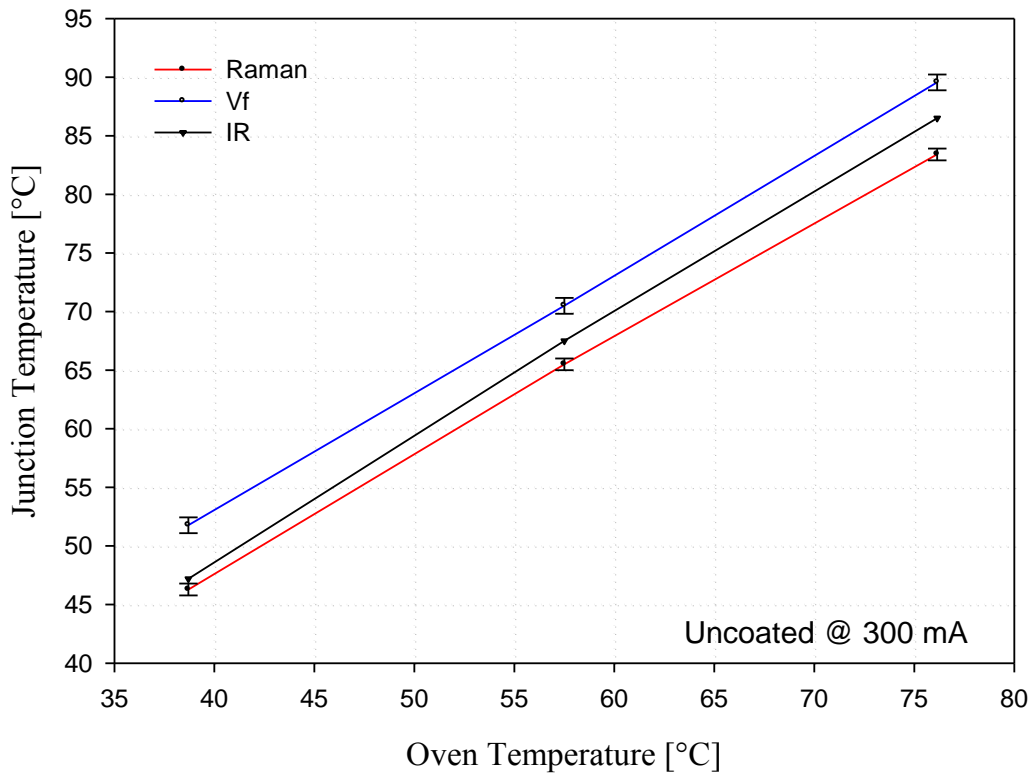
**Figure 63.** Comparison of coated and uncoated chip junction temperatures at 150mA

Figure 63a and Figure 63b present the results of coated and uncoated chips driven at 150mA. The obtained data for uncoated chip's junction temperatures are presented in Figure 63a within a couple of degrees difference between three methods. For the coated chip's, IR measurements showed a non-uniform temperature results through the surface, while the broad emission wavelengths with the light excitation coming from the phosphor coated chip is now changed and overlapped with the bandgap of GaN material in Raman spectroscopy.

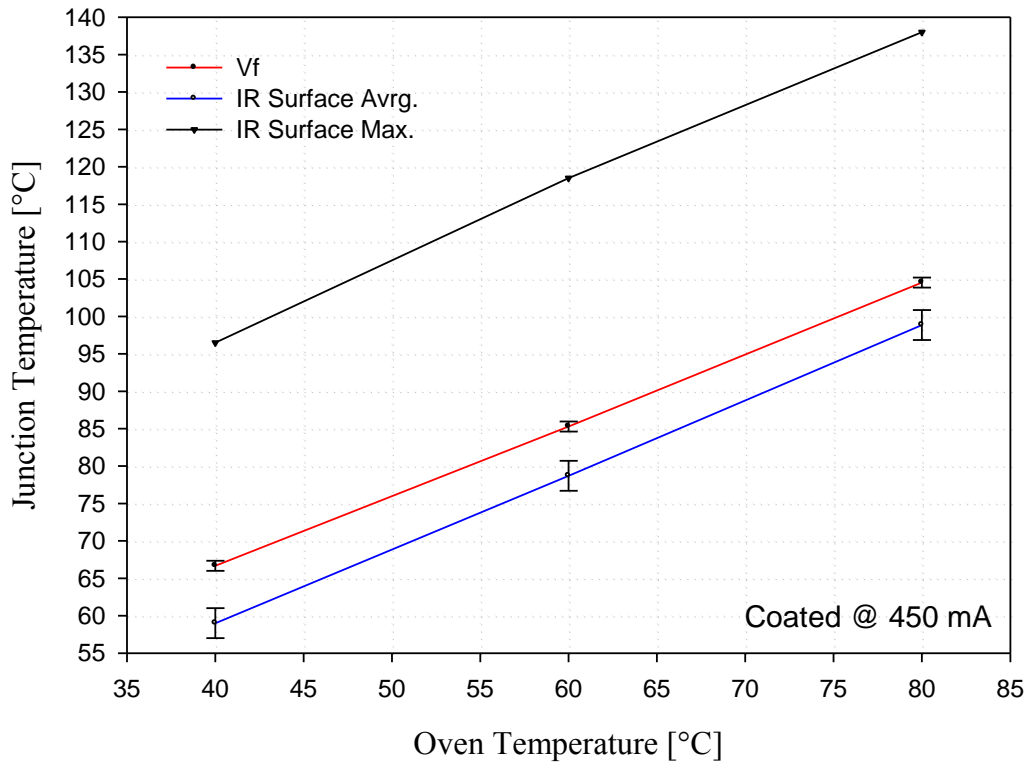
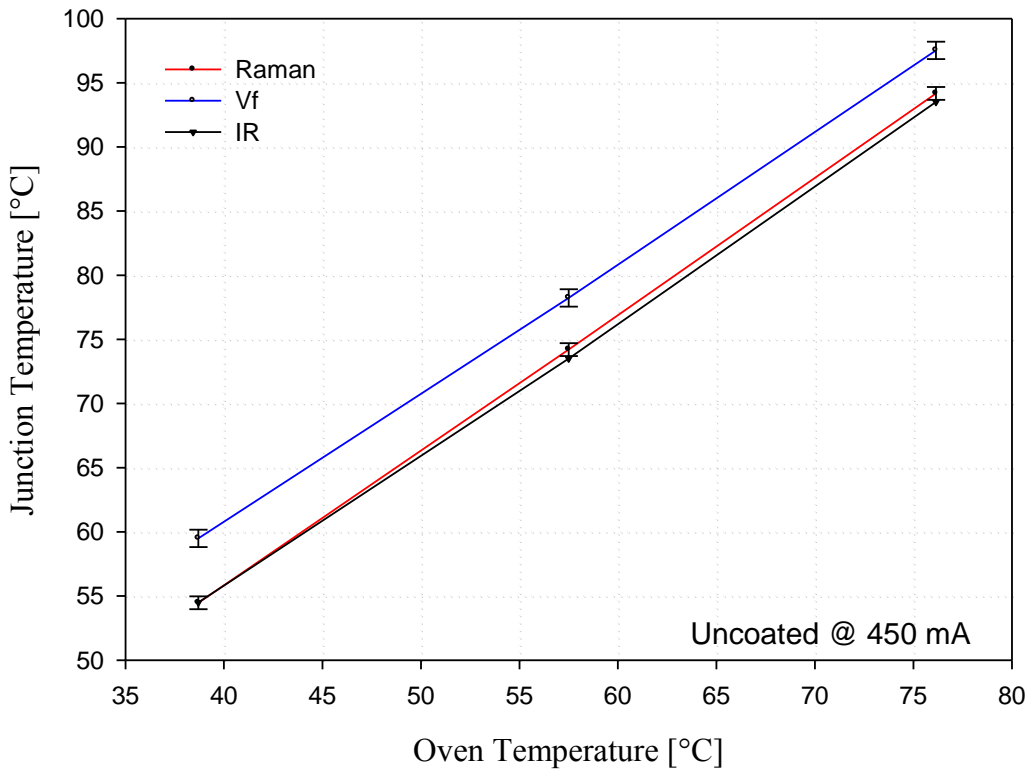
Due to the non-uniform temperature results over the chip surface, the maximum temperature that was observed at the center of the package was taken into account first and presented in the plots. Then, the average surface temperatures obtained from IR measurements were also added to the comparison plots, since the difference between obtained  $T_j$  values with forward voltage method and the maximum surface temperatures from IR measurements was higher.

However, forward voltage method has also measured the junction temperatures for varying oven conditions with the help of linear voltage drops affected by only temperature. The temperature measurements for 300 mA have been also presented in Figure 64a and Figure 64b. As observed before at 150 mA,  $T_j$  was measured with a small difference between each other for uncoated chips at 300 mA too. Moreover the same slope has been seen for varying oven temperatures. Furthermore,  $T_j$  values for coated chips with IR method have been repeated the changing behavior from side to center as shown in Figure 62 previously.

On the other hand, the same behaviors were observed from the measurements with 450 mA inlet current. Figure 65a and Figure 65b present the junction temperatures for coated and uncoated LED chips.



**Figure 64.** Comparison of coated and uncoated chip junction temperatures at 300mA



**Figure 65.** Comparison of coated and uncoated chip junction temperatures at 450mA



As a result, the LED junction temperatures are measured with Raman Spectroscopy, Infrared (IR) Imaging as well as Forward Voltage method (FVM) for uncoated and phosphor coated LED chip, individually. First, the uncoated bare chips were measured within a couple of degrees difference between three methods, while the coated packages have shown some unexpected differences. Due to the wide range light extraction from the coated package by itself, Raman Spectroscopy was not able to capture the peaks to the corresponding temperatures; as, the IR measurements for coated chips have shown non-uniform temperature distribution through the surface due to the lower thermal conductivity of the phosphor-epoxy mixture.

While different wavelength exciting lasers might be a solution for Raman Spectroscopy; changing coating thickness with a special interest on the optics through the surface might be a solution for IR measurements as well. On the other hand, Forward Voltage method determined the junction temperatures for both coated and uncoated packages. Moreover, the iterations of the experiments have shown repeatable results with a reliable slope of change on the voltage which supports the suitability of the method.

## CHAPTER VI

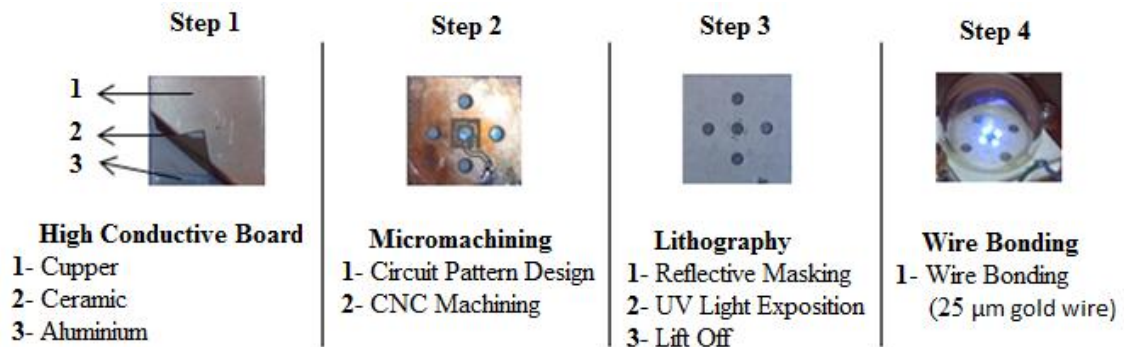
### THERMAL AND OPTICAL PERFORMANCE EXPERIMENTS FOR IMMERSION COOLED LEDS

Though there are several methods to produce white light in LEDs, the most common method is to use a blue chip and yellow phosphor. Blue light is produced in the semiconductor materials and then it is absorbed and reemitted by the phosphor layer. Also, there can be different phosphor usage methods in LEDs such as coating on led chip, dispersed phosphor particles on silicon and remote phosphor layer. Not only chips but also phosphor efficiency is less than %20 due to heat losses with poor cooling of package especially the phosphor and mismatching refractive index between chips to ambient [80,81]. Moreover, the conversion losses in the phosphor due to the Stokes Shift and quantum efficiency cause undesired heat generation. Furthermore, some applications practice higher phosphor temperature than LED junction due to this lower phosphor conversion efficiency. Thus, having white light from blue LED source with separated phosphor layer is commonly known as remote-phosphor systems. Although this idea has existed for more than 10 years, no one has studied yet the immersion liquid cooling between the LED chip and separated phosphor layer. In the current study, light extraction enhancement of each different proposed coating technology was tested and results were evaluated.

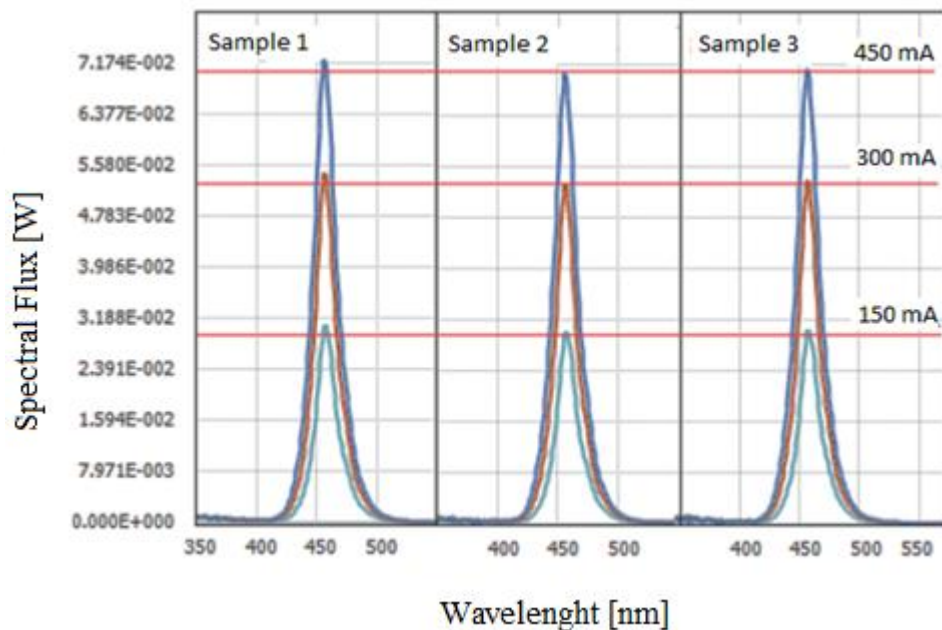
#### **6.1 Immersion Cooling of Suspended and Coated Nano-Phosphor LEDs and Light Extraction**

For the test specimen, thermally high conductive metal clad board with Al base, ceramic dielectric layer and copper electric conductive layer for circuit design has been chosen. As presented in Figure 66, the circuit pattern was designed first and then printed with a special micromachining tool. To have a homogenous reflectivity on the surface, it has

been masked with a special reflective coating material. Then, the coating was being lifted off from the undesired locations with UV light exposition for soldering the chip and wire bondings. Then, a number of test vehicles have been built accordingly by packaging with the same package dimensions as the Cree EZ1000 bare chips.



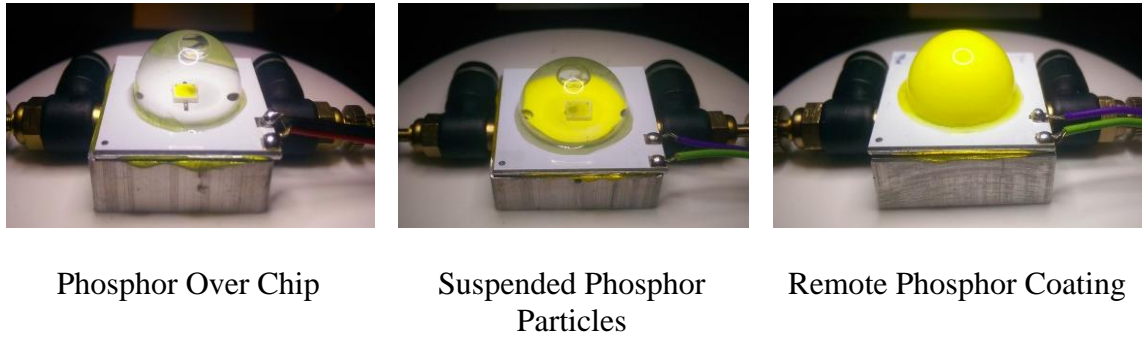
**Figure 66.** PCB manufacturing processes



**Figure 67.** Spectral fluxes for three test samples at various currents

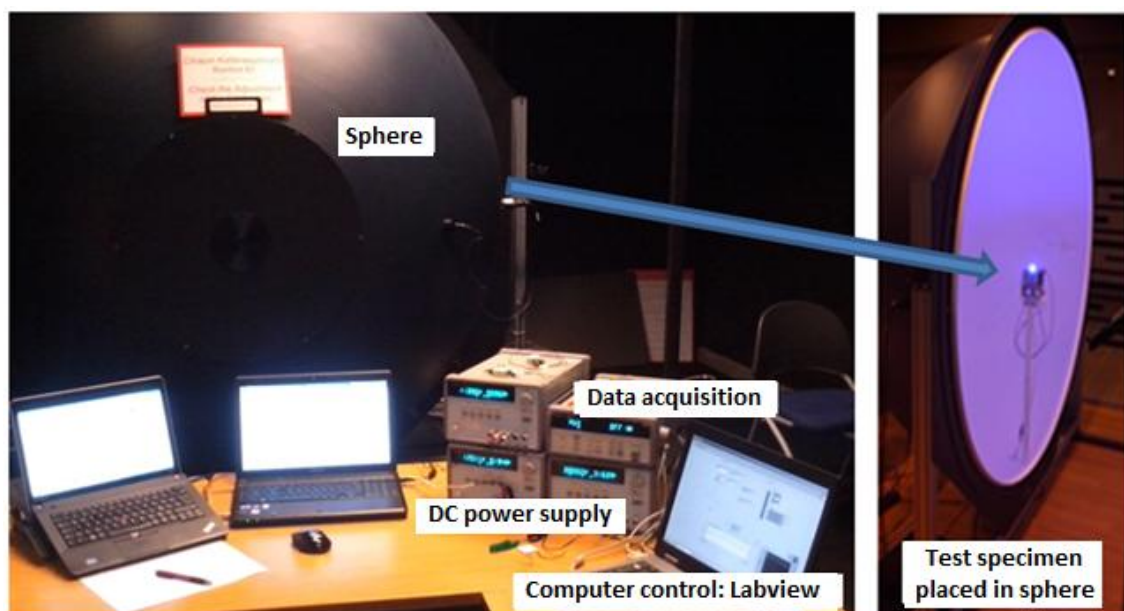
For an accurate comparison; the LED chip, phosphor, and final system configuration were considered as same except for the phosphor location. The initial conditions of samples have been investigated by measuring the radiant flux and peak wavelength values under the same input powers and the results are presented in Figure 67. As it can

be easily seen from the figure, the variation between samples is less than 0.25%. Once the initial properties were proven to be similar, different coated test vehicles, seen in Figure 68, were built with 2 prototypes of each for lower uncertainty.



**Figure 68.** Experimental setups for three different phosphor application technologies

The experimental setup was then designed and built for the current study as shown in Figure 69. The base temperature of each system has been controlled and kept at certain temperature (40°C), since the conversion efficiency of chip and phosphor are highly dependent on temperature [17].

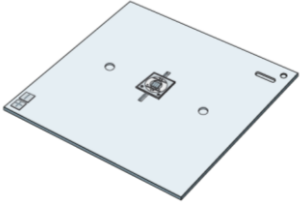
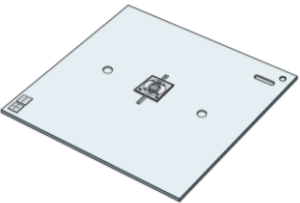
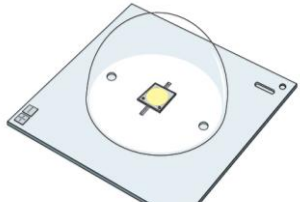


**Figure 69.** Junction temperature and optical experimental systems

The temperature variation at the back side of PCB due to the power variation on the chips has been compensated by controlling the power given to the thermoelectric with


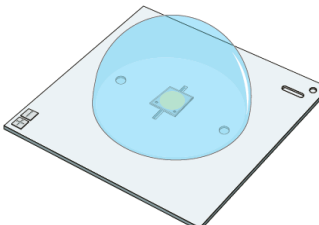
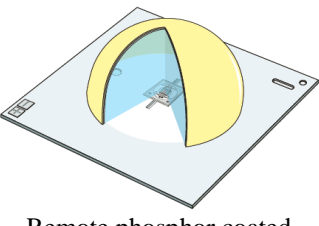
the help of Labview software. Two Agilent DC power supplies (E3634A) and an Agilent data acquisition (34972A) have been utilized for measurements. The optical measurements for obtaining lumen, lumen per watt (LPW), color rendering index (CRI), correlated color temperature (CCT), optical power, and spectral distribution were performed with an integrated sphere (2m diameter) manufactured by Labsphere Inc. as seen in Figure 69. Then, each coating ideas have been tested with and without immersion cooling with LS5238 dielectric coolant. Moreover, each experiment have been repeated minimum twice to assess the feasibility of light extraction of LED packages with different phosphor coating technologies and to compare their performances between each other accurately.

**Table 7.** Experimental junction temperature and light extraction results for corresponding technologies

Light Extraction Measurements			Test Vehicle	Junction Temperature Measurements		
<b>I (mA)</b>	<b>Lumen (Lm)</b>	<b>CCT (K)</b>	 Bare Chip	<b>T<sub>Base</sub> (°C)</b>	<b>T<sub>Junction</sub> (°C)</b>	<b>T<sub>Phosphor</sub> (°C)</b>
450	23,00	22000		40	58,33	-
300	17,20	22000		40	50,89	-
150	9,70	22000		40	44,06	-
<b>(A)</b>						
<b>I (mA)</b>	<b>Lumen (Lm)</b>	<b>CCT (K)</b>	 Silicone Coated Chip	<b>T<sub>Base</sub> (°C)</b>	<b>T<sub>Junction</sub> (°C)</b>	<b>T<sub>Phosphor</sub> (°C)</b>
450	23,00	22000		40	59,42	-
300	17,20	22000		40	51,03	-
150	9,70	22000		40	43,89	-
<b>(B)</b>						
<b>I (mA)</b>	<b>Lumen (Lm)</b>	<b>CCT (K)</b>	 Phosphor over Chip	<b>T<sub>Base</sub> (°C)</b>	<b>T<sub>Junction</sub> (°C)</b>	<b>T<sub>Phosphor</sub> (°C)</b>
450	68,50	4036		40	64,45	-
300	52,60	4038		40	55,20	-
150	30,50	4051		40	45,51	-
<b>(C)</b>						

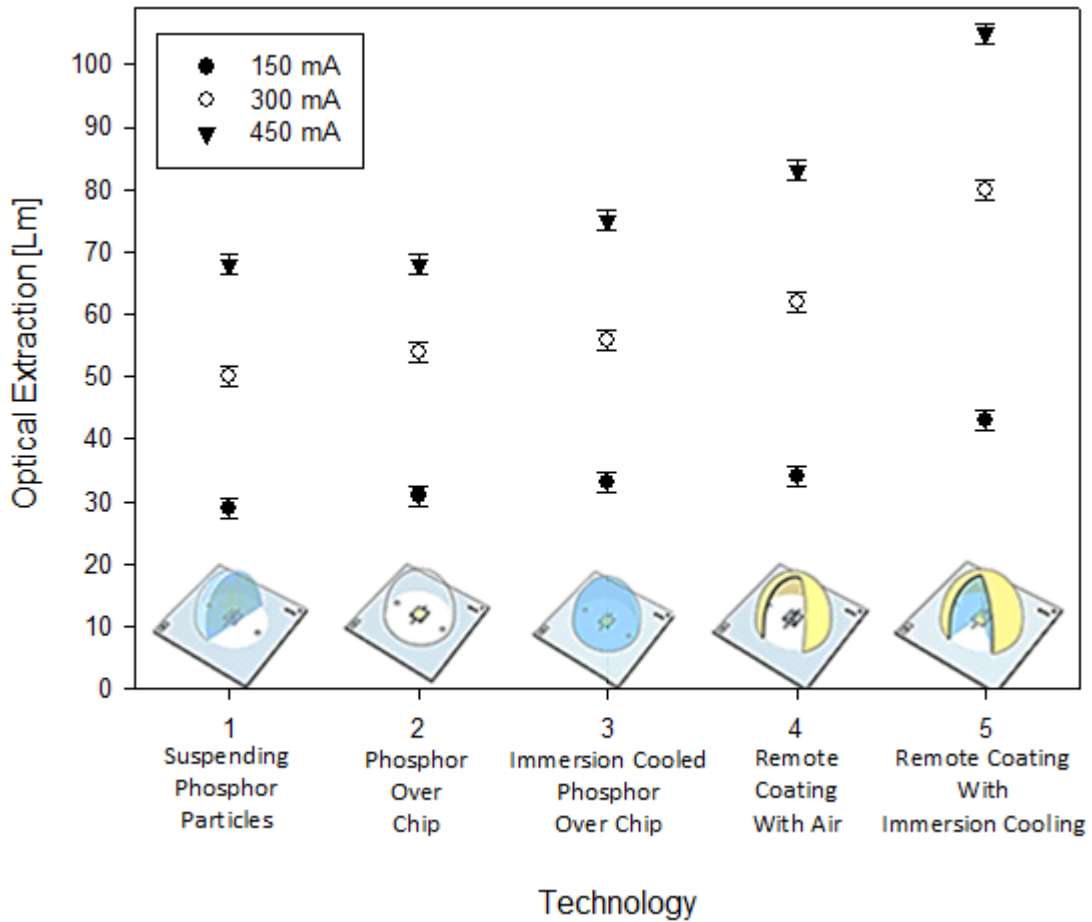
The steady state junction temperature and integrating sphere measurements for bare, silicone and phosphor coated chips are outlined in Table 7 below. There, the conventional coating technique and direct phosphor coating over chip has been chosen as the baseline light output. While A and B cases in which emit blue light, have shown similar junction temperatures, once the chip is phosphor coated as in C case, lumen extraction and also the junction temperature are increased as clearly seen in Table 7.

**Table 8.** Experimental junction temperature and light extraction results for corresponding technologies

Light Extraction Measurements			Test Vehicle	Junction Temperature Measurements		
I (mA)	Lumen (Lm)	CCT (K)		T <sub>Base</sub> (°C)	T <sub>Junction</sub> (°C)	T <sub>Phosphor</sub> (°C)
450	68,45	4005	 <p>Suspended phosphor inside the glass dome with dielectric coolant</p>	40	61,60	-
300	49,36	3972		40	52,04	-
150	27,64	3967		40	43,31	-
<b>(D)</b>						
450	73,60	4133	 <p>Immersion cooled phosphor over chip</p>	40	63,27	-
300	56,59	4134		40	54,53	-
150	32,77	4143		40	44,97	-
<b>(E)</b>						
450	105,00	4102	 <p>Remote phosphor coated glass dome with dielectric coolant</p>	40	56,87	-
300	78,93	4098		40	49,31	-
150	43,87	4091		40	42,79	-
<b>(F)</b>						

While, phosphor helps on converting the blue light to white light, which was resulted in higher lumen extraction; it caused extra heat generation inside the phosphor layer due to the conversion efficiency of phosphor particles by itself, which lead the chip to reach higher temperature as a result. Moreover, same procedures have been also utilized for remote-phosphor coating and dispersed phosphor particle systems with immersion cooling to compare temperatures and light extractions and their results were presented in Table 8. It is clearly seen from the Table 8 that junction temperatures get lowered while light extraction was increased with immersion cooling. While the lumen output from the chosen baseline LED system (phosphor over chip coating; case C in Table 7), shows 68.5 lumens at 450mA with a single LED chip, %7 enhancement has been observed once it is immersed with dielectric coolant with 73.6 lumens light extraction as seen in E case in Table 8. Additionally, dispersed phosphor case was also listed in the Table 8. Although the dispersed system has shown lower junction temperature, optical light extraction did not change much with 68.45 lumens light output. This was thought due to that more blue light has passed through the phosphor and liquid medium without touching the suspending phosphor particles.

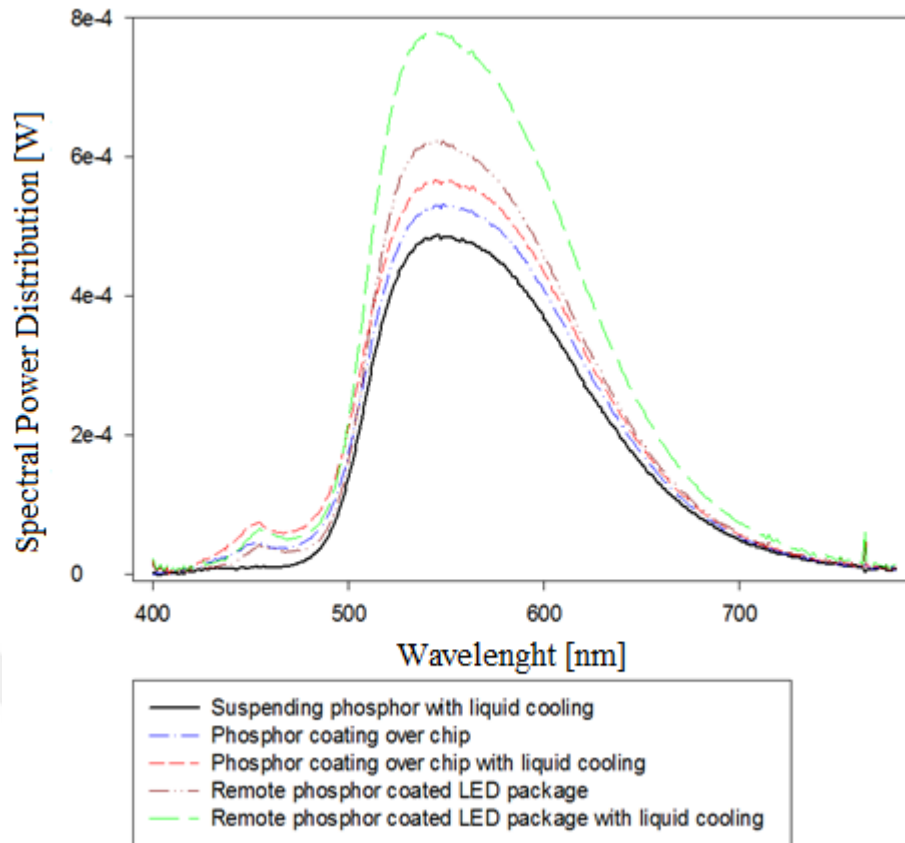
On the other hand, remote phosphor system has shown lower junction temperature and also better optical light extraction in comparison to baseline. As all proposed coating techniques were summarized in Figure 70, the dispersed phosphor package, technology 1, presented almost similar results of baseline shown as technology 2 in Figure 70. After immersion cooling of baseline study presented as technology 3, has resulted with a bit higher light extraction and a bit lower junction temperature. On the other hand, technology 5, remote phosphor with immersion liquid cooling has shown the highest light extraction with a light output of 105 lumens (53.2% increase) and the lowest junction temperature.



**Figure 70.** Optical light extractions according to the experimented technologies

Next, we looked at the spectral power distribution of each technique in Figure 71. While baseline LED system has shown less dense power distribution; decreasing the chip junction and especially the phosphor temperature resulted in a remarkably increase on the light extraction for 150 mA input current. Figure 70 shows the increase on the light output for varying input currents for each LED system. There, the superiority of remote phosphor LED system with immersion cooling has been proved once more again. While input power was not changed between baseline and remote phosphor liquid cooled system, the junction temperature has been decreased and also the light output has been increased about 53.3% in terms of efficiency (Lumen/Watt). The increase on light output mainly comes from the conversion efficiency enhancements at the chip and at the phosphor particles with decreasing temperature.





**Figure 71.** Spectral power distributions for proposed technologies

Moreover, the color maintenance results and peak wavelength shifts for the direct phosphor coated chip and remote phosphor system with and without liquid coolant prove the cooling effect on the light output. While the peak wavelength value for baseline system was measured as 544.99 nm, the shift at low temperature becomes to the right of spectrum (measured as 545.546 nm), against the blue corner of the CIE diagram after the same system has been cooled with immersion cooling. Moreover in the baseline system, the phosphor is placed on the LED chip and the phosphor temperature can be very close to the junction temperature of the LED. The conversion efficiency of the phosphor can drop with increasing temperature, thus there will be less yellow light from the phosphor and the overall LED color will shift against blue as observed from the wavelength shift. The color points of the remote-phosphor LED system have also shown the same wavelength shift trend against blue. But it is measured

smaller with the remote phosphor system since phosphor is far from the LED and heat stage. While the peak wavelength was measured as 544.210 nm for pure remote phosphor system, wavelength shift towards to right was measured as 544.542 nm once it was filed with liquid coolant between the phosphor and the LED chip. Although there was a shift observed, the amount of shift was not as much as measured at phosphor over chip system because of the phosphor temperature. As a result, the test of remote-phosphor systems in different configurations have shown increased light output with lower junction temperatures in comparison to other proposed techniques. When comparing remote phosphor with immersion cooling as a final user configuration, it has resulted as much as 53 percent more lumens than baseline system. Also, we have shown that the remote-phosphor system has a better color point stability over temperature; and this could be important depending on the specific lighting application requirement. Moreover, the blue light generated by the LED chip emits in all directions, as some of this light rays will interact with the phosphor on the LED chip and convert into light of different wavelengths, but mostly yellow light. These yellow lights are also emitted in all directions and some of them will head back to the LED chip and be absorbed, losing efficiency. In comparison, in a remote-phosphor system, the phosphor is placed far from the LED chip. As the blue light reaches the phosphor and the excitation-emission process occurs, the yellow light from the phosphor emits in all directions as in the white LED; but since the LED chip is far away, the chances of the yellow light hitting the chip and being absorbed are significantly lower. As long as the remote-phosphor system is well designed, the overall efficiency in a remote phosphor with immersion cooling system will be higher than the white LED. Moreover, in the baseline LED system where the phosphor is in direct contact with the LED chip, the phosphor can get very hot and lower its conversion efficiency. Furthermore, it can change the overall blue-to-yellow

light ratio and cause a color shift as explained previously. In contrast, the phosphor in the remote-phosphor is not affected by the LED temperature and thus can maintain a consistent conversion rate and overall color point.



## CHAPTER VII

### SUMMARY AND CONCLUSIONS

Possible fracture and ultimate device failures were intersected with large displacements inside the LED package due to the significant self-heating problems during LED operation. Furthermore, the elevated junction temperatures decrease the overall light conversion efficiency of the phosphor and leads to local hotspots and darkening of the phosphor particles. Moreover, the importance of understanding and evaluating the thermal resistance between the p-n junction and ambient have been clarified in details previously to reduce the junction temperature and improve device performance [4]. While, a major obstacle in estimating the thermal resistance for LEDs is determining the junction temperature especially for high power LEDs accurately, three main techniques; Forward Voltage, Raman Spectroscopy and Infrared (IR) imaging methods for determining the junction temperature were applied as proposed measurement techniques in the literature.

On the other hand, the need on the development of new technical solutions were explained, while the drawbacks and the inadequacy of the existing solutions, mentioned in previous sections. As the general aim for most of the previously explained cooling methods is to prevent the problems that are likely to occur due to the high heat formed in the chips during operation, local heating in the phosphor used for changing color in LEDs has lead the current study to immersion cooling with three different coating ideas (coated over chip, dispersed inside the liquid coolant as particles and remote coated under the dome) by evaluating their impact on LED performance.

Thus, topside immersion liquid cooling with optically-transparent liquids was applied to reduce the average chip temperatures and to improve the uniformity of chip and

phosphor temperature, leading to higher light extraction efficiencies. Furthermore, the study was involved in a number of key research areas such as liquid cooling with nano-phosphor fluids, optical losses due to phosphor white light conversion, computational modeling of heat transfer and optical behavior, and developing an experimental study to validate modeling results.

First, numerical models have been built with commercial computational software to capture the local temperature distributions over the LED light engine with a dome in the domain but especially over the LED chip. Moreover these studies have been applied for conduction, immersion cooled natural and forced convection cases individually. Later, attention has been turned into an opto-thermal evaluation for single and multi-phase heat transfer modes with dielectric fluids (LS5252, HFE7000, and silicone oil etc.).

While, a comparative study was made between air convection and liquid cooling, has clearly shown the cooling enhancement of dielectric liquids over air convection. Moreover, the vitality of temperature distribution over the dome surface has been explained with its effective share on the overall thermal management of the system. Thus, achieved higher heat transfer coefficients by dielectric liquids than air convection and conduction heat transfer with silicone has lead the researchers to focus on dielectric liquids. Also, forced convection heat transfer mechanism was applied beside of natural convection cooling. As a comparison purpose, the reference value of maximum temperature is set to a value that is obtained from natural convection case with 0.5 W chip powers and a dome filled with air. Thereafter, thermal resistances predicted in other cases were compared according to the reference value. While, 10% lower junction temperatures observed with conduction case; in case of air forced convection almost 80% lower thermal resistance values were obtained. Moreover, HFE 7200 has shown suitable thermal performance results with reasonable pumping power values.

After, evaluating the forced convection heat transfer mechanism for lighting systems, phase change heat transfer was in consideration due to the drawbacks have been mentioned in the previous section. Phase change heat transfer is very powerful method due to latent heat effect of the working fluids and provides several orders of magnitude higher performance than single phase heat transfer. However, the evaluation of the light extraction is more crucial than the thermal performance enhancement of multi-phase cooling due to bubbles occurs on the light path while functioning. Thus, a set of optical experimental studies were performed to evaluate light extraction before thermal performance evaluations. Then, they were compared with single phase natural convection heat transfer experiments utilized with LS5252, HFE 1230 and also silicone oil. Although the higher heat transfer performance expectations in multi-phase cooling, the negative impact of boiling on light extraction due to the phase change over the light path was observed. As a result, single phase liquid cooling has shown better optical light extraction with a reasonable thermal performance in comparison to boiling.

On the other hand, there are some performance differences among those liquids too, although the dielectric liquids have shown better cooling ability than air convection and silicone conduction. Thus, with a closer examination of analytical models, an ideal candidate liquid coolant has been found with a special understanding on the most effective fluid properties such, density, viscosity, volumetric expansion coefficient etc.

While NS13 and NS14 have presented lower heat removal behavior even than the existing dielectric liquids, NS15 has shown the best thermal performance. However, NS15 only computationally tested, thus experimental validation is required. Moreover, an optical study will make it much clear about the overall performance for such a lighting system.

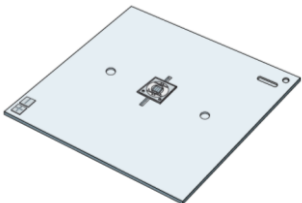
On the other hand, LED systems are also limited with their efficacy that is primarily due to the thermal, electrical and optical losses. Moreover, the resultant inefficiency in the phosphor manifests itself in heat and can further reduce the phosphor efficiency as suggested in the literature. All these factors in an LED optical package design can be quite challenging and also must be coupled with all the other factors including thermal design and reliability for the whole system to work at its optimum.

To capture the local temperature distributions over the LED light engine with a dome in the domain but phosphor at different positions; set of computational and experimental studies were utilized both for optical light extractions and also junction temperature measurements. Later, each technique has been compared to each other. Since the chip and the phosphor temperatures are affecting the conversion efficiency of both separately; the junction temperatures were also calculated individually for each step. First bare chip and pure silicone coated LED system have been tested and simulated for optical light output and junction temperatures for corresponding input power values as seen in Table 9 and Table 10. There a slight temperature increase has been observed while optical extraction stayed constant. After the coating, excited radiant power will pass through the phosphor particles where the 465 nm blue light is being converted to white light. While the phosphor is only capable of converting some portion of blue light to white light, rest of the radiant power remains inside the phosphor has been added to the phosphor layer as heat. The boundary conditions, input powers and corresponding results have also been presented in Table 11.

Accordingly, the junction temperature for phosphor coated bare LED package was being shown as the highest junction temperature in Table 11. Moreover, the CFD simulations enable the phosphor layer temperature measurements, where a slightly

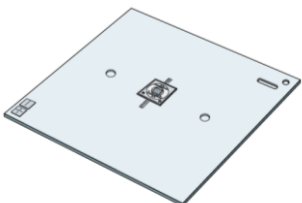
higher temperature than LED junction due to the extra heat generation because of lower phosphor conversion efficiency shown in Table 11.

**Table 9.** Both light extraction and junction temperature comparison for uncoated bare LED package



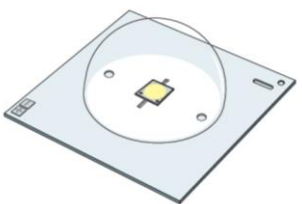
I (mA)	Optics		CFD		Experiment	
	Lumen (Lm)	CCT (K)	T <sub>Junction</sub> (°C)	T <sub>Phosphor</sub> (°C)	T <sub>Junction</sub> (°C)	T <sub>Phosphor</sub> (°C)
450	23,00	22000	57,95	-	58,33	-
300	17,20	22000	50,57	-	50,89	-
150	9,70	22000	44,53	-	44,06	-

**Table 10.** Both light extraction and junction temperature comparison for silicone coated LED package



I (mA)	Optics		CFD		Experiment	
	Lumen (Lm)	CCT (K)	T <sub>Junction</sub> (°C)	T <sub>Phosphor</sub> (°C)	T <sub>Junction</sub> (°C)	T <sub>Phosphor</sub> (°C)
450	23,00	22000	58,01	-	59,42	-
300	17,20	22000	50,61	-	51,03	-
150	9,70	22000	44,47	-	43,89	-

**Table 11.** Both light extraction and junction temperature comparison results for phosphor coated bare LED package

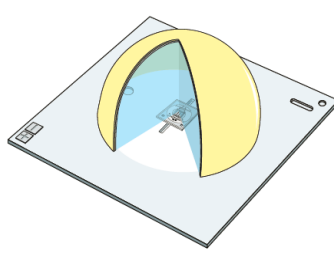


I (mA)	Optics		CFD		Experiment	
	Lumen (Lm)	CCT (K)	T <sub>Junction</sub> (°C)	T <sub>Phosphor</sub> (°C)	T <sub>Junction</sub> (°C)	T <sub>Phosphor</sub> (°C)
450	68,50	4036	60,05	60,08	64,45	-
300	52,60	4038	52,45	52,48	55,20	-
150	30,50	4051	45,71	45,74	45,51	-

On the other hand, Table 12 and Table 13 show the immersion cooling technologies with dielectric liquid filled glass dome including suspending phosphor, phosphor over chip and remote phosphor applications. It is clearly seen that moving away the phosphor layer from the LED chip decreases the junction temperatures.

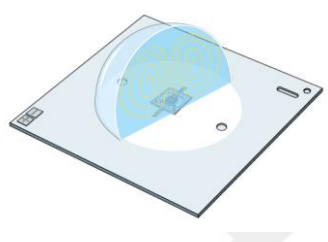


**Table 12.** Both light extraction and junction temperature comparison results for liquid cooled and remote phosphor coated LED package



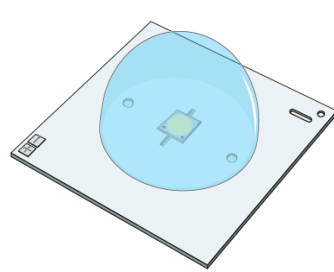
I (mA)	Optics		CFD		Experiment	
	Lumen (Lm)	CCT (K)	T <sub>Junction</sub> (°C)	T <sub>Phosphor</sub> (°C)	T <sub>Junction</sub> (°C)	T <sub>Phosphor</sub> (°C)
450	105,00	4102	57,84	-	56,87	-
300	78,93	4098	50,50	-	49,31	-
150	43,87	4091	44,40	-	42,79	-

**Table 13.** Both light extraction and junction temperature comparison results for liquid cooled with suspending phosphor particles



I (mA)	Optics		CFD		Experiment	
	Lumen (Lm)	CCT (K)	T <sub>Junction</sub> (°C)	T <sub>Phosphor</sub> (°C)	T <sub>Junction</sub> (°C)	T <sub>Phosphor</sub> (°C)
450	68,45	4005	58,70	-	61,60	-
300	49,36	3972	51,10	-	52,04	-
150	27,64	3967	44,84	-	43,31	-

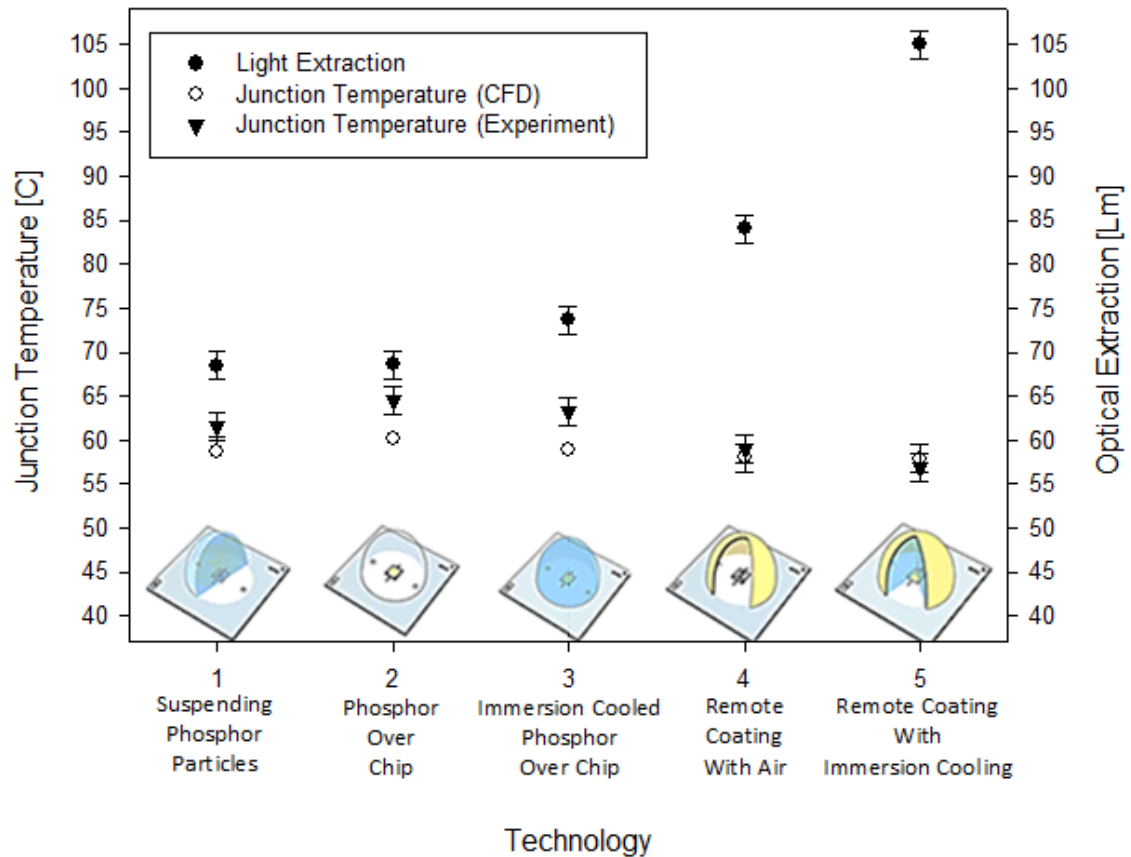
**Table 14.** Both light extraction and junction temperature comparison results for liquid cooled and phosphor coated LED package



I (mA)	Optics		CFD		Experiment	
	Lumen (Lm)	CCT (K)	T <sub>Junction</sub> (°C)	T <sub>Phosphor</sub> (°C)	T <sub>Junction</sub> (°C)	T <sub>Phosphor</sub> (°C)
450	73,60	4133	58,90	58,95	63,27	-
300	56,59	4134	51,76	51,78	54,53	-
150	32,77	4143	45,33	45,36	44,97	-

Moreover, CFD results have shown that the departed phosphor layer has practiced lower temperature in comparison to direct coating over the chip. While remote phosphor coating under the glass dome with dielectric liquid coolant has shown the lowest junction temperature, suspending phosphor case has shown slightly higher temperature. Even though immersion liquids have shown better cooling ability than air convection and silicone conduction, there are some performance differences among those coating technologies too as clearly seen in Figure 72. There the light extraction efficiency and

corresponding junction temperatures for each proposed technology have been presented. It is clearly seen from Figure 72 that with immersion cooling junction temperatures get lowered while light extraction was increased.

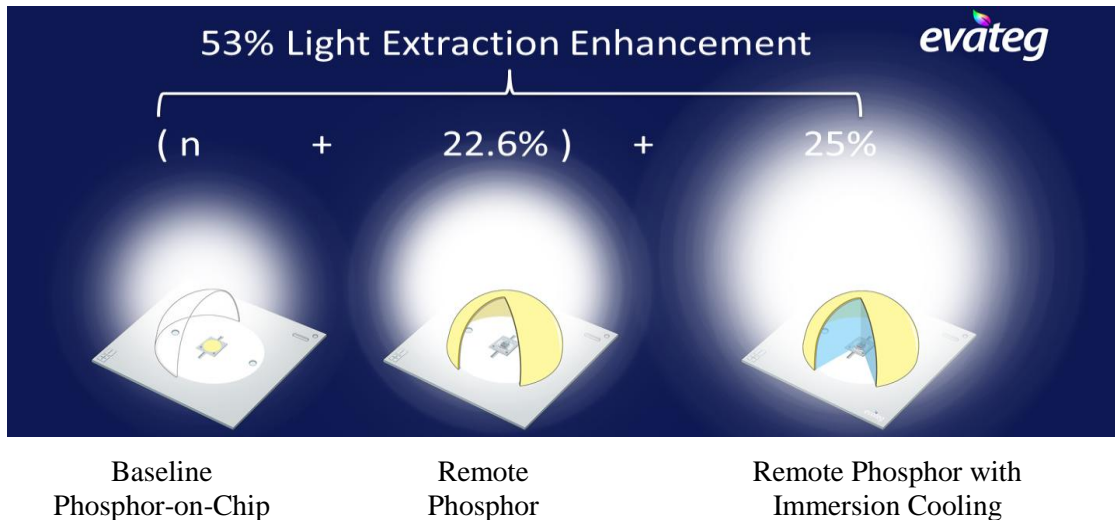


**Figure 72.** Both light extraction and junction temperature comparison results for all proposed technology

While the lumen output from the chosen baseline LED system (phosphor over chip coating), shows 68,5 lumens at 450mA with a single LED chip; %7 enhancement has been observed once it is immersed with dielectric coolant with 73,6 lumens light extraction. Although the dispersed system has shown lower junction temperature, optical light extraction were kept same with 68.45 lumens light output. This was thought due to that more blue light has passed through the phosphor & liquid medium without touching the suspending phosphor particles, thus with less light conversion efficiency. On the other hand, remote phosphor system has shown the better junction temperature and also better optical extraction in comparison to baseline. As all proposed

coating techniques were summarized in Figure 72, the remote phosphor system with dielectric liquid cooling has shown the highest light extraction with a light output of 105 lumens (%53,2 increase).

Moreover, the color maintenance results and peak wavelength shifts for the direct phosphor coated chip and remote phosphor system with and without liquid coolant prove the cooling effect on the light output. While the peak wavelength value for baseline system was measured as 544,99 nm, after the same system has been cooled with immersion cooling, the shift at low temperature is to the right (measured as 545,546 nm), against the blue corner of the CIE diagram. Moreover in the baseline system, the phosphor is placed on the LED chip and the phosphor temperature can be very close to the junction temperature of the LED. The conversion efficiency of the phosphor can drop with increasing temperature, thus there will be less yellow light from the phosphor and the overall LED color will shift against blue as observed from the wavelength shift. The color points of the remote-phosphor LED system have also shown the same wavelength shift trend against blue. But it is measured smaller with the remote phosphor system since phosphor is far from the LED and heat stage. While the peak wavelength was measured as 544,210 nm for pure remote phosphor system, once it was filled with liquid coolant between the phosphor and the LED chip, wavelength shift towards to right was measured as 544,542 nm. Although there was a shift observed, the amount of shift was not as much as measured at phosphor over chip system because of the phosphor temperature. Finally, the remote phosphor with immersion cooling LED system has resulted as much as 53 percent more lumens than baseline system as seen in Figure 73; when comparing remote phosphor with immersion cooling. Also, we have shown that the remote-phosphor has a better color point stability over temperature; this could be important depending on the specific lighting application requirement.



**Figure 73.** Visualization of invented technology

The main factor on the light output increase in remote phosphor with immersion liquid cooled LED system can be shown as the decrease on the chip and phosphor temperature. Moreover, the blue light generated by the LED chip emits in all directions, some of this light rays will interact with phosphor on chip and convert into light of different wavelengths, but mostly yellow light. These yellow lights are also emitted in all directions and some of them will head back to chip and be absorbed, losing efficiency. In comparison, in a remote-phosphor system, the phosphor is placed far from the LED chip. As the blue light reaches to the phosphor, the excitation-emission process occurs. Yellow light emits in all direction as in the white LED; but since the LED chip is far away, the chances of the yellow light hitting back the chip and being absorbed is significantly lower. As long as the remote-phosphor system is well designed, the overall efficiency in a remote phosphor with immersion cooling system will be higher than white LEDs. Moreover, baseline LED system can get very hot since the phosphor is in direct contact with the LED chip. Thus it can lower its conversion efficiency and cause a color shift. In contrast, the phosphor in the remote-phosphor system is not affected by the LED temperature and can maintain a consistent conversion rate.

## CHAPTER VIII

### SUGGESTIONS FOR FUTURE WORK

This thesis work provides fundamental understanding of the local hot spots in LED systems and the implications of direct immersion cooling over thermal and optical performance for both bare and phosphor coated LEDs. The understanding gained from this thesis work can be used to cool LED lamps in an efficient manner, to increase the durability and the amount of light to be obtained from LED lamps, and to reduce the weight thereof. In addition to summarizing the insights gained from our experiments and modeling, we outline future directions in this chapter.

#### 8.1 Summary of the Present Work

A set of experimental and computational studies were applied in the current thesis. Desired LED performances of the current available and proposed technologies were compared to each other. First, well-defined test devices were fabricated which allow for different coating and liquid filling approaches. Unlike past studies, our experimental characterization is immersed liquid cooling with possible different coating technologies. This liquid cooled integrated remote phosphor experiments were achieved after a set of applications was conducted within the previous liquid cooling studies and different coating technologies, individually. Consequently, our final experiments characterize the immersion liquid cooled LED packages with proposed different coating techniques.

We also developed a set of computational models to predict and validate the experimental findings. The models are developed by conserving mass, momentum, and energy in a control volume of the LED package with different proposed cooling

methods. The models predictions agree reasonably well with our first individual liquid cooling experiments as shown in conclusions. Encouraged by the good agreement between models and experiments, we further developed an immersed cooled and phosphor coated schemes. These studies have shown that we can cool down the LED package within reasonable thermal levels by immersion cooling for each different coating technique. In addition to that, optical measurements have shown a significant optical light extraction enhancement with immersed liquid cooling system. We extended the above characterization with immersion liquid cooled integrated with different phosphor coating ideas (coated over chip, dispersed inside the liquid coolant as particles and remote coated under the dome). While, the current phosphor over chip application has shown higher junction temperatures beside of lower conversion efficiency and possible color shifts since the phosphor is in direct contact with the LED chip; the phosphor in the remote coating system is not affected by the LED temperature and thus maintained a consistent conversion rate and overall color point. Moreover, the remote phosphor with immersion cooling system has extended the Lumen Extraction Limits of White LEDs in Excess of 53%, as long as the remote-phosphor system is well designed. Current study has demonstrated a new optical extraction technology for RGB and phosphor coated LEDs to extend the lumen extraction limits over 53%. An extensive research including computational and experimental validation has been performed. While conventional white light LED packages consist of silicone with or without phosphor mixture over the chip or remote phosphor, causing some significant optical losses due to refractive index mismatching, poor thermal management, local chip and phosphor heating issues resulting poor light extraction and reduced lifetime. This proposed and experimentally validated novel thermal management idea enhances the light extraction by locally cooling chip and phosphor, decreasing the chip junction

and phosphor temperatures with a carefully designed and demonstrated optical approach. While, the system comparison between the baseline (conventional RGB and white light LED packages) with air filled and fully silicone cured remote phosphor LED packages have shown an increase over the lumen output as 23%, 40%, respectively; this study has developed a novel approach enabling a 53% improvement over the conventional approach with opto-thermal fluid filled LED package.

This proven innovative idea brings the following key advantages over conventional LED approaches;

- Provides an effective cooling of LED light engines abating local temperature non-uniformities
- Reduces the thermal resistance between the chip and ambient significantly leading to high lumen extraction
- Key enabler technology for advanced IoT features for lighting systems
- Lowers the chip junction and phosphor temperatures with an exceptional increase in the lumen output and lifetime
- Higher conversion efficiency in phosphor with decreasing temperature
- Eliminates color shifts due to temperature overshoots
- Enables a better refractive index matching reducing optical losses
- Simplifies complex lighting system designs

## **8.2 Future Work**

The current study explains that we can improve the light extraction efficiency and thermal performance of LED systems by optimizing phosphor coating position and cooling method. The models and experiments show that the proposed innovative immersion cooled remote coating idea is suitable for both optical and thermal performance of an LED system. While the dielectric liquid coolants can provide on-

demand cooling; new approaches and ideas which may broaden the current research more on the optical and thermal enhancements. A brief list of suggestions for future work can be given as the following;

- Immersion cooling has shown as the most appropriate cooling mechanism for the problem in the current work for LEDs. Although, a special focus has been given to the dielectric coolant liquid in the current work; more can be given as listed below, since dielectric coolant has major importance in the cooling mechanism.
  - As theoretically shown in the current work, new possible dielectric coolants can be experimentally investigated according to the required performances. After system level characterization, it can also be used for cooling the next generation of high performance electronics.
  - Moreover, the candidate liquid coolants were studied with varying physical properties to meet the thermal performance expectations. However, it can be coupled with optical performance expectations too by controlling some other physical properties such as refractive index, transparency, etc.
  
- On the other hand, different approaches were tried to benefit from the thermal performance of boiling heat transfer, since it has shown inappropriate behavior for lighting applications.
  - It can be applied from the back side of the PCB, while single phase immersion liquid cooling is still active from the top side.
  - Moreover, two unmixing dielectric liquid have been used as a solution to the optical degradation problem in boiling heat transfer. There the liquid 1 with



higher density was objected to have higher saturation temperature; while the liquid 2 with lower density has lower saturation temperature. Thus, the liquid 1 will never change its phase but directly transport the undesired heat energy from LED die to the liquid 2 which will evaporate and condense at lower temperatures. But this idea only possible with downward lighting applications, and different liquids need to be researched according to the power level of the overall lighting system.

- Some part of the current work focuses on the coating technology and different approaches. Although, the effect of each idea has been successfully explained, much effort can be given on purely coating experiments.
  - The proposed phosphor coating approaches in the current work can be enlarged with varying thicknesses and phosphor types for different CCT and CRI values,
  - In the current work, 7-15 $\mu$ m diameter phosphor particles were used. The size of the particles would be changed and their effect on the light output and thermal management can be searched.
  - Beside of the yellow phosphor that is chosen for this study, different colors of phosphors would be nice to compare with similar coating techniques to see the effectiveness of the proposed coating ideas for different applications.
  - 2 cm diameter glass dome has been used in the current study. According to the experiments conducted, the results were quite satisfying. But the optimization of this glass dome size under different power conditions might bring new ideas to the LED packaging industry.

## REFERENCES

- [1] Arik M., Setlur A., Weaver S., and Shiang J. J. "Energy Efficient Solid State Lighting Systems." (2012).
- [2] Steigerwald D.A., Bhat J.C., Collins D., Fletcher R.M., Holcomb M.O., Ludowise M.J., "Illumination with solid state lighting technology", IEEE J Sel Top Quant Electron;2:310–20, (2002).
- [3] Tamdogan E., Arik M., and Dogruoz M. B. "Direct Liquid Cooling of High Flux LED Systems: Hot Spot Abatement." International Technical Conference and Exhibition on Packaging and Integration of Electronic and Photonic Microsystems, (2013).
- [4] Samudra Electronic System Pvt. Ltd., <http://www.samudraled.com>
- [5] Naoya M., Yusuke K., Yohtaro U., "Digital Color Shift Keying With Multicolor LED Array", Photonics Journal IEEE, vol. 8, pp. 1-13, 2016, ISSN 1943-0655.
- [6] Hye Oh J., Ji Yang S., Rag Do Y., "Light: Science and Applications", London 3.2 : e141, (Feb 2014).
- [7] Pryde J. R., Whalley D. C. and Malalasekera W., "A review of LED technology trends and relevant thermal management strategies," Fourteenth Intersociety Conference on Thermal and Thermomechanical Phenomena in Electronic Systems (ITherm), Orlando, FL , pp. 31-38, (2014).
- [8] Klaus D. J., Robin W. Mills, A brief history of LED photopolymerization, Dental Materials, Volume 29, Issue 6, Pages 605-617, (2013).
- [9] Isamu A., "Key inventions in the history of nitride-based blue LED and LD, Journal of Crystal Growth", Volume 300, Issue 1, Pages 2-10, (2007).
- [10] Holonyak N., Bevaqua S. F., Appl. Phys. Lett. 1, 82 (1962).
- [11] Bergh A. A., Dean P. J., "Light Emitting Diodes", Clarendon Press, Oxford (1976).
- [12] Holonyak, N. "From Transistors to Lasers and Light-Emitting Diodes", MRS Bulletin, 30(7), 509-515, (2005).
- [13] Nakamura S., Senoh M., Iwasa N., Nagahama S., Yamaka T., Mukai T., Jpn. J. Appl. Phys. 34, L1332 (1995).
- [14] United States Secretary of Energy,  
<<https://energy.gov/articles/history-light-bulb>>.
- [15] Arik M., Petroski J. and Weaver S., "Thermal challenges in the future generation solid state lighting applications: light emitting diodes," ITherm 2002. Eighth Intersociety Conference on Thermal and Thermomechanical Phenomena in Electronic Systems (Cat. No.02CH37258), pp. 113-120, (2002).

- [16] Schubert EF. "Light-emitting diodes", 2nd ed. New York: Cambridge University Press; [chapter 18], (2006).
- [17] King M. "Characteristics of high brightness LEDs", Electronic design online conference series, session 5; p. 1–16, June 22nd, (2010).
- [18] Timinger, A. and H. Ries. "Street-Lighting with LEDs.", Proceedings of SPIE - The International Society for Optical Engineering, v 7103.: 71030H-1 – 71030H-6, (2008).
- [19] City of Ann Arbor. "LEDs: Ann Arbor "Lights" the Way to Energy Savings." Green Sheet, City of Ann Arbor Environmental News September (2008). <[http://www.a2gov.org/government/publicservices/systems\\_planning/Document s/publicservices\\_systems\\_envtlcoord\\_greennews\\_ledlights\\_2008\\_09\\_08.pdf](http://www.a2gov.org/government/publicservices/systems_planning/Document%20s/publicservices_systems_envtlcoord_greennews_ledlights_2008_09_08.pdf)>.
- [20] Arik M., Utturkar Y., and Weaver S.. "Immersion cooling of light emitting diodes." In Thermal and Thermomechanical Phenomena in Electronic Systems (ITherm), 12th IEEE Intersociety Conference on, pp. 1-8. IEEE, (2010).
- [21] U.S. Department of Energy. "LED Basics." U.S. Department of Energy. PNNL-SA-58429, November (2009)a. <[http://apps1.eere.energy.gov/buildings/publications/pdfs/ssl/led\\_basics.pdf](http://apps1.eere.energy.gov/buildings/publications/pdfs/ssl/led_basics.pdf)>.
- [22] Cheng, J. et al. "Cooling Performance of Silicon-Based Thermoelectric Device on High Power LED." International Conference on Thermoelectrics, ICT, Proceedings.: 53–56, (2005).
- [23] Arik, M., and Weaver S. "Effect of Chip and Bonding Defects on the Junction Temperatures of High-Brightness Light-Emitting Diodes." Optical Engineering 44.11, (2005).
- [24] Weng, C, and B. Abbott. "Advanced Thermal Enhancement and Management of LED Packages." International Communications in Heat and Mass Transfer 36.3 (2009): 245–248. Web.
- [25] Yuan, L., et al. "Thermal Analysis of High Power LED Array Packaging with MicroChannel Cooler." 7th International Conference on Electronics Packaging Technology, ICEPT '06, (2007).
- [26] Luo, X. et al. "Design and Optimization of Horizontally-Located Plate Fin Heat Sink for High Power LED Street Lamps." Proceedings - Electronic Components and Technology Conference.: 854–859, (2009)a.
- [27] Arik M., Weaver S., Becker C., Hsing M., Srivastava A., "Effects of Localized Heat Generations Due to the Color Conversion in Phosphor Particles and Layers of High Brightness Light Emitting Diodes", ASME. International Electronic Packaging Technical Conference and Exhibition, Volume 1 ():611-619, (2003).
- [28] Cheng, Q. "Thermal Management of High Power LED Package." Electronic Packaging Technology, 2007. ICEPT, 8th International Conference on Electronic Packaging Technology, (2007).

- [29] Luo, X. et al. "Thermal Analysis of an 80 W Light-Emitting Diode Street Lamp." *IET Optoelectronics* 1.5: 191–196, (2007).
- [30] Nuttall, D. R., R. Shuttleworth, and G. Routledge. "Design of a LED Street Lighting System." *IET Conference Publications*: 436–440, (2008).
- [31] Petroski, J., Arik, M., and Gursoy, M., "Optimization of piezoelectric oscillating fan-cooled heat sinks for electronics cooling," *IEEE Trans. Components Packag. Technol.*, 33(1), pp. 25–31, (2010).
- [32] Kimber, M., and Garimella, S. V., "Measurement and prediction of the cooling characteristics of a generalized vibrating piezoelectric fan," *Int. J. Heat Mass Transf.*, 52(19-20), pp. 4470–4478, (2009).
- [33] Açıkalın, T., Garimella, S. V., Raman, A., and Petroski, J., "Characterization and optimization of the thermal performance of miniature piezoelectric fans," *Int. J. Heat Fluid Flow*, 28(4), pp. 806–820, (2007).
- [34] Petroski, J., Arik, M., and Gursoy, M., "Optimization of piezoelectric oscillating fan-cooled heat sinks for electronics cooling," *IEEE Trans. Components Packag. Technol.*, 33(1), pp. 25–31, (2010).
- [35] Bar-Cohen A., Wang P., "On-chip hot spot remediation with miniaturized thermoelectric coolers", *Micrograv. Sci. Technol*, vol. 21, no. 1, pp. 351-359, Aug. (2009).
- [36] Chu K.-H., et al., "Structured surfaces for enhanced pool boiling heat transfer," *Appl. Phys. Lett.*, vol. 100, p. 241603, (2012).
- [37] Lu M.-C., et al., "Critical heat flux of pool boiling on Si nanowire array-coated surfaces," *Int. J. Heat Mass Transfer*, vol. 54, pp. 5359-5367, (2011).
- [38] Li C. and Peterson G., "Experimental study of enhanced nucleate boiling heat transfer on uniform and modulated porous structures," *Front. Heat Mass Transfer*, vol. 1, (2010).
- [39] Chen R., et al., "Nanowires for enhanced boiling heat transfer," *Nano Lett.*, vol. 9, pp. 548-553, (2009).
- [40] Tamdogan E., and Arik M., "Numerical comparisons of passive and active cooling strategies on LEDs with optical concerns: Natural, forced and immersion cooling." *ICHMT DL*, (2014).
- [41] Cheung, C., Noska B., and Heide K. V. D., "Comparison of Passive and Active Cooling Effectiveness." *LED Professional Review*: 42–46. May/June (2009).
- [42] Wilcox, M. "Helping LEDs Keep Their Cool." *Photonics Spectra* 42.11: 64–66, (2008).
- [43] Christensen, A., and Graham S., "Thermal Effects in Packaging High Power Light Emitting Diode Arrays." *Applied Thermal Engineering* 29.2: 364–371,

- (2009).
- [44] Christensen, A., Ha M., and Graham S., "Thermal Management Methods for Compact High Power LED Arrays." Proceedings of SPIE—The International Society for Optical Engineering 6669, (2007).
  - [45] You J. P., He Y., and Shi F. G., "Thermal Management of High Power LEDs: Impact of Die Attach Materials." IMPACT: Microsystems, Packaging, Assembly and Circuits Technology.: 239–242, (2007).
  - [46] Kim, H. et al. "Thermal Transient Characteristics of Die Attach in High Power LED PKG." Microelectronics and Reliability 48.3: 445–454, (2008).
  - [47] Chen, K. C. et al. "Thermal Management and Novel Package Design of High Power Light-Emitting Diodes." Electronic Components and Technology Conference, 2008 Proceedings 58th.: 795–797, (2008).
  - [48] Arik, M. et al. "Thermal Management of LEDs: Package to System." Proceedings of SPIE—the International Society for Optical Engineering 5187: 64–75, (2004).
  - [49] Chi, W. et al. "Analysis of Thermal Performance of High Power Light Emitting Diodes Package." 10th Electronics Packaging Technology Conference, EPTC.: 533–538, (2008).
  - [50] Zhang K., Y. Chai, M. M. F. Yuen, D. G. W. Xiao, and P. C. H. Chan. "Carbon Nanotube Thermal Interface Material for High-Brightness Light-Emitting-Diode Cooling." Nanotechnology 19.21: 1–8, (2008).
  - [51] Ryu J.H., Choi D.H., Kim S.J., "Three-dimensional numerical optimization of a manifold microchannel heat sink", International Journal of Heat and Mass Transfer, Volume 46, Issue 9, Pages 1553-1562, (2003).
  - [52] Li J. and G. P. Peterson, "Geometric optimization of a micro heat sink with liquid flow," in IEEE Transactions on Components and Packaging Technologies, vol. 29, no. 1, pp. 145-154, March (2006).
  - [53] Knight R. W., Hall D. J., Goodling J. S. and Jaeger R. C., "Heat sink optimization with application to microchannels," in IEEE Transactions on Components, Hybrids, and Manufacturing Technology, vol. 15, no. 5, pp. 832-842, Oct (1992).
  - [54] Culham J. R. and Muzychka Y. S., "Optimization of plate fin heat sinks using entropy generation minimization," in IEEE Transactions on Components and Packaging Technologies, vol. 24, no. 2, pp. 159-165, June (2001).
  - [55] Huang, B. et al. "Development of High-Power LED Lighting Luminaires Using Loop Heat Pipe." Journal of Light & Visual Environment 32.2: 148–155, (2008).
  - [56] Huang, H.-S. et al. "Experimental Investigation of Vapor Chamber Module Applied to High-Power Light-Emitting Diodes." Experimental Heat Transfer

22.1.: 26–38, (2009).

- [57] Li, F., Chen D., Song X., and Chen Y., “Numerical Simulation on Heat Pipe for High Power LED Multi-Chip Module Packaging.” International Conference on Electronic Packaging Technology and High Density Packaging, ICEPT-HDP.: 393–397, (2009)b.
- [58] Tuckerman, D. B., and Pease, R. F., "Ultrahigh Thermal Conductance Microstructures for Cooling Integrated Circuits," Proceedings of the 32nd Electronics Components Conference, pp. 145-149, (1981).
- [59] Incropera, F. P., Kerby, J. S., Moffatt, D. F., and Ramadhyani, S., "Convection Heat Transfer From Discrete Heat Sources in a Rectangular Channel," Int. J. of Heat and Mass Transfer, Vol. 29, pp. 1051-1058, (1986).
- [60] Samant, K. R., and Simon, T. W., "Heat Transfer From a Small, High-Heat-Flux Patch to a Subcooled Turbulent Flow," Proceedings of the AIAA/ASME Heat Transfer and Thermophysics Conf, Boston, MA, (1986).
- [61] Ramadhyani, S., and Incropera, F. P., "Forced Convection Cooling of Discrete Heat Sources With and Without Surface Enhancement," Proceedings of the International Symposium on Cooling Technology for Electronic Equipment, Honolulu, HI, pp. 249-264, (1987).
- [62] Arik M., Kulkarni K. S., Royce C. and Weaver S., "Developing a standard measurement and calculation procedure for high brightness LED junction temperature," ITherm, 2014 IEEE Intersociety Conference on, Orlando, FL, pp. 170-177, (2014).
- [63] Jayasinghe L., Dong T., and Narendran N., “Is the thermal resistance coefficient of high-power LEDs constant?” Proc. SPIE 6669, Seventh International Conference on Solid State Lighting, 666911, September 17, (2007).
- [64] Todorov D.G., Kapisazov L.G., “LED Thermal Management”, Proc. Electronics, 24-26 September, Sozopol, Bulgaria, pp. 139-144, (2008).
- [65] Tamdogan E. and Arik M., “Natural convection immersion cooling and optical degradation of liquid cooled LED systems”, ASME Journal of Electronics Packaging, Vol. 137, Issue 4, November (2014).
- [66] Shailesh K.R., Kurian C. P., and Kini S. G., "Junction temperature measurement of a LED street light using forward voltage method", International Conference on Advances in Electronics Computers and Communications, (2014).
- [67] Xi Y., and Schubert E. F., “Junction-temperature measurements in GaN UV light-emitting diodes using the diode forward voltage”, International Journal of High Speed Electronics and Systems, Vol. 14, No. 3, pp. 708-713, (2004).
- [68] ANSYS Fluent 12.0, “Theory Guide“, April (2009).

- [69] Arik M., Uttukar Y., Weaver S., “Immersion Cooling of Light Emitting Diodes”, (2005).
- [70] 3M™ Novec™ Engineered Fluid HFE-7200. <http://www.3m.com>
- [71] Xi Y., and Schubert E. F., “Junction-temperature measurements in GaN UV light-emitting diodes using the diode forward voltage”, International Journal of High Speed Electronics and Systems, Vol. 14, No. 3, pp. 708-713, (2004).
- [72] Yuruker U.S., Tamdogan E., and Arik M., “An Experimental and Computational Study on Efficiency of White LED Packages with a Thermo-caloric Approach”, IEEE Transactions on Components, Packaging, and Manufacturing Technology, PP (99):1-7, (2017).
- [73] Chonko J., “Using Forward Voltage to Measure Semiconductor Junction Temperature”, Keithley Instruments, Inc., no. 2681, pp. 1-3, (2006).
- [74] Arik M. and Weaver S., “Chip Scale Thermal Management of High Brightness LED Packages”, SPIE – The International Society of Optical Engineering Annual Conference, Denver, August (2004).
- [75] JEDEC Standard JESD51-50, “Overview of Methodologies for the Thermal Measurement of Single- and Multi-Chip, Single- and Multi-PN Junction Light-Emitting Diodes (LEDs)”, April (2012).  
[www.jedec.org/sites/default/files/docs/jesd51-50.pdf](http://www.jedec.org/sites/default/files/docs/jesd51-50.pdf)
- [76] O. Ueda, S. J. Pearton, Materials and Reliability Handbook for Semiconductor Optical and Electron Devices, ISBN: 978-1-4614-4336-0 (Print) 978-1-4614-4337-7 (Online).
- [77] Choi S., Heller E. R., Dorsey D., Vetry R., and Graham S., “The Impact of Bias Conditions on Self-Heating in AlGaIn/GaN HEMTs”, IEEE Transactions on Electron Devices, Vol. 60, NO. 1, (2013).
- [78] Pavlidis G., Pavlidis S., Heller E. R., Moore E. A., Vetry R., Graham S., “Characterization of AlGaIn/GaN HEMTs using Gate Resistance Thermometry”, December 2016, IEEE Transactions on Electron Devices; PP(99):1-6, (2016).
- [79] Optotherm, Inc., [www.optotherm.com](http://www.optotherm.com)
- [80] Nguyen T.T., Jiun P.Y., and Frank G. S., "Effect of Phosphor Particle Size on Luminous Efficacy of Phosphor-Converted White LED," J. Lightwave Technol. 27, 5145-5150 (2009).
- [81] Xing Y., Frank W.M., David J.P., Martin F.S., Jong K.K., Jaehee C. and Fred S., “Refractive-Index-Matched Indium–Tin-Oxide Electrodes for Liquid Crystal Displays“, Published 7, The Japan Society of Applied Physics, December (2009).
- [82] TSE (Power Supply) and Tubitak UME (Spektrometer).
- [83] <http://www.cormusa.org/uploads/Scharpf-2015.pdf>

- [84] GUM, ISO. "Guide to the Expression of Uncertainty in Measurement, (1995), with Supplement 1, Evaluation of measurement data, JCGM 101: 2008." Organization for Standardization, Geneva, Switzerland (2008).
- [85] Webb P. W., "Thermal imaging of electronic devices with low surface emissivity," IEE Proc. G, Circuits, Devices Syst., vol. 138, no. 3, pp. 390–400, June (1991).
- [86] Vollmer M. and Möllmann K.-P., "Infrared Thermal Imaging: Fundamentals, Research and Applications", (2010).





## APPENDIX A

### UNCERTAINTY ANALYSIS

An analytical study was conducted in order to determine the measurement uncertainty for  $T_j$ ,  $V_f$ ,  $P$ ,  $\Phi_e$  and  $\lambda_{Dom}$ . Contribution of each component to the uncertainty calculation is made from the calibration certificates of used devices, their reference documents, laboratory and experiment records. Uncertainties for the oven system and source meter are added by considering the observations and standard deviations calculated in measurements.

For the integrating sphere measurements of radiant power and dominant wavelength, the uncertainty value for spectrometer, SCL 1400 lamp, LPS 150 power supply and Agilent power supply are taken from the calibration certificates given by the certified institutions [82], while uncertainty values of lifetime of SCL 1400 lamp, spectrometer nonlinearity, spectrometer drift, spectrometer stray light, sphere near field absorption and sphere non-uniformity are obtained from a guide presented by Labsphere [83]. Variations in temperature and air flow in the laboratory are also taken into consideration in calculations. The expanded uncertainties for individual Luminous flux, CCT, and CRI measurements are calculated according to the “Guide to the Expression of Uncertainty in Measurement (GUM, 2008)” within a 95% confidence interval, for which the uncertainties are given in Table 15, Table 16, and Table 17 [84].

Moreover, the propagated uncertainty for the junction temperature measurement of a blue chip is also given in Table 18. Results have shown that the junction temperature calculation is made with Forward Voltage Change Method below the range stated in the previous study.

**Table 15.** Integrating sphere – **Luminous flux (Lm)** measurement uncertainty

	Given or Expected Data	Distribution Type	Standard Measurement Uncertainty	Sensitivity Constant	Uncertainty Constant	Variant
<b>Reference Device or Related Uncertainty Components</b>						
Spectrometer (Wavelength Calibration)	0,7	Normal	0,35	1	0,35	0,1225
SCL 1400 Lamp	1,00	Normal	0,5	1	0,5	0,25
LPS 150 Power Supply (Direct Voltage)	0,005	Normal	0,0025	1	0,0025	0,00000625
LPS 150 Power Supply (Direct Current)	0,005	Normal	0,0025	1	0,0025	0,00000625
LPS 100 Power Supply (Direct Voltage)	0,005	Normal	0,0025	1	0,0025	0,00000625
LPS 100 Power Supply (Direct Current)	0,005	Normal	0,0025	1	0,0025	0,00000625
Agilent Power Supply (AC Voltage)	0,06	Normal	0,03	1	0,03	0,0009
Agilent Power Supply (Frequency)	0,01	Normal	0,005	1	0,005	0,000025
SCL 1400 Lamp Lifetime Uncertainty Constant	3,2332E-05	Rectangle	1,8667E-05	1	1,8667E-05	3,4844E-10
Spectrometer Non-linearity Uncertainty Constant	0,06	Normal	0,03	1	0,03	0,0009
Spectrometer Light Leakage Uncertainty Constant	0,05	Rectangle	0,02886751	1	0,02886751	0,00083333
Spectrometer Drift Based Uncertainty	0,05	Normal	0,025	1	0,025	0,000625
Sphere Space Absorptivity Uncertainty Constant	0,5	Normal	0,25	1	0,25	0,0625
Sphere Non-uniformity Uncertainty Constant	0,2	Normal	0,1	1	0,1	0,01
<b>Method Based Uncertainty</b>						
Temperature Based Uncertainty	0,77558493	Rectangle	0,44778417	1	0,44778417	0,20051066
Air Velocity Based Uncertainty	0	Rectangle	0	1	0	0
Experiment Repeatability Based Uncertainty	2,51197134	Normal	1,25598567	1	1,25598567	1,5775
						2,61022598
<b>Overall Measurement Uncertainty:</b>			1,61561938			
<b>Expanded Measurement Uncertainty:</b>			3,23123876			

**Table 16.** Integrating sphere – CCT measurement uncertainty

	Given or Expected Data	Distribution Type	Standard Measurement Uncertainty	Sensitivity Constant	Uncertainty Constant	Variant
<b>Reference Device or Related Uncertainty Components</b>						
Spectrometer (Wavelength Calibration)	0,7	Normal	0,35	1	0,35	0,1225
SCL 1400 Lamp	0,23	Normal	0,115	1	0,115	0,013225
LPS 150 Power Supply (Direct Voltage)	0,005	Normal	0,0025	1	0,0025	6,25E-06
LPS 150 Power Supply (Direct Current)	0,005	Normal	0,0025	1	0,0025	6,25E-06
LPS 100 Power Supply (Direct Voltage)	0,005	Normal	0,0025	1	0,0025	6,25E-06
LPS 100 Power Supply (Direct Current)	0,005	Normal	0,0025	1	0,0025	6,25E-06
Agilent Power Supply (AC Voltage)	0,06	Normal	0,03	1	0,03	0,0009
Agilent Power Supply (Frequency)	0,01	Normal	0,005	1	0,005	0,000025
SCL 1400 Lamp Lifetime Uncertainty Constant	3,2332E-05	Rectangle	1,8667E-05	1	1,87E-05	3,48E-10
Spectrometer Non-linearity Uncertainty Constant	0,06	Normal	0,03	1	0,03	0,0009
Spectrometer Light Leakage Uncertainty Constant	0,05	Rectangle	0,02886751	1	0,028868	0,000833
Spectrometer Drift Based Uncertainty	0,05	Normal	0,025	1	0,025	0,000625
Sphere Space Absorptivity Uncertainty Constant	0,5	Normal	0,25	1	0,25	0,0625
Sphere Non-uniformity Uncertainty Constant	0,2	Normal	0,1	1	0,1	0,01
<b>Method Based Uncertainty</b>						
Temperature Based Uncertainty	0,77558493	Rectangle	0,44778417	1	0,447784	0,200511
Air Velocity Based Uncertainty	0	Rectangle	0	1	0	0
Experiment Repeatability Based Uncertainty	3,46	Normal	1,73	1	1,73	2,9929
						9,016845
<b>Overall Measurement Uncertainty:</b>	3,002806195					
<b>Expanded Measurement Uncertainty:</b>	6,005612389					

**Table 17. Integrating sphere – CRI measurement uncertainty**

	<b>Given or Expected Data</b>	<b>Distribution Type</b>	<b>Standard Measurement Uncertainty</b>	<b>Sensitivity Constant</b>	<b>Uncertainty Constant</b>	<b>Variant</b>
<b>Reference Device or Related Uncertainty Components</b>						
Spectrometer (Wavelength Calibration)	0,7	Normal	0,35	1	0,35	0,1225
SCL 1400 Lamp	1,3	Normal	0,65	1	0,65	0,4225
LPS 150 Power Supply (Direct Voltage)	0,005	Normal	0,0025	1	0,0025	0,00000625
LPS 150 Power Supply (Direct Current)	0,005	Normal	0,0025	1	0,0025	0,00000625
LPS 100 Power Supply (Direct Voltage)	0,005	Normal	0,0025	1	0,0025	0,00000625
LPS 100 Power Supply (Direct Current)	0,005	Normal	0,0025	1	0,0025	0,00000625
Agilent Power Supply (AC Voltage)	0,06	Normal	0,03	1	0,03	0,0009
Agilent Power Supply (Frequency)	0,01	Normal	0,005	1	0,005	0,000025
SCL 1400 Lamp Lifetime Uncertainty Constant	3,2332E-05	Rectangle	1,8667E-05	1	1,8667E-05	3,4844E-10
Spectrometer Non-linearity Uncertainty Constant	0,06	Normal	0,03	1	0,03	0,0009
Spectrometer Light Leakage Uncertainty Constant	0,05	Rectangle	0,02886751	1	0,02886751	0,00083333
Spectrometer Drift Based Uncertainty	0,05	Normal	0,025	1	0,025	0,000625
Sphere Space Absorptivity Uncertainty Constant	0,5	Normal	0,25	1	0,25	0,0625
Sphere Non-uniformity Uncertainty Constant	0,2	Normal	0,1	1	0,1	0,01
<b>Method Based Uncertainty</b>						
Temperature Based Uncertainty	0,77558493	Rectangle	0,44778417	1	0,44778417	0,20051066
Air Velocity Based Uncertainty	0	Rectangle	0	1	0	0
Experiment Repeatability Based Uncertainty	0,14	Normal	0,07	1	0,07	0,0049
						<b>0,23774999</b>
<b>Overall Measurement Uncertainty:</b>	0,487596136					
<b>Expanded Measurement Uncertainty:</b>	0,975192271					

**Table 18.** Electrical, thermal and optical readings from experiments for blue chip

Parameters	Operating Currents (mA)		
	150 mA	300 mA	450 mA
V <sub>f</sub> (V)	2.4700	2.4501	2.4265
T <sub>j</sub> (°C)	32.31	44.04	57.93
P (Watts)	0.440	0.920	1.450
Φ <sub>e</sub> (Watts)	0.201	0.363	0.493
Q (Watts)	0.239	0.557	0.947
λ <sub>Dom</sub> (nm)	455.88	455.60	455.56

**Table 19.** Uncertainty analysis for the junction temperature of blue chip

No	Component	Symbol	Standard Uncertainty	Type	Sensitivity Coefficient	Contribution
1	Initial junction temperature	T <sub>j0</sub>	0.2	A	1	0.2
2	Steady voltage	V <sub>f</sub>	1	B	-0.8	0.8
3	Initial voltage	V <sub>f0</sub>	1	B	0.8	0.8
4	Voltage-temperature coefficient	KVT	0.006	B	15.12	0.089
4.1	Calibration junction temperature 1	T <sub>J1</sub>	1	A		0.4
4.2	Calibration junction temperature 2	T <sub>J2</sub>	1	A		-0.4
4.3	Calibration voltage 1	V <sub>f1</sub>	1	B		-0.5
4.4	Calibration voltage 2	V <sub>f2</sub>	1	B		0.5
<b>Total uncertainty</b>			<b>U(T<sub>j</sub>) = 1.33</b>			
<b>Expanded uncertainty (k = 2)</b>			<b>U(T<sub>j</sub>) = 2.66</b>			

**Table 20.** Integrating sphere overall measurement uncertainty summary

Parameters	Expanded uncertainty
Luminous Flux	3,23123876
CCT	6,005612389
CRI	0,975192271

Detailed measurements equations are shown below;

"T<sub>jx</sub>= Measured junction temperature"

"V<sub>fx</sub>= Steady forward voltage under the measured junction temperature"

"T<sub>jo</sub>= Initial junction temperature"

"V<sub>fo</sub>= Initial forward voltage"

"KVT= Voltage-temperature coefficient"

$$T_{jx} = T_{jo} + \frac{V_{fx} - V_{fo}}{KVT}$$


---

"V<sub>f1</sub> and V<sub>f2</sub>; Measured forward voltages at ambient temperatures of T<sub>1</sub> and T<sub>2</sub>"

"T<sub>j1</sub> and T<sub>j2</sub>; Junction temperatures after thermal equilibrium"

$$KVT = \frac{V_{f1} - V_{f2}}{T_{j1} - T_{j2}}$$


---

"The standard uncertainty of junction temperature T<sub>J</sub> is given by;"

$$A = U^2$$

$$A_{Tj} = A_{Tjo} + \frac{1}{KVT^2} \cdot (A_{Vfx} + A_{Vfo}) + \frac{(V_{fx} - V_{fo})^2}{KVT^4} \cdot A_{KVT}$$


---

"The standard uncertainty of the voltage-temperature coefficient; KVT, is given by;"

$$A_{KVT} = \left[ \frac{(V_{f1} - V_{f2})^2}{(T_{j1} - T_{j2})^4} \right] \cdot (A_{Tj1} + A_{Tj2}) + \frac{1}{(T_{j1} - T_{j2})^2} \cdot (A_{Vf1} + A_{Vf2})$$

## APPENDIX B

### LED CHIP EFFICIENCY MEASUREMENT STUDY

It is known that some portion of the input electrical energy 'E' is converted to light (radiant power) 'L' at the p-n junction of an LED chip, and the remaining portion is converted to heat 'Q'. Thus, it can be presented in the following equation as;

$$E=Q+L \quad (10)$$

The ratio of the generated radiant power to the given electrical power denotes the efficiency of an LED package. In order to measure the amount of the electrical energy that is converted to heat at the junction of the LED chip; this current projected method has been developed consisting of two distinct approaches; transparent unpainted LED test sample and fully absorbing painted LED system. In the unpainted case, the chip operates until steady state condition is reached, and meanwhile it emits light out through its transparent silicone optical path. Conversely, in the fully absorbing painted case, the dome of the LED chip is painted in absorbing-black with a thermal emissivity of over 0.95. This causes absorption of the emitted light at the outer surface of the dome and generates heat in the amount of the emitted radiant power. These two cases are investigated both experimentally and computationally in order to determine the generated light and heat percentages for various power inputs.

#### **Fully Transparent Unpainted LED Study**

While there is not any coating over the LED as shown in Figure 74, the chip emits white light when it operates at a certain wavelength after it reaches to steady condition. Optical and thermal behavior of the LED chip is measured using an integrating sphere for optical characteristics, and a microscopic IR camera in addition to thermocouples attached to the chip.

**Table 21.** Optical properties of the LED package

Driving Current[mA]	Lumen/W	CCT	CRI
200	194	5198	69.7
300	169	5171	69.4
400	141	5150	69.2
500	111	5119	69.0
600	78	5088	68.8

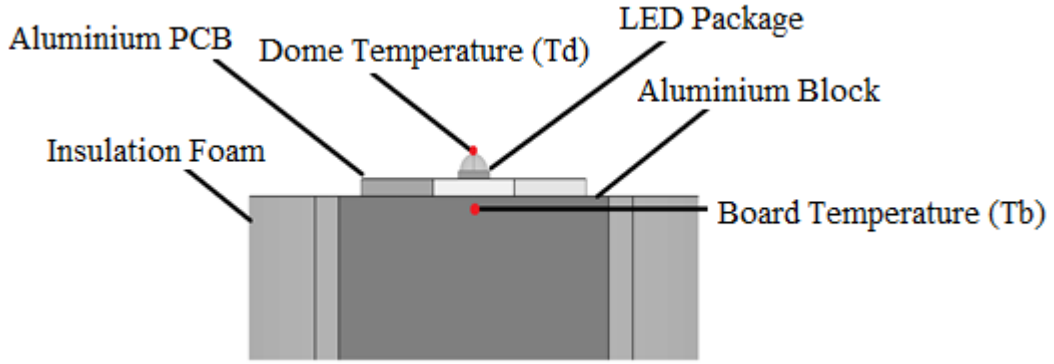
A rectangular aluminum block with a 9 cm height and 3 cm width is produced. A multi-chip LED package is placed and screwed on top surface of the aluminum block. The LED package is from CREE Inc. and its optical properties are shown in Table 21. A thermal paste with a thermal conductivity of 2 W/m-K is used as the thermal interface material.



**Figure 74.** The experiment sample for unpainted case

To minimize possible heat losses at the experimental setup, the aluminum block is then covered with foam for thermal insulation purpose. The optical and thermal measurements were performed simultaneously inside the integrating sphere. First, the sample is placed inside the integrating sphere where the optical and thermal measurements were performed for five different current levels increasing linearly between 200 mA to 600 mA. While the optical measurement is done by the spectrometer inside the sphere, the temperature of the board is measured from the top of the aluminum block as shown in Figure 74 by a T-Type thermocouple that is connected to a data acquisition system. Electrical power is supplied by a DC power supply and both current and voltage values are measured with a data acquisition system.





**Figure 75.** Schematic of the temperature measurement points

The results of the experimental measurements are given in Figure 75. By using the experimental results, we can determine the generated heat by subtracting the radiant power from input electrical power as shown in Table 22.

**Table 22.** Optical and thermal performance results of the unpainted experiments

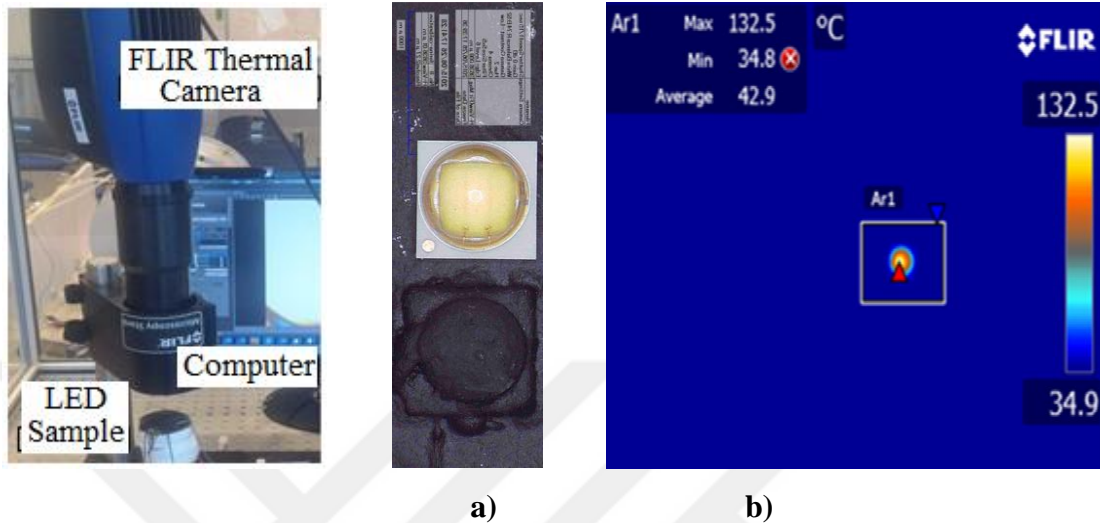
Current [mA]	$E_{in}$ [W]	$T_b$ [°C]	L[W]	$E_{in}-L = Q$ [W]
200	0.608	29.1	0.254	0.354
300	0.946	35.4	0.357	0.590
400	1.303	39.6	0.453	0.850
500	1.672	45.4	0.538	1.134
600	2.068	50.7	0.617	1.451

### Fully Absorbing Painted LED Study

In this part of the study, the chip is completely painted with a black paint having an emissivity value of over 0.95 and no light is leaked out from the dome surfaces. All of the radiant power is absorbed at the surface and converted to heat, which means all of the electrical input to the LED is converted to heat eventually.

This case has a similar method for understanding the portion of the heat generation at the p-n junction of the chip. The portion of the generated light is converted to heat at the dome surface, thus, an overheating occurs at the dome surface and the temperature drastically increases. Similar measurements have been found in literature that, the

temperature of the surface is observed using a FLIR thermal camera alongside with the board temperature measurement with a T-type thermocouple as in the unpainted case as shown in Figure 76 [85,86].

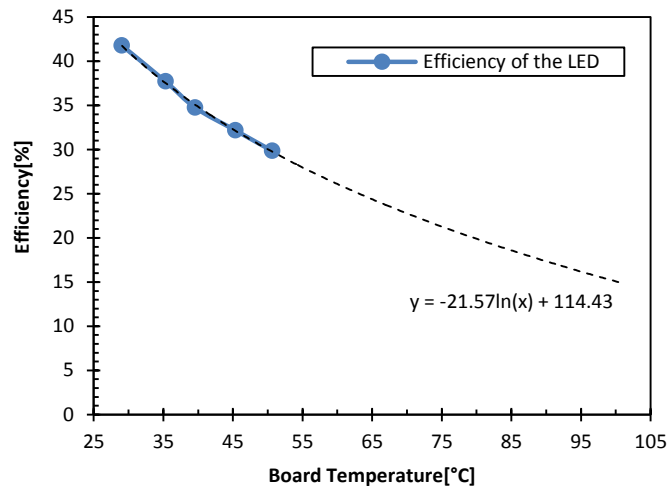


**Figure 76.** a)Experimental setup, b)Painted and unpainted LED packages close up view

Because the temperature of the dome is enormously high due to the light absorption, 0.6 W power (200 mA) is the maximum power given to the chip in this phase as seen in Table 23. For obtaining accurate results with a low uncertainty, it is very important to make sure that there is no leakage of light from the silicone dome for the painted case, otherwise the leaked light would not be accounted for in the simulation, and the temperature distribution on the dome would be different than that of without any leakage (Presumably results in lower temperatures since not all of the light is converted to heat).

**Table 23.** Optical and thermal performance results of the painted experiments

$E_{in}[W]$	$T_b[°C]$	$T_d[°C]$	$L[W]$
<b>0.28</b>	29.5	98.5	0
<b>0.44</b>	32.9	132	0
<b>0.59</b>	36.2	163.5	0



**Figure 77.** Change of efficiency with increasing board temperature

Accordingly, the related chip efficiencies are measured and reported in Figure 77 in which the x-axis represents the various board temperatures and y-axis represents the corresponding chip efficiencies. The blue line is the result of the actual experiment values and the dashed line is the extrapolated efficiency line for further board temperatures with a logarithmic relationship assumed.

As it was discussed in the earlier sections, due to high elevated temperatures at the fully absorbing painted LED case, the peak board temperature one would get without compromising the accuracy was limited to 50 °C (163°C dome temperature ( $T_d$ )). Consequently, only the data points until the peak value are represented in this study, and the dotted line is an estimated trend based on those experimental findings and they do not represent experimentally validated values. While, the efficiency for 30 °C is measured as 42%, with the current idea, it is expected to drop to 30% for 50°C board temperature. If one assumes a logarithmic relationship between the efficiency and the board temperature, the efficiency drops approximately to 15% when the temperature reaches to 100°C. Since most of the LEDs operating board temperature are between 80°C - 100°C, it can be concluded as the efficiencies of the LED chips may be around 20% for a wide range of elevated temperatures.

## APPENDIX C

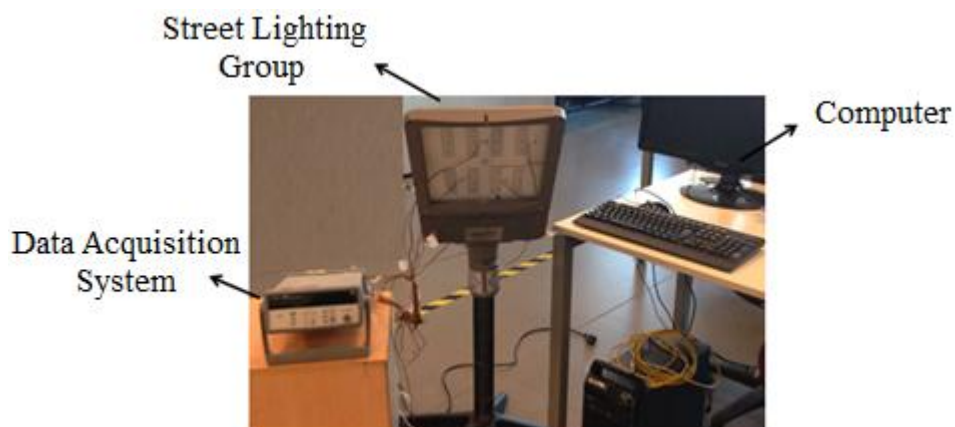
### LED STREET LIGHTING: HEAT SINK OPTIMIZATION

Implementing LEDs to street lighting have many advantages for local governments. Outdoor lighting applications may generate anything between 5000 and 58000 lumens depending on the standards and specific application needs. While the technology is moving towards LEDs, one of the biggest issues is the size and weight that LEDs are posing due to bulky heat sinks.

This study focused on the experimental and computational study of a 114 W, LED outdoor lighting module. Computational models are validated with an experimental study to understand thermal performances. Critical system components are identified and further component interactions are presented.

#### Experimental Setup

An experimental study has been performed with a 114 W LED street lamp. For this study, an experimental system has been designed and built (Figure 78). There is a small cabinet to assembly power box in the presented street light. An aluminum plate is functioned as a platform to carry the box, while the plate is also for thermal spreading to reduce the temperature on the box surface.



**Figure 78.** Experimental setup of street lighting

While, temperature is the main parameter of the experiment, it is measured from 15 different locations as noted in Table 24 with 15 T-type thermocouples (Cu-Cu Ni). In this study, a street light is cooled by external heat sinks connected to the main body by natural convection. The experiment has been done twice for each two different conditions and the temperature values have been noted while they are showing stabilized results. The presented street light positioned horizontally for the initial condition while the lamp has been positioned 45° angular with the horizontal axis for the second condition. The result will be analyzed in the further sections.

**Table 24.** Measured temperatures on different location

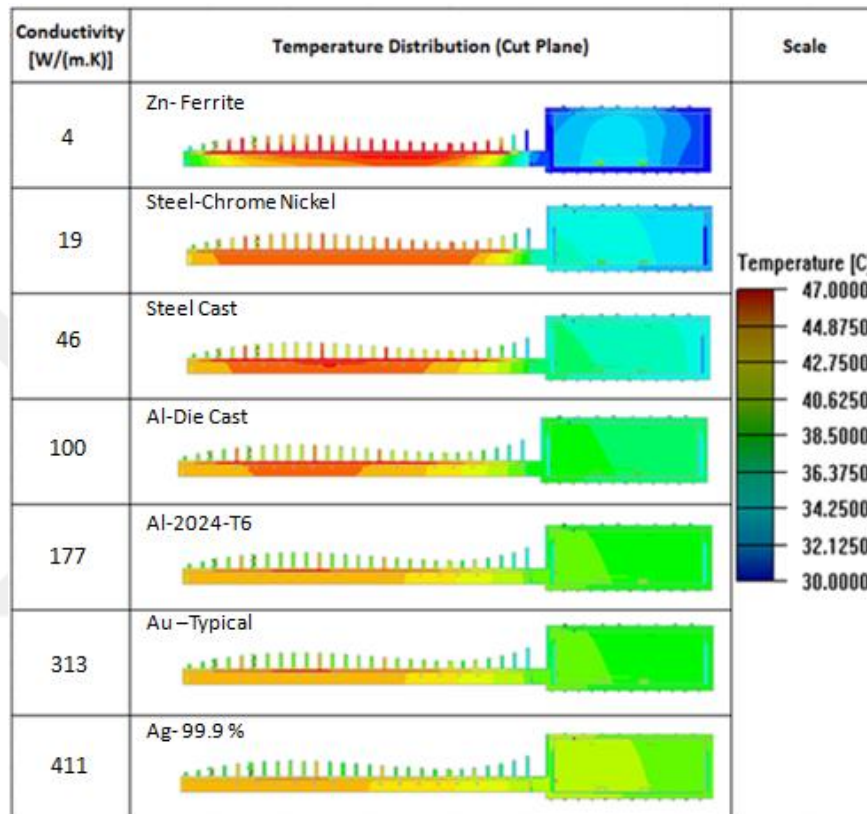
Thermocouple No	Location
103	Ambient
106	LED Lighting Area
111	
114	
116	
118	
108	LED Fin Area
113	
115	
117	
119	Power Box Cabinet Fin Area
120	
107	Power Box Cabinet Lid Fin Area
109	Power Box (driver) Cabinet
110	
112	

### Computational Domain

A three-dimensional geometry of the domain of analysis is simulated with commercially available software Ansys – Icepak. There, computational studies are carried out with different angular positions and different design conditions such as changing the fin height, fin thickness and fin numbers.

## Outer Thermal Path Results

As it seen on Figure 79, thermal distributions for different materials (Zn-Ferrite, Steel-Chrome nickel, Steel Cast, Al-Die Cast, Al-2024-T6, Au–Typical and Ag-99.9%) with different conductivities are chosen to determinate thermal behavior with different material.



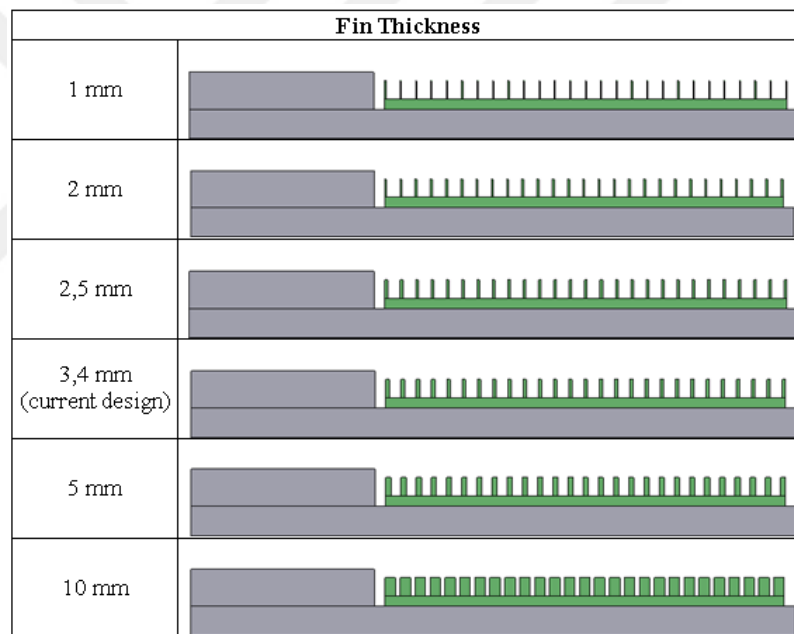
**Figure 79.** Temperature distribution on cut plane

As it is seen on Figure 79, on the first picture, Zn- Ferrite material with  $k: 4[W/ (m. ^\circ K)]$  conductivity has poor heat transfer capacity therefore heat is accumulated and could not disappears to ambient. While conductivity is increased, as it is seen on the other pictures, heat could spread towards driver cabinet and transfer to ambient. Thus high conductivity, high temperature area becomes smaller and move forward through edge area, while conductivity arises. The first fin and last three fins do not perform sufficiently to transfer the heat to ambient. Temperature distribution on cut plane is seen on Figure 79.

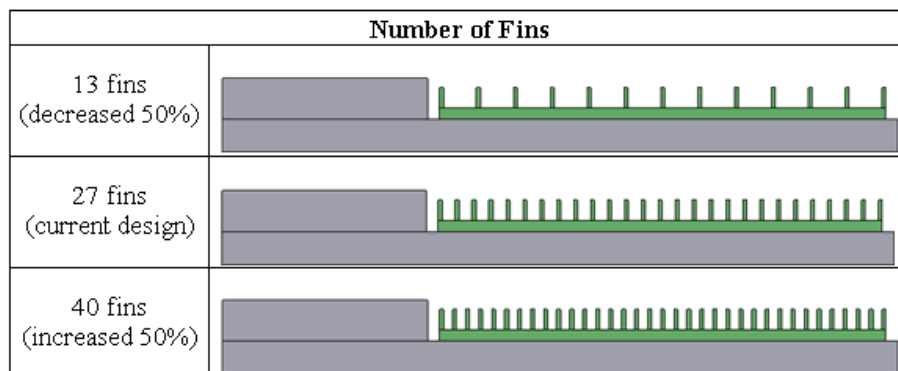
**Table 25.** Temperature for different materials

Thermocouple Number	Temperatures for different materials conductivities (°C)						
	4 [W/(m.K)]	19 [W/(m.K)]	46 [W/(m.K)]	100 [W/(m.K)]	177 [W/(m.K)]	313 [W/(m.K)]	411 [W/(m.K)]
103	21,2	21,0	21,2	21,2	21,2	21,2	21,2
108	54,0	49,5	47,1	45,2	44,0	42,8	42,2
113	57,1	52,6	50,3	48,4	47,3	46,0	45,4
115	54,2	47,1	45,3	44,5	42,3	41,5	41,4
120	29,4	29,8	31,3	32,6	33,7	34,2	34,4
107	28,0	30,7	32,4	33,7	34,6	35,1	35,2

Thereafter, geometrical changes have also been applied. Initially, fin thickness was changed for five different materials. Current fin thickness value is 3, 4 mm. This value was increased to 5mm and 10 mm and decreased to 1mm, 2mm and 2.5mm can be seen in Figure 80.



**Figure 80.** Various design with different fin thickness



**Figure 81.** Various design with different number of fins

However, reducing the fin thickness to 1 mm, 2 mm and 2.5 mm affects the system in a positive way and decreased the temperature values. However, changing the fin thickness as 5mm and 10mm has not shown same behavior; unlike, temperature values rise when fin thickness were increased seen in Table 26, due to decrease the distance between fins.

Another revision has applied to lighting group by changing the fin number. In current design, fin number is 27. This number was increased and decreased 50% to observe the fin number affect (Table 27). Other physical properties such as fin thickness and fin height were not changed.

**Table 26.** Temperature distribution for current material on variable thickness

Temperature values on different fin thickness for conductivity of 205 W/m-K (°C)						
Object	1mm	2mm	2,5mm	current 3,4 mm	5mm	10mm
Led 14	49,03	48,47	49,3	49,42	50,45	56,22
Led 6	49,04	48,49	49,3	49,41	50,43	56,2
Led 4	49,04	48,49	49,28	49,4	50,45	56,2
Led 12	49,03	48,47	49,28	49,4	50,46	56,21
Led 22	48,98	48,41	49,22	49,38	50,4	56,16
Led 20	48,98	48,42	49,2	49,37	50,41	56,16
Led 43	48,98	48,45	49,24	49,35	50,39	56,13
Led 45	48,97	48,45	49,26	49,35	50,38	56,14

**Table 27.** Temperature distribution for current material on variable fin number (k=205W/m-K)

Temperature values on different fin numbers (°C)			
Object	13 fins	current (27fins)	40 fins
Led 6	51,87	49,41	49,61



It is found that temperature variation between fins is less than  $1^{\circ}\text{C}$  so it is decided that the comparing the results from single location (LED6) will be sufficient. It is also shown that the optimum fin number is 27 which is in the current design. Otherwise, temperature values increase between  $0.2^{\circ}\text{C}$  and  $1.5^{\circ}\text{C}$ .

To sum up, the street light thermal regime is monitored experimentally with fifteen thermocouples and temperatures have been monitored while the street light is oriented at different positions. Thermal resistance analysis also carried out computationally to compare the results. Those studies show that the temperature on the chip is approximately  $45^{\circ}\text{C}$ . The temperature is higher on the edge area and even further increases while the street light positioned is angled ( $45^{\circ}$ ) with the horizontal axis. Inner and outer areas were studied in this study. Thermal analysis of the street light has been carried out in different materials and design options.

While, geometrical changes have been observed on different material and their variations such as fin thickness, fin heights and fin numbers. Ideal fin number is found 27fins which is current status and increasing the fin height effects in positive way to system. Also increasing the thermal conductivity decreases the temperature values as parabolic.

Reducing the fin thickness 2 mm and changing material with cheaper one, temperature increase maximum  $19^{\circ}\text{C}$  (with  $k:19\text{ W/m}\cdot^{\circ}\text{K}$ ). These modifications can be applied according to thermal requirements.

## BIBLIOGRAPHY



**Dr. Enes Tamdoğan**

### Research Areas

Cooling technologies in electronics (Direct-Indirect Liquid Cooling, etc), heat transfer on structured surfaces, CFD analysis and experimental studies for single and 2 Phase Natural&Forced Convection

### PhD

Özyeğin University 2017

### Graduate

Brandenburg University of Technology, Cottbus, 2011

### Undergraduate

Uludağ University, 2009

*Enes Tamdoğan obtained his B.Sc. in Mechanical Engineering from Uludağ University in 2009 and completed his M.Sc. in Mechanical Engineering at Brandenburg University of Technology, Cottbus in 2011 with his thesis on “Numerical Study On Swirling Flows in a Pulverized Oxy-Coal Burner”. There, he also focused on sustainable energy supply techniques beside of the computational studies of nature friendly combustion systems (Carbon Capture and Storage Technology). Since he has experienced short term team works in USA and Germany between 2004-2009, he also participated for a long term international project as a researcher in BTU Cottbus for two years after 2009.*

*After his M.Sc. he joined to Özyeğin University, Mechanical Engineering department for his Ph.D. There, he worked with research interests of cooling technologies (Direct-Indirect Liquid Cooling, etc) in electronics, heat transfer on structured surfaces, CFD analysis and experimental studies for single and 2 Phase Natural&Forced Convection problems and also took place in a variety of projects where novel approaches are being applied for thermal management of electronics and at OzU as RA/TA. During his Ph.D., he also worked at Georgia Institute of Technology as a visitor researcher.*

*At the end of his study, 6 journals, 8 conference papers, 2 USA patents (1 pending), 1 book chapter have been served to the literature. Moreover, his researches have been awarded in USA (IMECE 2013) as “**Best Poster Presentation**” and in USA (DARPA RevCon Thermal Connector Design Competition) as “**Best Commercial Potential**”.*